GRAVITY, SURFACTANTS, AND INSTABILITIES

OF TWO-LAYER SHEAR FLOWS

by

ADAM SCHWEIGER

DAVID HALPERN, COMMITTEE CHAIR
LAYACHI HADJI
TSUN ZEE MAI
BETH A. TODD
WEI ZHU

A DISSERTATION

Submitted in partial fulfillment of the requirements
for the degree of Doctor of Philosophy
in the Department of Mathematics
in the Graduate School of
The University of Alabama

TUSCALOOSA, ALABAMA

2013

ABSTRACT

A linear stability analysis of a two-layer plane Couette-Poiseuille flow of two immiscible fluid layers with different densities, viscosities and thicknesses, bounded by two infinite parallel plates moving at a constant relative velocity to each other, with an insoluble surfactant monolayer along the interface and in the presence of gravity is carried out. A normal modes approach is applied to the continuity and the Navier-Stokes equations that govern the fluid motion in the two layers, yielding two Orr-Sommerfeld equations for the perturbed vertical components of velocity in the two layers. These equations together with boundary conditions at the plates and the interface form a linear eigenvalue problem. When inertia is neglected the eigenfunctions can be determined analytically, and a dispersion equation for the increment, that is the complex growth rate, is obtained where coefficients depend on the aspect ratio, the viscosity ratio, the basic velocity shear, the Marangoni number Ma that measures the effects of surfactant, and the Bond number Bo that measures the influence of gravity. An extensive investigation is carried out that examines the stabilizing or destabilizing effects of these parameters on the flow within the two layers. Since the dispersion equation is quadratic in the growth rate, there are two branches: a robust branch that exists even when there is no surfactant, and a surfactant branch that vanishes when $\mathrm{Ma} \downarrow 0$. Although $\mathrm{Bo} > 0$ has a stabilizing effect, the results show that for certain parameters the small-amplitude long-wave disturbances may grow due to the destabilizing effects of surfactant, no matter how large the magnitude of Bo. When $\mathrm{Bo} < 0$ gravity is destabilizing but surfactants can be either stabilizing or destabilizing depending on the parameters.

DEDICATION

I dedicate this dissertation, foremost, to Herb and Donna Schweiger, my parents. Their support, encouragement and love continues to be invaluable. To the rest of my family, I am grateful and blessed. To my friends for all the great times that kept me sane (Danvillian Civilians) JCSells, JDooley, SSlack, JRothwell, CGuill, ECropp, SEdmunds, ETurner, ANewcomb, (JMU peeps) SWilliamsL, ASmith, MGeyer, JGilliam, BGeorge, (RMFT) DHopcraft, CGeorge, MSendral. To my first and longest friend in Alabama, Nathan Jackson, for all his generosity through my days living in Tuscaloosa. Also, to Kyle Edwards for everything before and after the tornado on April 27, 2011. Finally, to Rebecca Vosghanian who stuck by my side through all the years I worked to finish this dissertation. Her patience, understanding, and help has been crucial to my progress and happiness.

LIST OF ABBREVIATIONS AND SYMBOLS

In this dissertation the superscript * will denote dimensional variables. The important variables and parameters are:

z^*-axis is the spanwise, vertical, coordinate perpendicular to the moving plates

x^*-axis is chosen so that it is parallel to the plates.

t^* represents the time.

$\sigma^*$the surface tension at the interface

Γ^*insoluble surfactant monolayer concentration

$\eta^*(x^*, t^*)$ deflection of the interface

ρ_j density

μ_j viscosity

$\boldsymbol{v}_j^* = (u_j^*, w_j^*)$ is the fluid velocity vector

u_j^* horizontal component

w_j^* vertical component

p_j^* pressure

g gravity

$m = \mu_2/\mu_1$ ratio of viscosities,

$n = d_2/d_1$ thickness ratio of the liquid layers

$r = \rho_2/\rho_1$ is the ratio densities

s shear of the basic velocity at the interface

$\mathrm{Pe} = \sigma_0 d_1/\mu_1 D_\Gamma$ is the Péclet number

$\mathrm{Re} = \rho_1 \sigma_0 d_1 / \mu_1^2$ is the Reynolds number

$\mathrm{Ma} = \frac{E\Gamma_0}{\sigma_0}$ is the Marangoni number

$\mathrm{Bo} = \mathrm{Bo}_1 - \mathrm{Bo}_2 = \frac{(\rho_1 - \rho_2) g d_1^2}{\sigma_0}$ is the effective Bond number

α wavenumber of the disturbance

$\gamma = \gamma_R + i\gamma_I$ increment (complex growth rate)

R "robust branch,"

S "surfactant branch,"

Q-sectors Q_1 $(1 < n^2 < m)$ and Q_2 $(m < n^2 < 1)$

R-sectors R_1 $(1 < m < n^2)$ and R_2 $(n^2 < m < 1)$

S-sectors S_1 $(1 < n < \infty$ and $0 < m < 1)$ and S_2 $(0 < n < 1$ and $1 < m < \infty)$

ζ discriminant

ACKNOWLEDGMENTS

First and foremost I thank Dr. David Halpern for his willingness to take on the task of advising me through this dissertation. His guidance and help was always above and beyond anything a graduate student could ever ask. Also, Dr. Alexander Frenkel was always available for suggestions, support, and encouragement throughout this research. Their patience, skill, insight, and inspiration has been the backbone to my survival as a graduate student.

To Dr. Tan-Yu Lee who worked with me on the "Volume" project and helping me obtain the NSF GK-12 fellowship (program #0742504). This fellowship guided by Dr. Beth Todd allowed me to meet many wonderful people while working in Sumter County Alabama and while studying abroad in Peru. Specifically, Mrs. Gloria Clark, my GK-12 high school teacher pair was always available with words from the wise.

I would also like to thank my committee members, Dr. Layachi Hadji, Dr. Tsun Zee Mai, Dr. Beth Todd, and Dr. Wei Zhu for their time and suggestions. Thank you Dr. Zhijian Wu, the department chair, the Mathematics Department staff, especially Michele Farley, Marcia Black, and Sam Evers, and the many professors for always believing in my success.

Thanks to Dr. Debra Warne, my undergraduate advisor, who saved my career at JMU and Dr. Laura Taalman for my calculus background. Finally, to everyone who taught me valuable mathematics growing up. From adding money with Grandma and Papa to budgeting and saving by Mom and Dad. The lessons learned will last a lifetime.

CONTENTS

LIST OF FIGURES

I. INTRODUCTION

In this dissertation the stability of two fluid layers of different densities and viscosities that are sheared by the relative motion of two parallel plates between the layers is investigated. An insoluble surfactant monolayer present at the interface between the two layers significantly affects the character of the instability, and its interplay with gravity is the novel aspect of this work. There continues to be a great deal of interest in these types of flows in many industrial and biomedical applications, for example, coating in photography (Kistler and Schweizer [24]) and oil recovery entrapped in water (Slattery [41]). The core-annular flow is another well studied example of a two-fluid system of immiscible fluids that fill a circular pipe and flow along its axis. Applications include power generation by separation of steam (Joseph and Renardy [23]), the transportation of crude viscous oils in lubricated pipelines (Joseph and Renardy [23]), and the closure of the small airways of the lung that are liquid lined (Halpern and Grotberg [21], Otis et al. [32]). A summary of thin film literature and their applications are given by Oron et al. [30] and Craster and Matar [12].

The interest is in viscous fluid arrangements that are bounded by two parallel plates which could be stationary or moving relative to each other. Yih [55] was one of the very first researchers to consider interfacial instability between two fluids subject to a shear flow. He found that an instability could occur provided there was a viscosity difference and the effects of inertia were included. Yiantsios and Higgins [53] extended the results of Yih [55] by considering the effects of interfacial tension and gravity on the stability of two immiscible layers in plane Poiseuille flow. A review of the Yih instability can be found in Joseph and Renardy [23].

Surfactants are surface active compounds that reduce the surface tension between two

fluids, or between a fluid and a solid. Typically they are organic compounds containing hydrophobic and hydrophilic groups, and their alignment at an interface alters the surface properties of an interface. The effect of introducing an insoluble surfactant has been shown to be stabilizing for a certain class of two layer flows where the interfacial velocity shear is zero (Anshus and Acrivos [1], De Wit et al. [13], Lin [28], Rubinstein and Bankoff [39], Whitaker [50], Whitaker and Jones [51], Yih [54]) and also in multifluid systems with no base flow (Kwak and Pozrikidis [26]). Frenkel and Halpern [14] (hereafter referred to as FH) and Halpern and Frenkel [19] (hereafter referred to as HF) discovered what is believed to be the first example of a stable system of two fluids with different viscosities of a sheared flow that becomes unstable in the presence of an interfacial surfactant monolayer in the absence of inertia. More recently, it has been shown that the inclusion of surfactants may be stabilizing or destabilizing in sheared viscous multilayer systems (Bassom et al. [3, 4], Blyth and Bassom [5], Blyth et al. [6], Blyth and Pozrikidis [7, 8, 9], Frenkel and Halpern [15, 16], Gao and Lu [17, 18], Halpern and Frenkel [20], Levy and Shearer [27], Peng and Zhu [33], Pozrikidis [35, 36], Pozrikidis and Hill [37], Suman and Kumar [43], Wei [45, 46, 47, 48], Wei and Rumschitzki [49]). Next, a description of how surfactants may destabilize a flow is provided.

Interfacial flows may be driven by surface tension gradients at the interface which depend on the properties that characterize the fluid at the interface of two fluids or at a free surface, such as, the temperature or chemical concentration. These types of flows are called Marangoni flows. Consider two fluids separated by a flat interface that are sheared by the relative motion of two parallel plates, and assume that the surfactant concentration along the interface is initially constant. If the interface is slightly perturbed from its uniform state, the flow within the two layers may modify the surfactant distribution along the interface. For instance, an accumulation of surfactant at the troughs causes a flow from troughs to

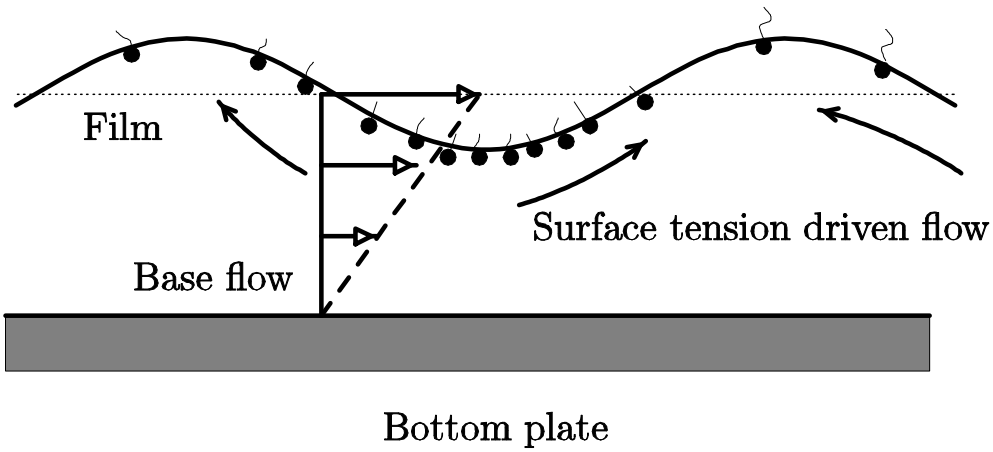

FIG. 1: Diagram of the surfactant driven Marangoni instability.

crests indicating that surfactants can be destabilizing. A diagram of the surfactant induced Marangoni instability mechanism is given in figure 1.

The linear stability analysis carried out by FH to demonstrate surfactants could have a destabilizing effect was restricted to longwaves, and then extended to cover all wavenumbers in HF. A description of their stability analysis is given next. The equations that govern the flow in the two layers are the Navier-Stokes and continuity equations for incompressible Newtonian fluids. At the channel walls no slip and no penetration conditions are applied, while at the interface between the two liquids there are balances of tangential and normal stresses, and continuity of velocity conditions are imposed. There is also a transport equation for the surfactant concentration and the kinematic boundary condition for the interfacial deflection. The equations and boundary conditions are nondimensionalized, and this allows one to compare the order of magnitudes of dimensionless variables that will represent the quantitative properties of the physical system, that in turn dictates how to neglect certain terms and approximate the system. Only infinitesimally small disturbances are considered so that the equations and boundary conditions can be linearized with re-

spect to the base (unperturbed) state. The method of normal modes is used to express the disturbances as complex exponential functions of time (growth rate–time frequency) and location (wavenumber–spatial frequency). Due to linearity, disturbances can be expressed as a superposition of the normal modes. A system of differential equations is obtained for the perturbed velocity component, the pressure, the surfactant concentration, and the interfacial deflection. Because two dimensional flows are considered, it is possible to eliminate the pressure and one of the velocity components, and obtain two fourth order ordinary differential equations known as the Orr-Sommerfeld equations (Orr [31], Sommerfeld [42]). These equations together with the boundary conditions form an eigenvalue problem. When inertia is neglected, the eigenfunctions can be determined analytically, and the growth rate satisfies a quadratic equation for the complex increment γ with lengthy complex coefficients that depend on the wavenumber α, aspect ratio n, viscosity ratio m, shear of the basic velocity at the interface s, Marangoni number Ma (that measures the effect of surfactant), and effective Bond number Bo (that measures the influence of gravity). There are two branches, the increment branch that is non-zero for zero Marangoni number is defined as the "robust branch," R, and the other increment branch, that vanishes as $\mathrm{Ma} \downarrow 0$, is the "surfactant branch," S.

Stability is achieved when the perturbation decays for all wavenumbers, while instability is observed provided the growth rate $\gamma_R = \mathrm{Re}(\gamma)$ is positive for at least one single wavenumber. In the limit as $\alpha \downarrow 0$, which is considered by FH, solutions to the Orr-Sommerfeld equations take the form of a polynomial, while solutions for arbitrary wavenumber comprise of transcendental functions. FH and HF identified six sectors of longwave instability in the (n, m)-plane that characterize the stability properties, and are: the Q-sectors, Q_1 $(1 < n^2 < m)$ and Q_2 $(m < n^2 < 1)$; the R-sectors, R_1 $(1 < m < n^2)$ and R_2 $(n^2 < m < 1)$;

the S-sectors, S_1 ($1 < n < \infty$ and $0 < m < 1$) and S_2 ($0 < n < 1$ and $1 < m < \infty$). In the S sectors, they showed that the growth rate corresponding to the surfactant branch is positive, and hence this mode is unstable, while in the R sectors the growth rate of the robust branch is positive. In the Q sectors both branches are stable. They also found a midwave instability where the growth rate $\gamma_R > 0$ for finite α-interval bounded away from $\alpha = 0$ for Ma $> 5/2$ and $m > n^2$ (Q_1 sector). The midwave instability and the semi-infinite thickness case will be explored thoroughly in this dissertation.

The effect of gravity on the surfactant instability is also investigated. Gravity can be stabilizing when the lighter fluid layer is on top of the heavier fluid layer, or destabilizing when heavier fluid is above the lighter fluid. The latter is the well-known Rayleigh-Taylor instability (RTI) Rayleigh [38], Taylor [44] that has been studied extensively. Rayleigh [38] investigated the stability of stratified fluids or fluids with different densities along a vertical axis, and Taylor [44] showed that equivalently the interface between two inviscid fluids with different densities could be unstable to small perturbations if the fluids are accelerated in the direction of the heavier fluid. Reviews of the RTI are given in Kull [25] and Chandrasekhar [10], with applications found in Arnett et al. [2], Hinds et al. [22], Lindl et al. [29], Rudraiah et al. [40], Whitehead and Luther [52]. In this dissertation, the arrangements with the heavier fluid layer above the lighter fluid (RTI) and vice versa are considered.

In section II the stability problem is formulated for finite values of the aspect ratio n, and a comprehensive analysis using normal modes is given in the six stability sectors in the (n, m)-plane and their borders, while in section III the infinite aspect ratio case is considered. Section IV provides some concluding remarks and possible future work.

II. STABILITY PROBLEM FORMULATION FOR FINITE THICKNESS

The formulation used in this dissertation is similar to that of HF and is as follows. A two-dimensional system of two immiscible fluid layers with different densities, viscosities and thicknesses bounded by two infinite parallel plates, a distance $d = d_1 + d_2$ apart, where the upper plate is moving at a constant relative velocity, U, is shown in figure 2. The z^*-axis is the spanwise, vertical, coordinate perpendicular to the moving plates with the upper plate located at $z^* = d_2$ and the lower plate located at $z^* = -d_1$ where $z^* = 0$ is the chosen reference frame and defines the location of the unperturbed liquid-liquid interface. (The symbol * indicates a dimensional quantity.) The direction of the horizontal x^*-axis is chosen so that it is parallel to the plates. At the interface, the surface tension, σ^*, depends on the concentration of the insoluble surfactant monolayer, Γ^*. The basic flow is driven by the combination of the steady motion of the the upper plate and a constant pressure gradient parallel to the plate motion. The frame of reference is fixed at the liquid-liquid interface so that the velocity of the lower plate is $-U_1$, and that of the upper plate is U_2. In the base state, the horizontal velocity profiles are quadratic in z^*, the interface is flat, and the surfactant concentration is uniform. Once disturbed, the surfactant concentration is no longer uniform and the deflection of the interface is represented by the function $\eta^*(x^*, t^*)$ where t^* represents the time.

The continuity equation and the Navier-Stokes momentum equations govern the fluid motion in the two layers (with $j = 1$ for the lower liquid layer and $j = 2$ for the upper liquid layer). They are

$$\nabla^* \cdot \boldsymbol{v}_j^* = 0, \tag{1}$$

$$\rho_j \left(\frac{\partial \boldsymbol{v}_j^*}{\partial t^*} + \boldsymbol{v}_j^* \cdot \nabla^* \boldsymbol{v}_j^* \right) = -\nabla^* p_j^* + \mu_j \nabla^{*2} \boldsymbol{v}_j^* - \rho_j g \hat{\mathbf{z}}, \tag{2}$$

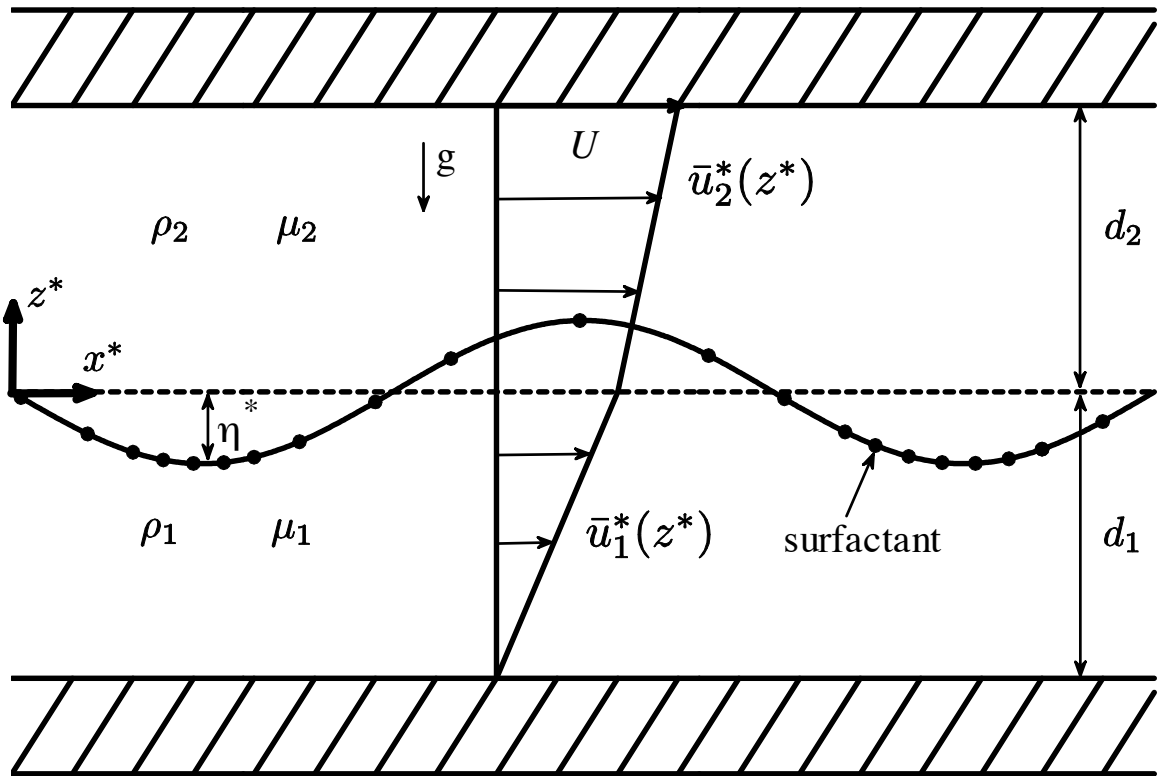

FIG. 2: Definition sketch for two-layer viscous flow between a fixed plate at $z^* = -d_1$ and a moving plate at $z^* = d_2$ with constant velocity U. The disturbed interface is located at $z^* = \eta^*(x^*, t^*)$ and is coated with an insoluble surfactant monolayer whose concentration is $\Gamma^*(x^*, t^*)$.

where ρ_j is the density, $\boldsymbol{v}_j^* = (u_j^*, w_j^*)$ is the fluid velocity vector with horizontal component u_j^* and vertical component w_j^*, $\nabla^* = (\partial/\partial x^*, \partial/\partial z^*)$, p_j^* is the pressure, μ_j is the viscosity, g is the gravity, and $\hat{\mathbf{z}}$ is the unit vector in the upward z^* direction.

At the plates, $z^* = -d_1$ and $z^* = d_2$ the no-slip and no-penetration boundary conditions are applied:

$$u_1^*(-d_1) = -U_1^*,\ w_1^*(-d_1) = 0,\ u_2^*(d_2) = U_2^*,\ w_2^*(d_2) = 0. \tag{3}$$

The interfacial boundary conditions are as follows. The velocity of the fluid at interface must be continuous:

$$[\boldsymbol{v}^*]_1^2 = 0, \tag{4}$$

where $[A]_1^2 = A_2 - A_1$ denotes the jump in A across the interface, $z^* = \eta^*(x^*, t^*)$. Taking into account the gradient of surface tension and the capillary jump in the normal stresses, the interfacial balances of the tangential and normal stresses are, respectively,

$$\frac{1}{1+\eta_{x^*}^{*2}}\left[(1-\eta_{x^*}^{*2})\mu(u_{z^*}^* + w_{x^*}^*) + 2\eta_{x^*}^{*2}\mu(w_{z^*}^* - u_{x^*}^*)\right]_1^2 = -\frac{\sigma_{x^*}^*}{(1+\eta_{x^*}^{*2})^{1/2}}, \tag{5}$$

$$[(1+\eta_{x^*}^{*2})p^* - 2\mu(\eta_{x^*}^{*2}u_{x^*}^* - \eta_{x^*}^*(u_{z^*}^* + w_{x^*}^*) + w_{z^*}^*)]_1^2 = \frac{\eta_{x^*x^*}^*}{(1+\eta_{x^*}^{*2})^{3/2}}\sigma^*, \tag{6}$$

where the subscripts indicate partial differentiation, for example, $\eta_{x^*}^* = \partial\eta^*/dx^*$. The kinematic interfacial condition is

$$\eta_{t^*}^* = w^* - u^*\eta_{x^*}^*. \tag{7}$$

The surface concentration of the insoluble surfactant on the interface, $\Gamma^*(x^*, t^*)$, obeys the following transport equation, which for the one-dimensional case becomes

$$\frac{\partial}{\partial t^*}(H^*\Gamma^*) + \frac{\partial}{\partial x^*}(H^*\Gamma^* u^*) = D_\Gamma \frac{\partial}{\partial x^*}\left(\frac{1}{H^*}\frac{\partial \Gamma^*}{\partial x^*}\right), \tag{8}$$

where $H^* = (1+\eta_{x^*}^{*2})^{1/2}$ and D_Γ is the surface molecular diffusivity of the surfactant. Only infinitesimal deviations of the concentration Γ^* from its basic value Γ_0 are considered thus the surface tension dependence on the surface concentration is linearized and

$$\sigma^* = \sigma_0 - E(\Gamma^* - \Gamma_0), \tag{9}$$

where σ_0 is the basic surface tension and E is a constant.

The governing equations and boundary conditions are nondimensionalized by introducing

the following dimensionless variables:

$$(x, z, \eta) = \frac{(x^*, z^*, \eta^*)}{d_1},\ t = \frac{t^*}{d_1\mu_1/\sigma_0},\ \boldsymbol{v} = (u_j, w_j) = \frac{(u_j^*, w_j^*)}{\sigma_o/\mu_1},$$

$$p_j = \frac{p_j^*}{\sigma_0/d_1}\ ,\ \Gamma = \frac{\Gamma^*}{\Gamma_0},\ \sigma = \frac{\sigma^*}{\sigma_0}. \tag{10}$$

Therefore, equations (1) and (2) become

$$\nabla \cdot \boldsymbol{v}_j = 0, \tag{11}$$

$$Re_j \left(\frac{\partial \boldsymbol{v}_j}{\partial t} + \boldsymbol{v}_j \cdot \nabla \boldsymbol{v}_j \right) = -\nabla p_j + m_j \nabla^2 \boldsymbol{v}_j - \mathrm{Bo}_j \hat{\mathbf{z}}, \tag{12}$$

where $\mathrm{Re}_j = \rho_j \sigma_0 d_1/\mu_1^2$ is the Reynolds number, $m_j = \mu_j/\mu_1$ is the viscosity ratio (when $j = 2$), and $\mathrm{Bo}_j = \rho_j g d_1^2/\sigma_0$ is the Bond number. The plate boundary conditions (3) become

$$u_1(-1) = -U_1,\ w_1(-1) = 0,\ u_2(n) = U_2,\ w_2(n) = 0 \tag{13}$$

where $U_j = U_j^* \mu_1/\sigma_0$ are capillary numbers and $n = d_2/d_1$ is the thickness ratio of the liquid layers. The dimensionless continuity of velocity equation (4), the tangential stress condition (5), and the normal stress condition (6) are, respectively,

$$[\boldsymbol{v}]_1^2 = 0, \tag{14}$$

$$\frac{1}{1+\eta_x^2} \left[(1-\eta_x^2) \frac{\mu}{\mu_1} (u_z + w_x) + 2\eta_x^2 \frac{\mu}{\mu_1} (w_z - u_x) \right]_1^2 = -\frac{\sigma_x}{(1+\eta_x^2)^{1/2}}, \tag{15}$$

and

$$[(1+\eta_x^2)p - 2\frac{\mu}{\mu_1}(\eta_x^2 u_x - \eta_x(u_z + w_x) + w_z)]_1^2 = \frac{\eta_{xx}}{(1+\eta_x^2)^{3/2}}\sigma. \tag{16}$$

The surfactant transport equation (8) becomes

$$\frac{\partial}{\partial t}(H\Gamma) + \frac{\partial}{\partial x}(H\Gamma u) = \frac{1}{\mathrm{Pe}}\frac{\partial}{\partial x}\left(\frac{1}{H}\frac{\partial \Gamma}{\partial x}\right), \tag{17}$$

where $\mathrm{Pe} = D_\Gamma \mu_1/\sigma_0 d_1$ is the surface Péclet number. The kinematic boundary condition (7) becomes

$$\eta_t = w - u\eta_x, \tag{18}$$

and the equation of state for the surface tension (9), is given by

$$\sigma = 1 - \mathrm{Ma}(\Gamma - 1). \tag{19}$$

The dimensionless velocity field of the basic Couette-Poiseuille flow, with a flat interface, $\eta = 0$, uniform surface tension, $\bar{\sigma} = 1$, and corresponding surfactant concentration, $\bar{\Gamma} = 1$ (where the overbar indicates a basic state quantity), is

$$\bar{w}_1 = 0,\ \bar{u}_1(z) = sz + qz^2, \text{ and } \bar{p}_1 = -\mathrm{Bo}_1 z + 2qx \quad \text{for} \quad -1 \le z \le 0, \tag{20}$$

$$\bar{w}_2 = 0,\ \bar{u}_2(z) = \frac{1}{m}\bar{u}_1(z), \text{ and } \bar{p}_2 = -\mathrm{Bo}_2 z + 2qx \quad \text{for} \quad 0 \le z \le n, \tag{21}$$

where $m = m_2 = \mu_2/\mu_1$. The constants s and q are used to characterize the flow in place of the pressure gradient and the relative velocity of the plates (see HF page 193 for the relationships). Here the shear of the basic velocity at the interface is $s = D\bar{u}_1(0)$ where

$D = d/dz$. The stability of the flow does not depend on q because when evaluating $\bar{u}_1$ and $D\bar{u}_1$ at the interfacial reference frame, $z = 0$, the terms involving q disappear.

The perturbed state with small deviations from the basic configuration is given by

$$\eta = \tilde{\eta},\ u_j = \bar{u}_j + \tilde{u}_j,\ w_j = \tilde{w}_j,\ p_j = \bar{p}_j + \tilde{p}_j,\ \Gamma = \bar{\Gamma} + \tilde{\Gamma}. \tag{22}$$

The normal modes are disturbances of the form

$$(\tilde{\eta},\ \tilde{u}_j,\ \tilde{w}_j,\ \tilde{p}_j,\ \tilde{\Gamma}) = [h,\ \hat{u}_j(z),\ \hat{w}_j(z),\ \hat{f}_j(z),\ G]e^{i\alpha x+\gamma t}, \tag{23}$$

where $\hat{u}_j(z)$, $\hat{w}_j(z)$, and $\hat{f}_j\ (z)$ are the complex amplitudes that depend on the depth, α is the wavenumber of the disturbance, G and h are constants, and γ is the complex increment, $\gamma = \gamma_R + i\gamma_I$. The stability of the flow depends on the sign of γ_R, the growth rate: if $\gamma_R > 0$ for some normal modes then the system is unstable; and if $\gamma_R < 0$ for all normal modes then the system is stable. The continuity equation (11) becomes

$$\hat{u}_j = \frac{i}{\alpha} D\hat{w}_j, \tag{24}$$

and the linearization of the horizontal and vertical components of the momentum equations (12) yield ($j = 1,\ 2$)

$$m_j(D^2 - \alpha^2)\hat{u}_j - i\alpha\hat{f}_j = r_j \mathrm{Re}[\gamma\hat{u}_j + i\alpha\bar{u}_j\hat{u}_j + \hat{w}_j D\bar{u}_j], \tag{25}$$

$$m_j(D^2 - \alpha^2)\hat{w}_j - D\hat{f}_j = r_j \mathrm{Re}[\gamma\hat{w}_j + i\alpha\bar{u}_j\hat{w}_j], \tag{26}$$

where $m_1 = 1$, $m_2 = m$, $r = \rho_2/\rho_1$ is the ratio of densities, $r_1 = 1$ and $r_2 = r$. It is assumed

that the inertial forces will be small compared to the viscous forces and thus Re $\ll 1$ (Stokes' flow). Therefore, the inertia terms will be neglected from here on. Eliminating the pressure disturbances $\hat{f}_j$ from equations (25) and (26), yields the well-known Orr-Sommerfeld equations [34] for the velocity disturbances,

$$m_j(D^2 - \alpha^2)^2 \hat{w}_j = 0. \tag{27}$$

The disturbances of the velocities are subject to the boundary conditions at the plates and at the interface. The boundary conditions are written as linear homogeneous equations in terms of the disturbance amplitudes. On applying equation (24), the boundary conditions at the plates (13) are given by

$$D\hat{w}_1(-1) = 0,\ \hat{w}_1(-1) = 0,\ D\hat{w}_2(n) = 0,\ \hat{w}_2(n) = 0. \tag{28}$$

The linearized kinematic boundary condition (18) and surfactant transport equation (17) are, respectively,

$$\gamma h - \hat{w}_1 = 0\ (z = 0), \tag{29}$$

$$\gamma G - D\hat{w}_1 + si\alpha h = 0\ (z = 0). \tag{30}$$

The last term in (30) comes from the Taylor expansion of the base state fluid velocities at $z = \eta(x, t)$. Continuity of velocity at the interface given by equation (14) yields

$$\hat{w}_1 - \hat{w}_2 = 0\ (z = 0), \tag{31}$$

and

$$D\hat{w}_2 - D\hat{w}_1 - i\alpha sh\left(\frac{1-m}{m}\right) = 0 \ (z=0). \tag{32}$$

(To obtain (32) first one takes the Taylor series $[\bar{u}_j + \tilde{u}_j]_1^2$ and keeps only the linear terms. Then once in terms $\hat{u}_j$, h and s equation (24) is used to write $\hat{u}_j$ in terms of $\hat{w}_j$.)

To obtain the linearized homogeneous normal stress condition (16), the complex pressure amplitude, $\hat{f}_j$, is first written in terms of $\hat{w}_j$. From equation (25) it is given by

$$\alpha^2 \hat{f}_j = m_j(D^2 - \alpha^2)D\hat{w}_j. \tag{33}$$

After linearization, the interfacial tangential stress (15) condition becomes

$$mD^2\hat{w}_2 - D^2\hat{w}_1 + \alpha^2(m\hat{w}_2 - \hat{w}_1) - \alpha^2 G\mathrm{Ma} = 0 \ (z=0), \tag{34}$$

where $\mathrm{Ma} = \frac{E\Gamma_0}{\sigma_0}$ is the Marangoni number, and using equation (33) the normal stress condition reduces to

$$mD^3\hat{w}_2 - 3m\alpha^2 D\hat{w}_2 - D^3\hat{w}_1 + \mathrm{Bo}\alpha^2 h + 3\alpha^2 D\hat{w}_1 + \alpha^4 h = 0 \ (z=0), \tag{35}$$

where Bo is the effective Bond number

$$\mathrm{Bo} = \mathrm{Bo}_1 - \mathrm{Bo}_2 = \frac{(\rho_1 - \rho_2)gd_1^2}{\sigma_0}. \tag{36}$$

Note that from (36) Bo can be either positive or negative. If Bo $<$ ($>$) 0 the heavier (lighter) fluid is on top of the lighter (heavier) fluid corresponding to a configuration where gravity is (de-)stabilizing. A formula for the complex growth rate is derived in section

II A and its dependence on the wavenumber α and the parameters n, m, s, Ma, and Bo is investigated throughout.

A. Derivation of the dispersion relation

For finite aspect ratio, n, the general solutions of (27) are given by

$$\hat{w}_j(z) = a_j \cosh(\alpha z) + b_j \sinh(\alpha z) + c_j z \cosh(\alpha z) + d_j z \sinh(\alpha z), \tag{37}$$

where the coefficients a_j, b_j, c_j, and d_j are determined by the boundary conditions up to a common normalization factor, which is chosen to be $a_1 = 1$. Then $a_2 = 1$ so that (31) is satisfied.

Applying the plate velocity conditions, equation (28), the coefficients c_1 and d_1 are expressed in terms of b_1, and the coefficients c_2 and d_2 are expressed in terms of b_2:

$$\begin{aligned}\hat{w}_1(z) = \cosh(\alpha z) + b_1 \sinh(\alpha z) + \left[1 + \frac{1}{\alpha}\left(s_\alpha c_\alpha - s_\alpha^2 b_1\right)\right] z \cosh(\alpha z) \\ + \frac{1}{\alpha}\left[c_\alpha^2 - \left(s_\alpha c_\alpha - \alpha\right) b_1\right] z \sinh(\alpha z),\end{aligned} \tag{38}$$

and

$$\begin{aligned}\hat{w}_2(z) = \cosh(\alpha z) + b_2 \sinh(\alpha z) - \frac{1}{\alpha n^2}\left[\alpha n + s_{\alpha n} c_{\alpha n} + s_{\alpha n}^2 b_2\right] z \cosh(\alpha z) \\ + \frac{1}{\alpha n^2}\left[\left(s_{\alpha n} c_{\alpha n} - \alpha n\right) b_2 + c_{\alpha n}^2\right] z \sinh(\alpha z)\end{aligned} \tag{39}$$

where, as in HF,

$$c_\alpha = \cosh(\alpha),\ s_\alpha = \sinh(\alpha)\,,\ c_{\alpha n} = \cosh(\alpha n),\ s_{\alpha n} = \sinh(\alpha n)\,. \tag{40}$$

Equations (29) and (30) yield h (note that $\hat{w}_1(0) = 1$) and G:

$$h = \frac{1}{\gamma}, \tag{41}$$

$$G = \frac{1}{\gamma^2\alpha}\left(s_\alpha c_\alpha \gamma - is\alpha^2 + \gamma\alpha\right) - \frac{1}{\alpha\gamma}(s_\alpha^2 - \alpha^2)b_1. \tag{42}$$

The interfacial conditions (32), (35), and (34) then provide the following three equations involving b_1, b_2, and γ:

$$\begin{aligned} -\frac{1}{\alpha}\left(s_\alpha^2 - \alpha^2\right)b_1 + \frac{1}{\alpha n^2}\left(s_{\alpha n}^2 - \alpha^2 n^2\right)b_2 + \frac{1}{n}(n+1) \\ + \frac{1}{\alpha n^2}\left(n^2 s_\alpha c_\alpha + s_{\alpha n}c_{\alpha n}\right) - \frac{is\alpha}{\gamma m}(m-1) = 0, \end{aligned} \tag{43}$$

$$2b_2 m - 2b_1 - \frac{1}{\gamma\alpha}\left(\mathrm{Bo} + \alpha^2\right) = 0, \tag{44}$$

and

$$\begin{aligned} \left[\frac{\alpha\mathrm{Ma}}{\gamma}(s_\alpha^2 - \alpha^2) - 2(\alpha - s_\alpha c_\alpha)\right]b_1 + \frac{2m}{n^2}\left(s_{\alpha n}c_{\alpha n} - \alpha n\right)b_2 \\ + 2\frac{mc_{\alpha n}^2}{n^2} - 2c_a^2 - 2\alpha^2(1-m) - \frac{\alpha\mathrm{Ma}}{\gamma}\left(\alpha + s_\alpha c_\alpha - \frac{is\alpha^2}{\gamma}\right) = 0. \end{aligned} \tag{45}$$

From (44) b_2 is expressed in terms of b_1

$$b_2 = \frac{1}{2\gamma\alpha m}\left(2b_1\gamma\alpha + \mathrm{Bo} + \alpha^2\right). \tag{46}$$

This is then substituted into (43) which yields b_1, and thus b_2, in terms of γ. Therefore, (43) and (45) are written as a system of two linear equations in terms of b_1 of the form

$$\begin{bmatrix} A_{11} & A_{12} \\ A_{21} & A_{22} \end{bmatrix} \begin{bmatrix} b_1 \\ 1 \end{bmatrix} = \begin{bmatrix} 0 \\ 0 \end{bmatrix}, \tag{47}$$

where nontrivial solutions are only possible if $\det(A) = A_{11}A_{22} - A_{12}A_{21} = 0$. The coefficients A_{11}, A_{12}, A_{21}, and A_{22} are given in Appendix A 1. Here it is convenient to multiply $\det(A) = 0$ by $-\frac{mn^2\gamma^2}{2\alpha^2}$ to yield the dispersion equation which is quadratic in γ:

$$F_2\gamma^2 + F_1\gamma + F_0 = 0. \tag{48}$$

The two solutions are written in the form

$$\gamma = \frac{1}{2F_2}\left(-F_1 + \left[F_1^2 - 4F_2F_0\right]^{1/2}\right) = -\frac{F_1}{2F_2} + \left[\left(\frac{F_1}{2F_2}\right)^2 - \frac{F_0}{F_2}\right]^{1/2}, \tag{49}$$

where the complex square root has two values. The coefficients F_2, F_1, and F_0 (split into real and imaginary parts) are

$$\begin{aligned} \mathrm{Re}(F_2) = \frac{1}{\alpha^4}\Big\{&\left(s_\alpha^2 - \alpha^2\right)\left(\alpha^2 n^2 + c_{\alpha n}^2\right) m^2 \\ &+ 2\left(\alpha^4 n^2 + s_\alpha c_\alpha s_{\alpha n} c_{\alpha n} - \alpha^2 n\right) m \\ &+ \left(\alpha^2 + c_\alpha^2\right)\left(s_{\alpha n}^2 - \alpha^2 n^2\right)\Big\} > 0, \end{aligned} \tag{50}$$

$$\mathrm{Im}(F_2) = 0, \tag{51}$$

$$\begin{aligned}\mathrm{Re}(F_1) = \frac{1}{2\alpha^3}\Big\{ & m\mathrm{Ma}(\alpha n + s_{\alpha n}c_{\alpha n})\left(s_\alpha^2 - \alpha^2\right) \\ & + \mathrm{Ma}(s_{\alpha n}^2 - \alpha^2 n^2)\left(\alpha + s_\alpha c_\alpha\right) \\ & + \frac{1}{\alpha^2} m(s_{\alpha n}c_{\alpha n} - \alpha n)\left(s_\alpha^2 - \alpha^2\right)\left(\mathrm{Bo} + \alpha^2\right) \\ & + \frac{1}{\alpha^2}(s_{\alpha n}^2 - \alpha^2 n^2)\left(s_\alpha c_\alpha - \alpha\right)\left(\mathrm{Bo} + \alpha^2\right)\Big\}, \end{aligned} \tag{52}$$

$$\mathrm{Im}(F_1) = \frac{s}{\alpha^2}(m-1)(\alpha n^2 - n^2 s_\alpha c_\alpha + \alpha n - s_{\alpha n}c_{\alpha n}), \tag{53}$$

$$\mathrm{Re}(F_0) = \frac{\mathrm{Ma}}{4\alpha^4}(s_{\alpha n}^2 - \alpha^2 n^2)(s_\alpha^2 - \alpha^2)\left(\mathrm{Bo} + \alpha^2\right), \tag{54}$$

$$\mathrm{Im}(F_0) = \frac{\mathrm{Ma}}{2\alpha} s(s_\alpha^2 n^2 - s_{\alpha n}^2). \tag{55}$$

Note that $\mathrm{Im}(F_0)$ is negative (positive) for $n > (<)\ 1$. The zero gravity limit studied in FH and HF is recovered by letting $\mathrm{Bo} = 0$ and then making the substitution $\gamma = -i\alpha c$. One of the goals of this dissertation is to investigate the dependence of n, m, s, Ma, and Bo on the growth rates, $\gamma_R(\alpha) = \mathrm{Re}(\gamma)$, which are continuous functions of wavenumber α.

It is well known in calculus of complex variables that there are two analytic (and thus continuous) branches of the complex square root function in every simply connected domain that does not contain the origin. Therefore, there are two continuous branches of the (complex) increment γ (49), and correspondingly two continuous branches of the (real) growth rate γ_R. If $\mathrm{Ma} \downarrow 0$ then $\gamma_1\gamma_2 = F_0/F_2 \downarrow 0$ and $\gamma_1 + \gamma_2 = -F_2/F_1 \not\to 0$ and so either $\gamma_1 \downarrow 0$ or $\gamma_2 \downarrow 0$. The increment branch that is non-zero at $\mathrm{Ma} = 0$ is defined as the "robust branch," R, and the other increment branch that vanishes as $\mathrm{Ma} \downarrow 0$ is the "surfactant branch," S. These are known as the robust and surfactant branches of the growth rate. It is possible for the two growth rate branches to cross, and therefore the discriminant of (49) can be zero at some points. This can cause difficulties in determining

which branch is the surfactant branch and which is the robust branch. However, γ_R is always defined to be continuous in α. It is shown in section (II C 5) that when $m = 1$ the discriminant is never zero.

B. Main concepts, dependencies, and some examples

Typical dispersion curves of stable and unstable cases look like those in figure 3 and are similar to FH and HF. The unstable branch starts at $\alpha = 0$ and $\gamma_R = 0$, grows with wavenumber, attains a maximum value of $\gamma_{R\,\max}$ at some $\alpha = \alpha_{\max}$, then decreases and crosses the α-axis so that $\gamma_R = 0$ at some non-zero wavenumber, α_0, called the marginal wavenumber. The other, stable, branch also starts at $\alpha = 0$ and $\gamma_R = 0$ but then decreases with wavenumber. The values of α_0, $\gamma_{R\,\max}$, and $\alpha_{\max}$ depend on the parameters n, m, s, Ma, and Bo.

It is pointed out in FH that at least one of the modes for each given α is stable. When one branch is unstable and thus growing with time (i.e., $\gamma_R > 0$) for some interval of wavenumbers, $0 < \alpha < \alpha_0$, then the other branch is stable (i.e., $\gamma_R < 0$) for all $\alpha > 0$. This result is extended for Bo ≥ 0, and is proven by using the relationship between the roots and the coefficients of (49). One should note that this result does not apply for the Rayleigh-Taylor configuration.

First note that the real parts of the coefficients $\mathrm{Re}(F_2)$, $\mathrm{Re}(F_1)$, and $\mathrm{Re}(F_0)$ (equations (50), (52), and (54)) are always positive for Bo ≥ 0 and for $\alpha > 0$ since $\sinh(\alpha) > \alpha$ and $\cosh(\alpha) > 1$. The signs of the imaginary parts depend on the values of n and m. Let the two solutions of (49) be $\gamma_1 = \gamma_{R1} + i\gamma_{I1}$ and $\gamma_2 = \gamma_{R2} + i\gamma_{I2}$, where the real parts of the solutions must satisfy $\gamma_{R1} + \gamma_{R2} = -\,\mathrm{Re}(F_1)/F_2 < 0$. So if either γ_{R1} or γ_{R2} is positive

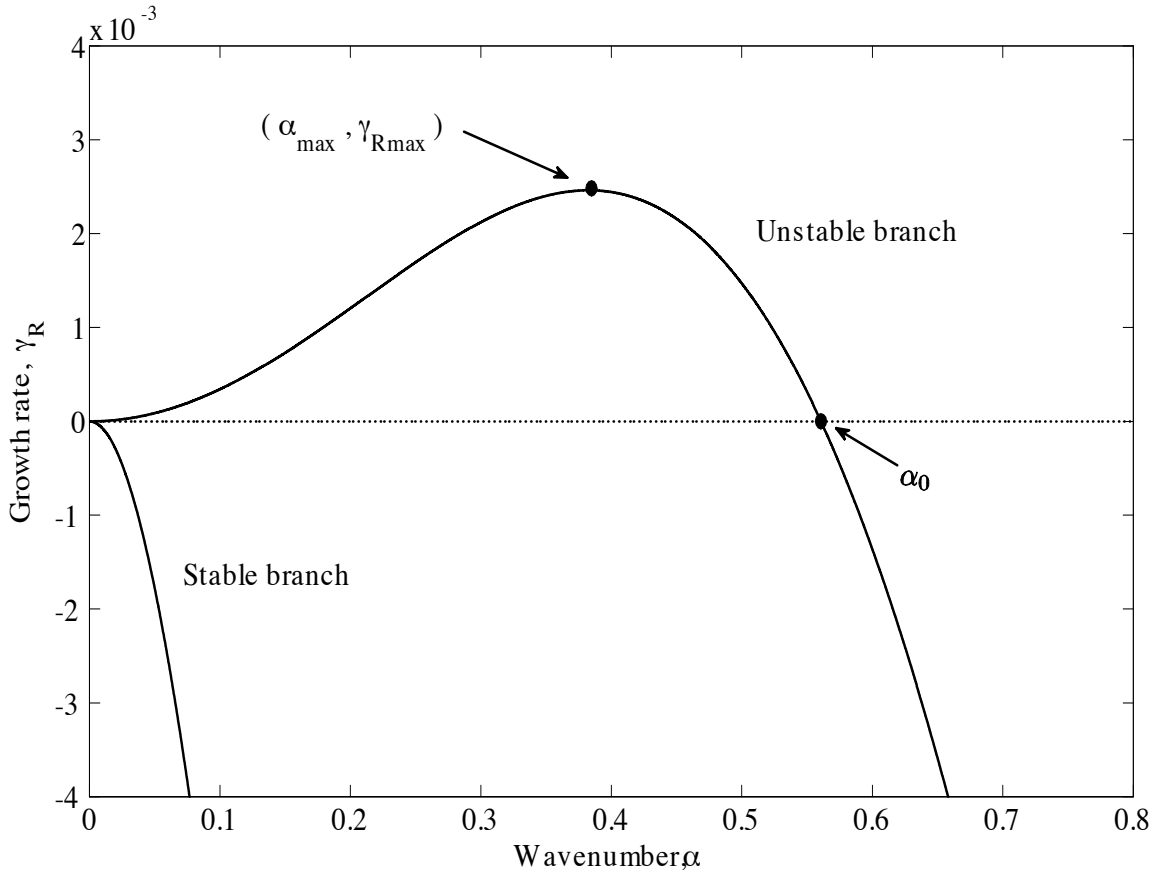

FIG. 3: Two normal modes: (1) the unstable branch attains a maximum at $(\alpha_{\max}, \gamma_{R\max})$ and then decays eventually becoming stable for $\alpha > \alpha_0$ and (2) the stable branch.

(unstable) then the other must be negative (stable).

Some of the types of dependencies that are investigated throughout this dissertation are introduced in figures 4 and 5. In figure 4 the marginal wavenumber, α_0, is plotted as a function of Ma with fixed $n = 2$ and $s = 1$, two values of the Bond number, Bo $= 0$ and Bo $= 0.1$ for each $m = 0.5$ and $m = 2$. For fixed Ma, α_0 decreases with increasing Bo and remains unstable or α_0 does not exist. The latter case suggests there is a critical Ma, Ma_{cL}, where $\alpha_0 = 0$ such that when $\mathrm{Ma} < \mathrm{Ma}_{cL}$ gravity is completely stabilizing.

However, gravity is not completely stabilizing in some regions of the (n, m) plane. This

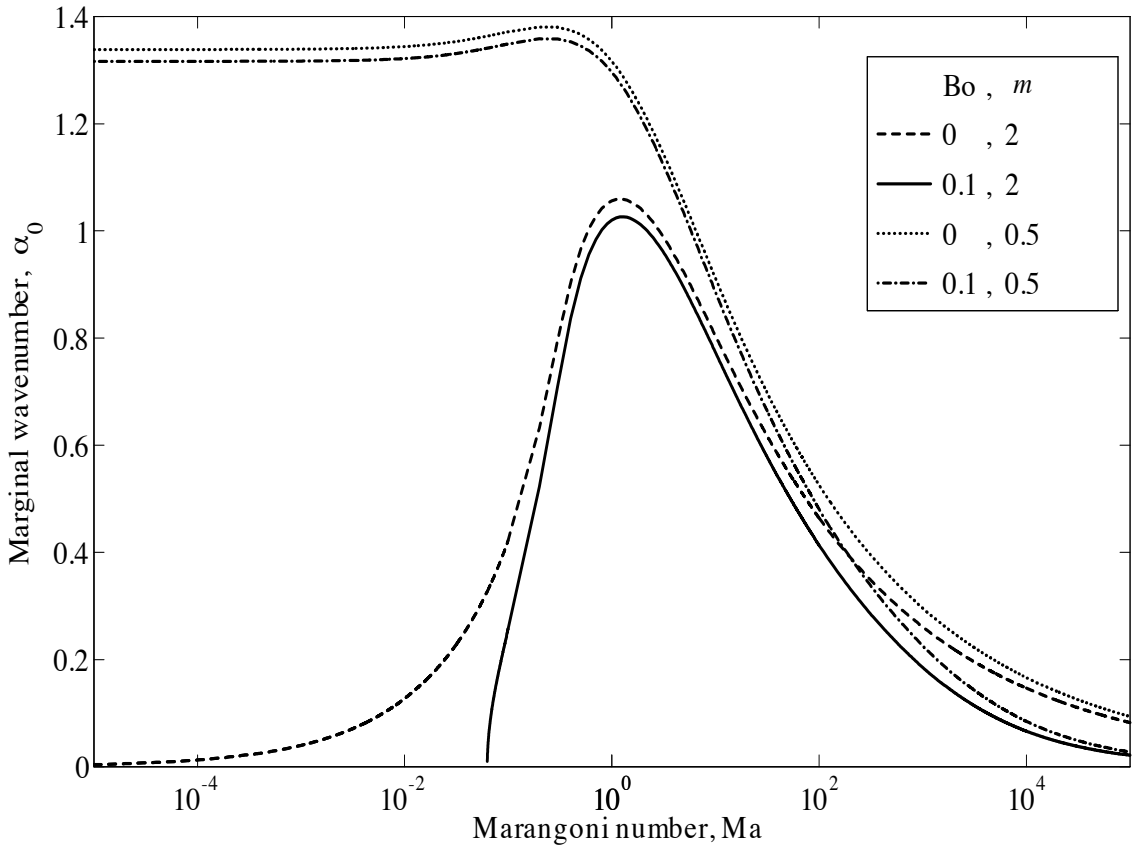

FIG. 4: Marginal wavenumber vs Marangoni number for the parameters indicated in the legend. Here $n = 2$ and $s = 1$.

feature is discussed in more detail in section II C 3 but is also seen in figure 5, where $\gamma_{R\max}$ plotted as a function of Bo for $n = 2$, $m = 5$, Ma $= 0.1$, and $s = 1$. In this case, $\gamma_{R\max} \downarrow 0$ as Bo $\uparrow \infty$ illustrating that gravity may never be completely stabilizing. Also, $\gamma_{R\max}$ increases linearly as Bo $\downarrow -\infty$. The impact of surfactant on the Rayleigh-Taylor instability is investigated more in section II C 4.

In order to compute the maximum growth rate, $\gamma_{R\max}$, the wavenumber corresponding to the maximum growth rate, $\alpha_{\max}$, and the marginal wavenumber, α_0, it is convenient to split the dispersion equation (48) into its real and imaginary parts,

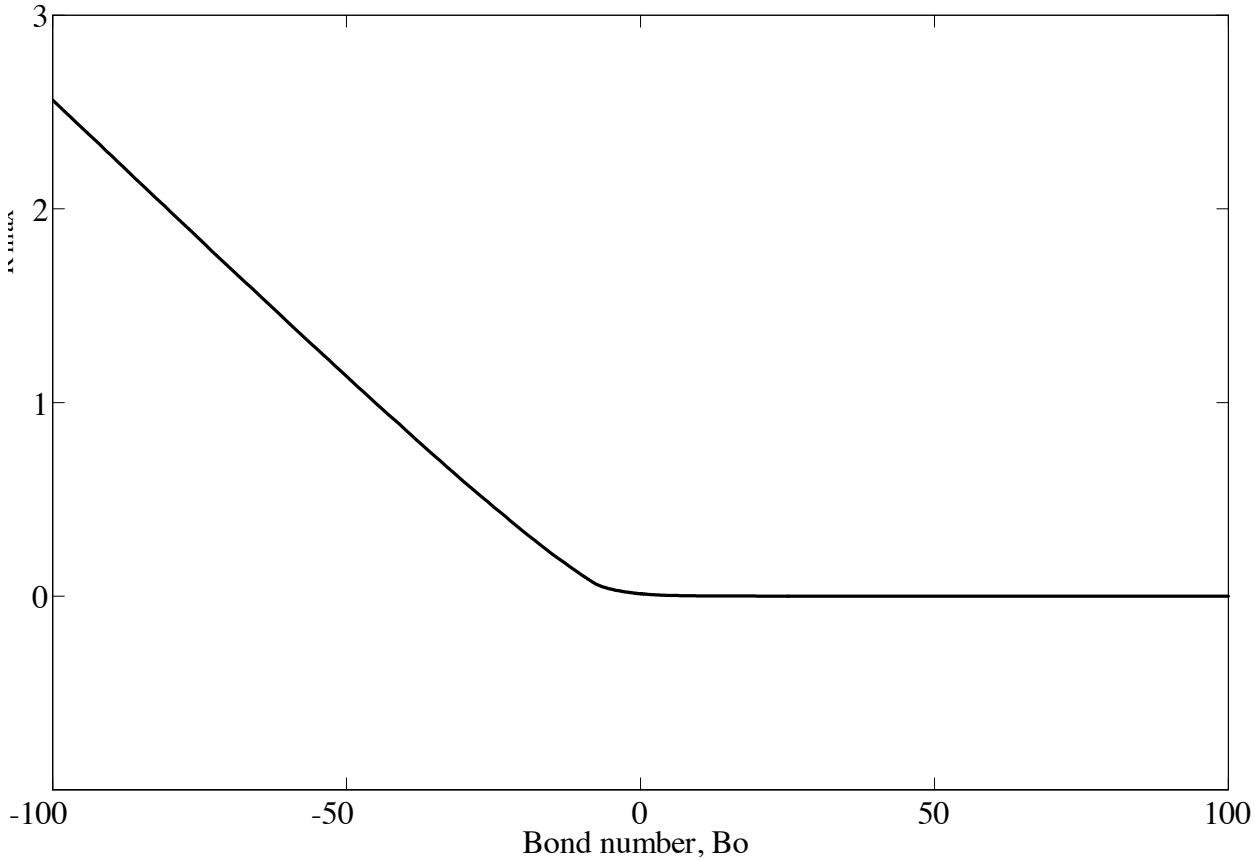

FIG. 5: Maximum growth rate vs Bond number for $s = 1$, Ma $= 0.1$, $n = 2$, and $m = 0.5$.

$$F_2\gamma_R^2 - F_2\gamma_I^2 + \mathrm{Re}(F_1)\gamma_R - \mathrm{Im}(F_1)\gamma_I + \mathrm{Re}(F_0) = 0, \tag{56}$$

$$2F_2\gamma_R\gamma_I + \mathrm{Re}(F_1)\gamma_I + \mathrm{Im}(F_1)\gamma_R + \mathrm{Im}(F_0) = 0. \tag{57}$$

The imaginary part of the growth rate γ_I is expressed in terms of γ_R using equation (57)

and then substituted it into (56) to obtain the following quartic equation for γ_R,

$$4\,{F_2}^3\gamma_R^4 + 8F_2^2\,\mathrm{Re}(F_1)\gamma_R^3 + F_2\left[4\,F_2\,\mathrm{Re}(F_0) + \mathrm{Im}(F_1)^2 + 5\;\mathrm{Re}(F_1)^2\right]\gamma_R^2$$
$$+\,\mathrm{Re}(F_1)\left[\mathrm{Re}(F_1)^2 + 4F_2\,\mathrm{Re}(F_0) + \mathrm{Im}(F_1)^2\right]\gamma_R - F_2\,\mathrm{Im}(F_0)^2$$
$$+\,\mathrm{Re}(F_1)^2\,\mathrm{Re}(F_0) + \mathrm{Re}(F_1)\,\mathrm{Im}(F_1)\,\mathrm{Im}(F_0) = 0. \tag{58}$$

Since $\gamma_R = 0$ at the marginal wavenumber, α_0, equation (58) becomes

$$-F_2\,\mathrm{Im}(F_0)^2 + \mathrm{Re}(F_1)\,\mathrm{Im}(F_1)\,\mathrm{Im}(F_0) + \mathrm{Re}(F_1)^2\,\mathrm{Re}(F_0) = 0, \tag{59}$$

the marginal wavenumber equation. This equation (59) is a polynomial in Ma and B

$$k_{20}\mathrm{Ma}^2 + k_{11}\mathrm{MaB} + k_{31}\mathrm{Ma}^3\mathrm{B} + k_{22}\mathrm{Ma}^2\mathrm{B}^2 + k_{13}\mathrm{MaB}^3 = 0 \tag{60}$$

where $\mathrm{B} = \mathrm{Bo} + \alpha^2$ and the coefficients k_{ij} are given in appendix A 1. The wavenumber $\alpha_{\max}$ corresponding to the maximum growth rate $\gamma_{R\max}$ is obtained by simultaneously solving (58) and the equation obtained by differentiating (58) with respect to α, taking into account that $d\gamma_R/d\alpha = 0$ at the maximum. The latter equation is written as

$$\gamma_R^4\frac{d}{d\alpha}C_4(\alpha) + \gamma_R^3\frac{d}{d\alpha}C_3(\alpha) + \gamma_R^2\frac{d}{d\alpha}C_2(\alpha) + \gamma_R\frac{d}{d\alpha}C_1(\alpha) + \frac{d}{d\alpha}C_0(\alpha) = 0 \tag{61}$$

where C_j denotes the coefficient of the γ_R^j term that appears in equation (58). (For example, $C_4 = 4F_2^3$.)

C. The longwave approximation

As mentioned earlier, from the longwave approximation by FH (Bo = 0), six sectors in the (n, m)-plane were identified that characterize the stability of the flow. Based on the longwave results given later in this section the same six sectors are found: the Q-sectors Q_1 $(1 < n^2 < m)$ and Q_2 $(m < n^2 < 1)$; the R-sectors R_1 $(1 < m < n^2)$ and R_2 $(n^2 < m < 1)$; the S-sectors S_1 $(1 < n < \infty$ and $0 < m < 1)$ and S_2 $(0 < n < 1$ and $1 < m < \infty)$. Figure 6 shows the six sectors and their borders. Stability properties of the robust and surfactant branches can change significantly as one moves from sector to sector. Note that for Bo = 0 there is symmetry about the point $n = 1$ and $m = 1$.

1. *General growth rate expressions in the R, S, and Q sectors*

The general growth rate expressions in the R, S, and Q sectors are given in this section but additional results in each sector will be discussed in later sections. First the coefficients F_2, F_1, and F_0 (50)-(55) in the dispersion equation (48) are expanded in a Taylor series about $\alpha = 0$. The leading order terms are given in Appendix A 2. For $m \neq 1$, $|F_1^2| \gg |F_2 F_0|$ since $|F_1^2| \approx \mathrm{Re}\,(F_1^2) \sim \alpha^2$ and $|F_2 F_0| \approx \mathrm{Im}(F_2 F_0) \sim \alpha^3$ (see Appendix A 2). Therefore, the two increments (49), to the two leading terms, are

$$\gamma \approx \frac{1}{2F_2}\left(-F_1 \pm F_1\left[1 + \frac{1}{2}\left(-\frac{4F_2F_0}{F_1^2}\right)\right]\right), \tag{62}$$

or,

$$\gamma \approx -\frac{F_1}{F_2} + \frac{F_0}{F_1}, \tag{63}$$

and

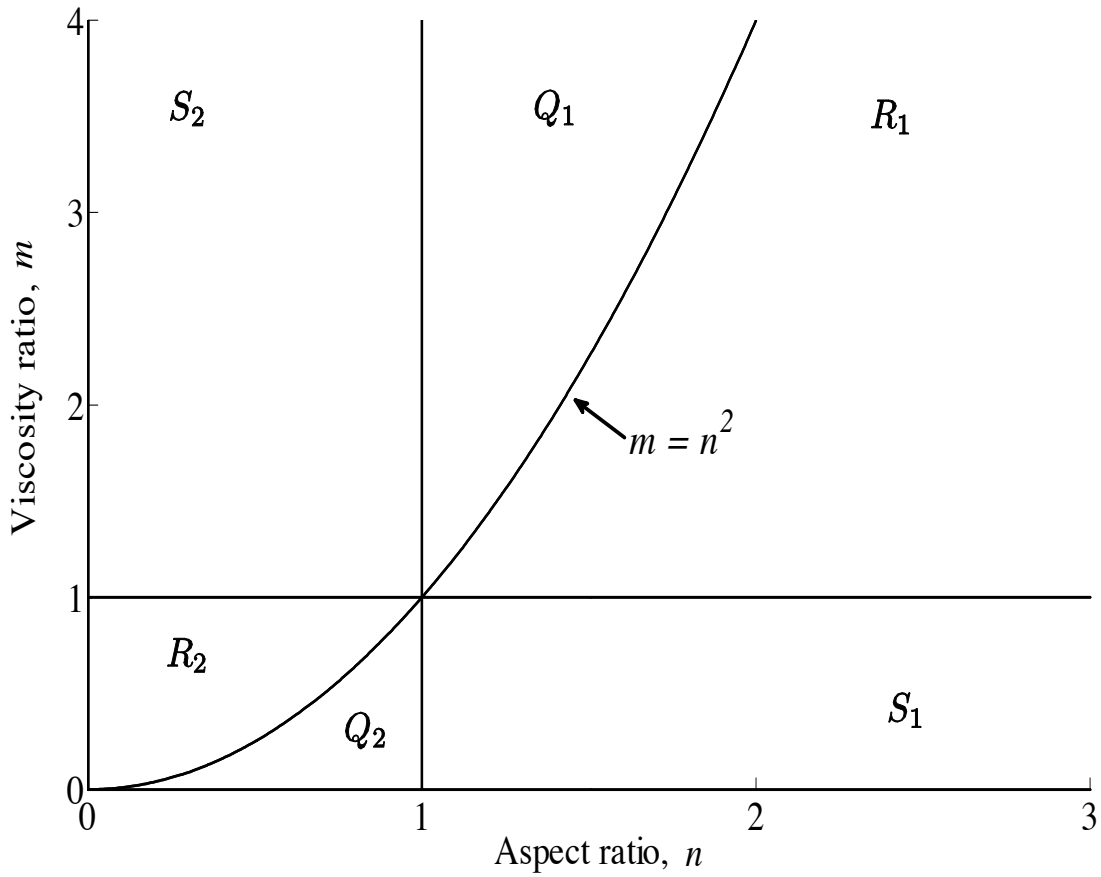

FIG. 6: The (n, m) plane consists of six sectors as regards to different stability properties.

$$\gamma \approx -\frac{F_0}{F_1} - \frac{F_2 F_0^2}{F_1^3}. \tag{64}$$

The growth rates for the robust (63) and surfactant (64) branches are approximately given by

$$\gamma_R \approx \left(\frac{\varphi\,(m - n^2)}{4\,(1-m)\,\psi} \mathrm{Ma} - \frac{n^3(n+m)}{3\psi} \mathrm{Bo} \right) \alpha^2, \tag{65}$$

and

$$\gamma_R \approx \frac{(n-1)\mathrm{Ma}}{4(1-m)} \alpha^2, \tag{66}$$

where

$$\varphi = 3\,mn + m + n^3 + 3\,n^2, \tag{67}$$

and

$$\psi = m^2 + n^4 + 6\,mn^2 + 4\,mn^3 + 4\,mn. \tag{68}$$

Also, note that the growth-rate superposition principle, $\gamma_R\,(\mathrm{Ma},\,\mathrm{Bo}) = \gamma_R\,(\mathrm{Ma},\,0) + \gamma_R\,(0,\,\mathrm{Bo})$, holds for the robust branch in the longwave limit given by equation (65). In contrast, the growth rate superposition principle does not hold for the S branch.

In the longwave limit the marginal wavenumber equation (59) is approximated by substituting the longwave coefficients (A15)-(A19) into (59) and keeping only the two leading terms in α:

$$\begin{aligned}
&\left\{\frac{1}{108}s^2(n-1)(n+1)^2(m-n^2)\varphi\mathrm{Ma}\right.\\
&\left.+\frac{1}{81}n^3s^2(n-1)(n+1)^2(m-1)(n+m)\mathrm{Bo}\right\}\\
&+\left\{\frac{1}{134}n^2(m+n^3)^2\mathrm{Ma}^2\mathrm{Bo}+\frac{1}{486}n^4(n+m)(m+n^3)\mathrm{MaBo}^2\right.\\
&\left.+\frac{1}{2916}n^6(n+m)^2\mathrm{Bo}^3+\frac{1}{81}s^2n^3(n-1)(n+1)^2(m-1)(n+m)\right\}\alpha^2 = 0.
\end{aligned} \tag{69}$$

The behavior of the growth rate as a function of the various system parameters is described in the upcoming longwave sections. The borders are discussed separately due to certain discontinuities that could occur. For example, equation (66) for $m = 1$.

2. Instability in the R-sectors

In the R-sectors, defined as R_1 $(1 < m < n^2)$ and R_2 $(n^2 < m < 1)$, the surfactant branch (66) is always stable and the robust branch (65) is unstable for a range of $\mathrm{Bo} > 0$. If $\mathrm{Bo} > \mathrm{Bo}_c$, where

$$\mathrm{Bo}_c = \frac{3\varphi(m - n^2)}{4n^3(1-m)(n+m)}\mathrm{Ma}, \tag{70}$$

gravity is strong enough to overwhelm the destabilizing Marangoni effect and thus the robust branch is also stable. The asymptotic expression (65) is only valid for $\alpha \ll 1$. For $n = m = 2$ and $s = \mathrm{Ma} = \mathrm{Bo} = 1$ the error is than 1% when $\alpha < 0.044$.

The window of unstable wavenumbers diminishes as $\mathrm{Bo} \uparrow \mathrm{Bo}_c$. To obtain the approximation for α_0 it is convenient to express the Bond number as

$$\mathrm{Bo} = \mathrm{Bo}_c - \ \Delta. \tag{71}$$

Equation (71) is substituted into (69) and when retaining the leading order terms in Δ and α^2 becomes

$$\begin{aligned} -\frac{1}{81}n^7 s^2(n-1)(n+1)^2(m-1)(n+m)\Delta + \Bigg\{ \frac{1}{2916}n^{10}(n+m)^2\mathrm{Bo}_c^3 \\ +\frac{1}{486}n^8(m+n^3)(n+m)\mathrm{Bo}_c^2\mathrm{Ma} + \frac{1}{324}n^6(m+n^3)^2\mathrm{Bo}_c\mathrm{Ma}^2 \\ +\frac{1}{81}n^7 s^2(n-1)(n+1)^2(m-1)(n+m)\Bigg\}\alpha^2 = 0. \end{aligned} \tag{72}$$

An asymptotic expression for the marginal wavenumber is obtained by solving equation (72)

$$\alpha_0 \approx \left[1 + \frac{1}{36}\frac{n^3(n+m)\,|n-1|\,\psi^2}{\left[\varphi s(m-n^2)(n+1)\right]^2|m-1|}\mathrm{Bo}_c^3\right]^{-1/2}\Delta^{1/2}. \tag{73}$$

Note here that Ma has been written in terms of Bo_c using equation (70). If $\mathrm{Bo}_c \ll 1$ (i.e., $\mathrm{Ma} \ll 1$) equation (73) simplifies to

$$\alpha_0 \approx \Delta^{1/2}. \tag{74}$$

For example, the relative error of the asymptotic expression (74) for $n = m = 2$, $s = 1$, Bo $= 10^{-6}$, and $\mathrm{Ma} = 10^{-6}$ to $\mathrm{Ma} = 10$ is less than 10% for $\Delta < 0.2$.

The critical Bond number given by (70) is represented as a surface above the (n, m)-plane. Figures 7 (a) and (b) represent the surface of Bo_c for the R_1 and R_2 sectors, respectively. These figures, where $\mathrm{Ma} = 0.1$ and $s = 1.0$, show how n and m affect the critical Bond number. It is clear figures 7 (a) and (b) as well as from equation (70) that in both the R_1 and R_2 sectors $\mathrm{Bo}_c \uparrow \infty$ as $m \to 1$ and $\mathrm{Bo}_c \downarrow 0$ as $m \to n^2$.

3. Instability in the S-sectors

In sectors S_1 ($1 < n < \infty$ and $0 < m < 1$) and S_2 ($0 < n < 1$ and $1 < m < \infty$), the robust branch is always stable (63) but the surfactant branch is unstable (64) for $\mathrm{Bo} > 0$. The asymptotic expression (66) is only valid for $\alpha \ll 1$, for example, the relative error is less than 1% for $n = 2$, $m = .5$, $\mathrm{Ma} = .1$, and $s = \mathrm{Bo} = 1$ when $\alpha < 0.092$.

As mentioned earlier in section II B, the surfactant branch is never completely stabilized

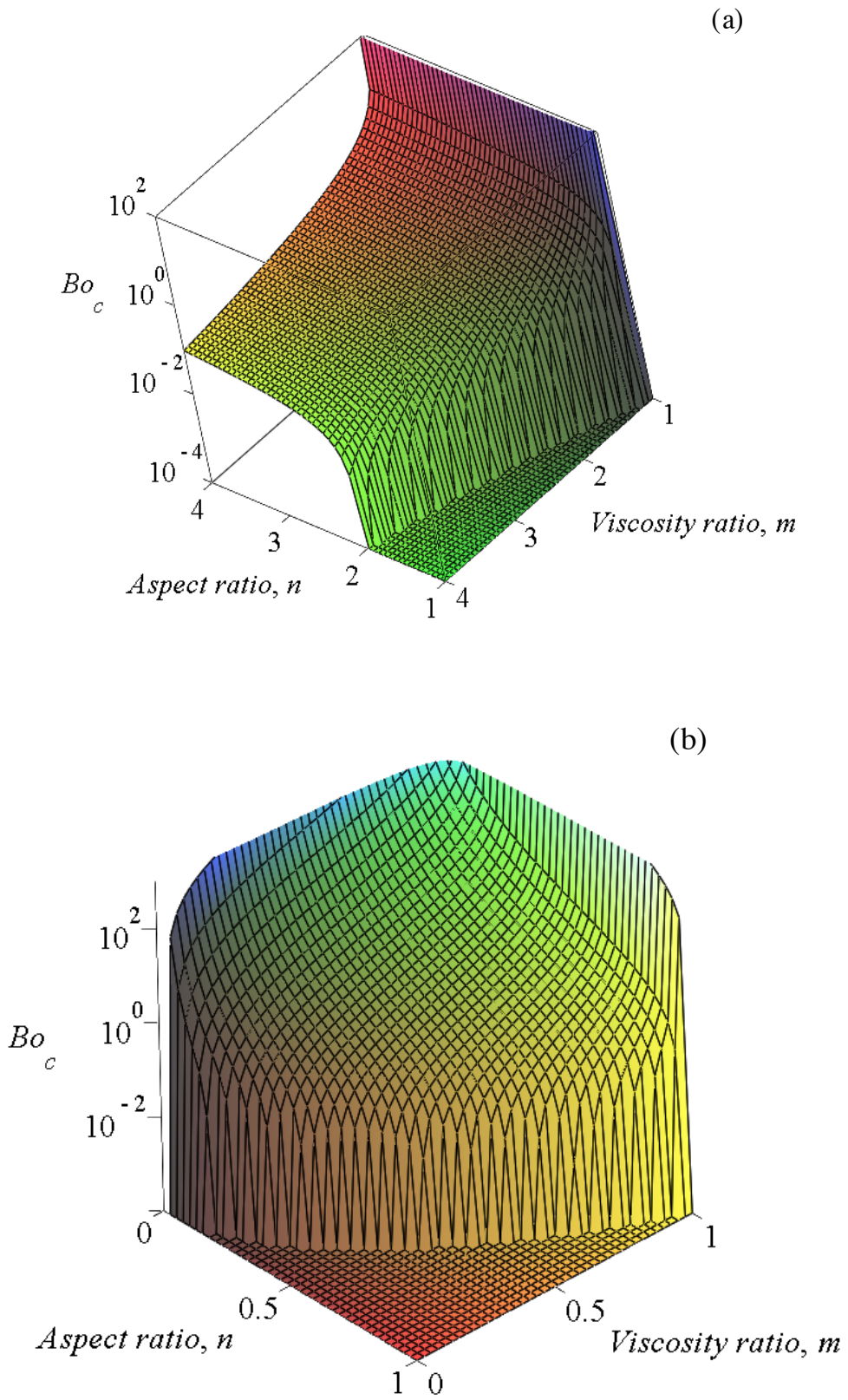

FIG. 7: The critical Bond number Bo_c as a function of the aspect ratio and viscosity ratio (a) in the R_1 sector, and (b) in the R_2 sector. Here $\mathrm{Ma} = 0.1$ and $s = 1$

by gravity in the S sectors. In the limit Bo $\uparrow \infty$, equation (69) reduces to

$$s^2(n-1)(n+1)^2(m-1) + 36n^3(n+m)\alpha^2\mathrm{Bo}^2 = 0, \tag{75}$$

Thus an asymptotic formula for α_0 is obtained by solving (75) for α

$$\alpha_0 \approx \left[\frac{36s^2(n+1)^2(1-m)(n-1)}{n^3(n+m)}\right]^{1/2} \mathrm{Bo}^{-1}. \tag{76}$$

The relative error of (76) for $n = 2$, $m = 0.5$, Ma $= 0.1$ and $s = 1$ is less than 1% when Bo > 9.9. In contrast to the R sectors, the marginal wavenumber expression (76) is independent of (small) Marangoni number and no amount of gravity will completely stabilize the flow.

If the Bond number is sufficiently negative then both the robust branch and surfactant branch are positive and cross under certain conditions. However, there are no crossings as $\alpha \downarrow 0$, and so this discussion is reserved for section II D where additional results for arbitrary wavenumber and Bond number are given.

It has been shown that for positive values of the Bond number a longwave instability can occur in the R and S sectors, but this is not possible in the Q sectors. Next, it is shown that in the Q sectors the flow is stable for Bo > 0 and becomes unstable for Bo < 0.

4. Instability in the Q-sectors

For the Q-sectors Q_1 $(1 < n^2 < m)$ and Q_2 $(m < n^2 < 1)$ the surfactant branch (64) is always stable while the stability of the robust branch (63) depends on the interaction between the stabilizing Ma terms and the destabilizing Bo term (when Bo < 0). When Bo < 0 the robust branch is stabilized if Ma exceeds a critical Marangoni number, Ma_{cL}. By

setting $\gamma_R = 0$ in (65) Ma_{cL} is given by

$$\mathrm{Ma}_{cL} = \frac{4n^3(1-m)(n+m)}{3\varphi\,(m-n^2)}\mathrm{Bo}. \tag{77}$$

When Ma is close to Ma_{cL} the marginal wavenumber is expressed in terms of $\Delta = \mathrm{Ma}_{cL} - \mathrm{Ma} > 0$

$$\alpha_0 \approx \left[1 - \frac{3}{256}\frac{\varphi\psi^2\,|n-1|\,|m-n^2|}{\left[n^3 s(n+m)(n+1)(m-1)^2\right]^2}\mathrm{Ma}_{cL}^3\right]^{-1/2}\Delta^{1/2}. \tag{78}$$

Figure 8 shows some comparisons between the full α_0 solution given by (59) and the approximate formula given by (78) for $n = 2$, $m = 5$, $s = 1$. In this figure α_0 is plotted as a function of Bo for $\mathrm{Bo} < \mathrm{Bo}_c$ where Bo_c is determined from (77) by setting $\mathrm{Ma} = \mathrm{Ma}_{cL}$. There is good agreement between the approximation (78) and the exact numerically computed α_0.

From equation (77) a threshold stabilization factor $\mathrm{Ma}_{cL}/(-\mathrm{Bo})$ in terms of (n, m) is obtained. The surface of this factor is shown in figure 9. Below the surface the flow is longwave unstable and above it the flow is stable. Note that $\mathrm{Ma}_{cL}/(-\mathrm{Bo}) \to \infty$ as $m \to n^2$ and $\mathrm{Ma}_{cL}/(-\mathrm{Bo}) \to 0$ as $m \to 1$.

5. *Instabilities on the (n, m)-sector borders*

The borders $m = 1$, $m = n^2$, and $n = 1$ are considered separately because of singularities that can occur in the expressions for the growth rates and the marginal wavenumber derived in the previous sections for the R, S, and Q sectors.

First the $m = 1$ and $n \neq 1$ case is considered. In the longwave limit, $F_1^2 \ll |F_2 F_0|$ since $F_1^2 \sim \alpha^4$ (A30) and $|F_2 F_0| \sim \mathrm{Ma}\alpha^3$ (A33) and (A32). Therefore, the roots to the dispersion

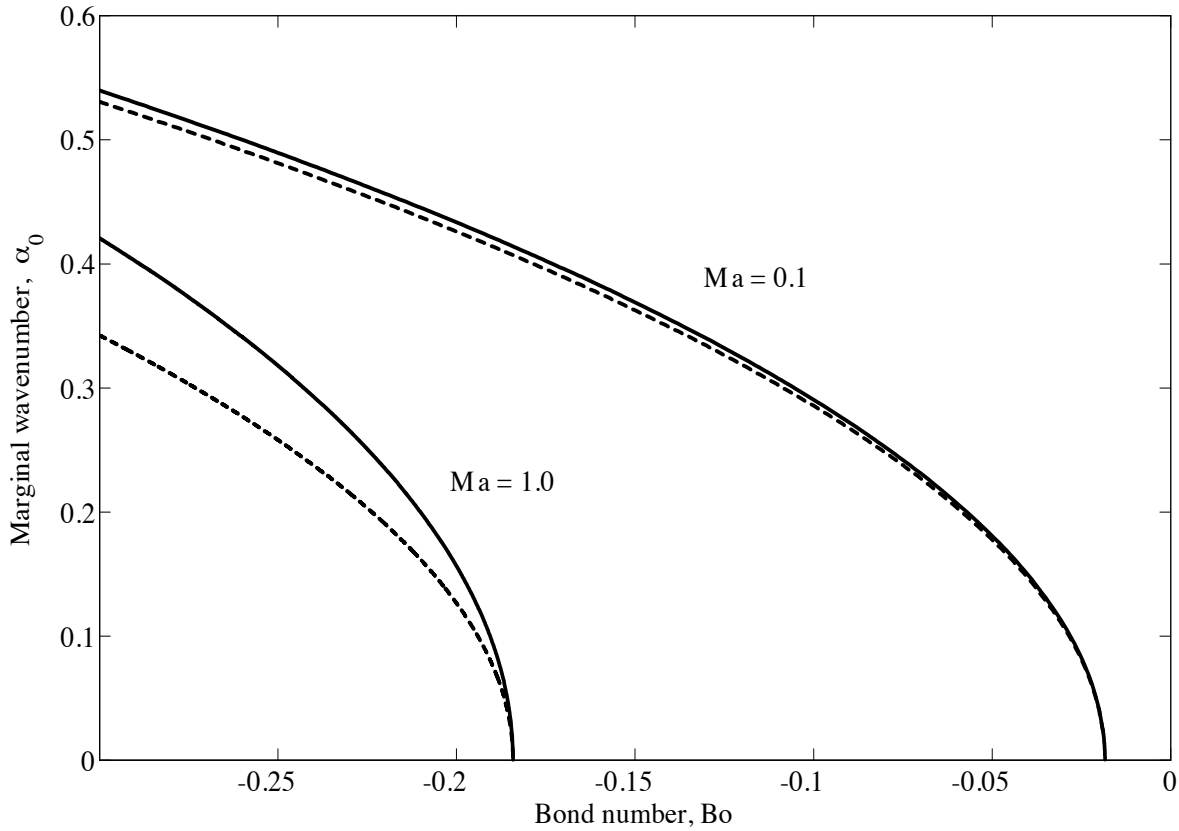

FIG. 8: α_0 vs Bo for $n = 2$, $m = 5$ (Q_1 sector), $s = 1$ and for the two values of Ma indicated in the figure. The solid lines represent the full solutions, equation (59), and the dashed lines represent the asymptotics given by (78). The intersections with the horizontal axis correspond to the critical values $\mathrm{Bo}_c \approx -0.0184$ for $\mathrm{Ma} = 1.0$ and $\mathrm{Bo}_c \approx -0.184$ for $\mathrm{Ma} = 1$.

equation (49), are approximated by

$$\gamma \approx \frac{1}{2F_2}\left(-F_1 + (4F_2F_0)^{1/2}\left[1 + \frac{1}{2}\left(-\frac{F_1^2}{4F_2F_0}\right)\right]\right). \tag{79}$$

Hence, the growth rates of the two branches are

$$\gamma_R = \frac{-\operatorname{Re}(F_1) + \operatorname{Re}(\sqrt{\zeta})}{2F_2} \tag{80}$$

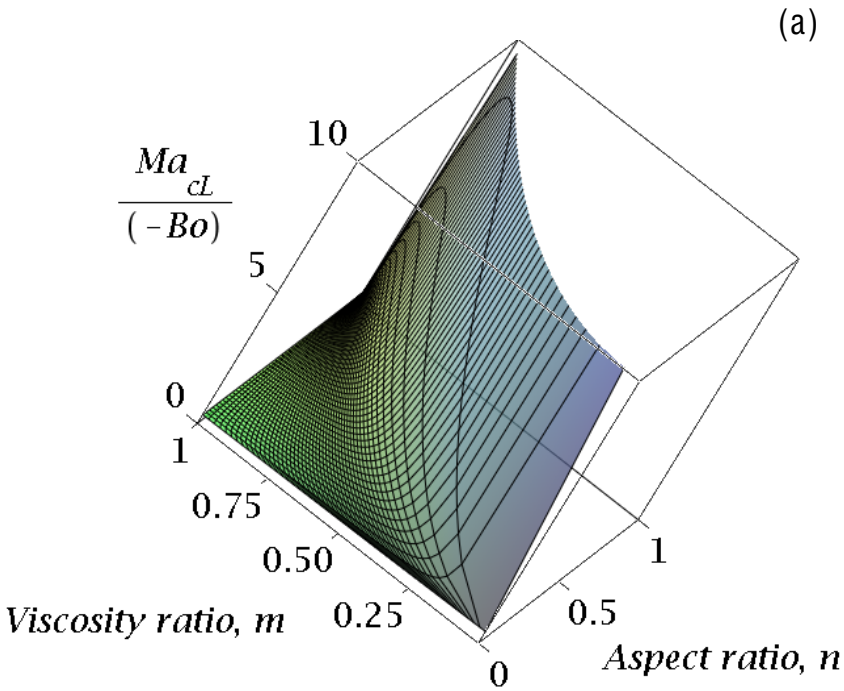

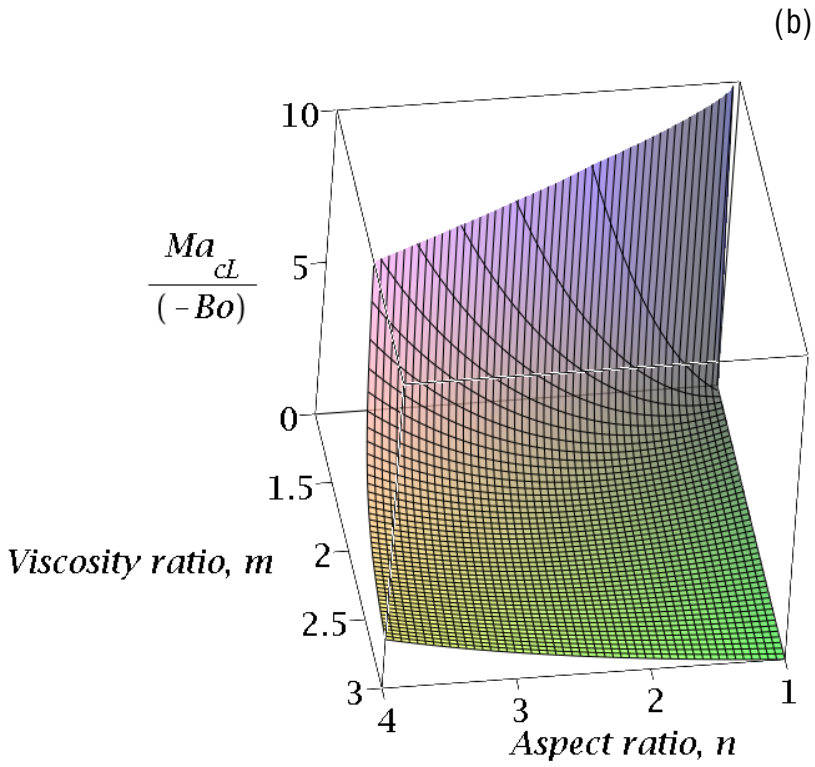

FIG. 9: The dependence of the stabilization factor Ma/(-Bo) on the aspect ratio n and viscosity ratio m (a) in the Q_2 sector, and (b) in the Q_1 sector. Here $s = 1$

where ζ is the discriminant of (49)

$$\zeta = F_1^2 - 4F_0F_2. \tag{81}$$

To leading order in α, equation (80) reduces to

$$\gamma_R \approx \frac{\mathrm{Re}(\sqrt{\zeta})}{2F_2} = \pm\frac{n\left[|n-1|\,(n+1)s\mathrm{Ma}\right]^{1/2}}{2(n+1)^2}\alpha^{3/2}. \tag{82}$$

This result does not depend on the Bond number and is the same as FH and HF. Note also that expression (82) is valid as $\alpha \downarrow 0$ with the Marangoni number fixed but it is not good as $\mathrm{Ma} \downarrow 0$ with the wavenumber fixed. It is unclear from equation (82) whether the unstable growth rate corresponds to the surfactant branch or the robust branch. Recall, as $\mathrm{Ma} \downarrow 0$ the identity of each branch is clear since the surfactant branch vanishes. Starting from there each branch is tracked to the asymptotic region of small α where equation (82) is valid and thus the branches will be identified there.

The two branches of $\gamma(\alpha,\mathrm{Ma})$ given by (49) are continuous functions corresponding to the two continuous branches of the function $\sqrt{\zeta}$. The two distinct analytic branches of the function $\sqrt{\zeta}$ exist in any simply connected domain in the complex plane that does not contain the origin. The complex growth rate, γ, is expressed as a composite function of (α,Ma) through ζ. The discriminant ζ is a single-valued (in general, complex) continuous function of (α,Ma) which therefore maps the first quadrant of the (α,Ma) plane into some simply-connected domain D in the complex ζ-plane. When $m = 1$, $n \neq 1$, and $s \neq 0$

$$\mathrm{Im}(\zeta) = -4F_2\,\mathrm{Im}(F_0) > 0 \quad (\text{or} < 0) \tag{83}$$

depending on whether $n > 1$ (or < 1) (see equation (55)). Because $\mathrm{Im}(F_1) = 0$, D lies entirely in the upper-half (or lower-half) plane when $n > 1$ (or < 1). Therefore, by continuity of the increment branches, it is concluded that the surfactant branch will always be obtained by taking the value of $\zeta^{1/2}$ with positive real part for arbitrary Ma provided the real part of the square root is always positive for one branch and is always negative for the other branch.

The two values of the square root of the discriminant are $f(\zeta) = \sqrt{\zeta}$ where $\zeta = re^{i(\theta+2\pi k)}$ with $k = 0, 1$. First the $n > 1$ case is considered with domain $\tilde{D} = \{\zeta \mid r > 0,\ 0 < \theta < \pi\}$, which clearly contains D. The function $w = \sqrt{\zeta}$ has two branches with different ranges because $\tilde{D}$ is a simply connected domain that does not contain the origin. When $k = 0$, the range of $\sqrt{\zeta}$ is $R_I = \left\{w = \rho e^{i\phi} \mid \rho > 0,\ 0 < \phi < \pi/2\right\}$ so that the real part of $\sqrt{\zeta}$ is always positive, and when $k = 1$, the range of $\zeta^{1/2}$ is $R_{II} = \left\{w = \rho e^{i\phi} \mid \rho > 0,\ \pi < \phi < 3\pi/2\right\}$ so that the real part of $\sqrt{\zeta}$ is always negative. The $n < 1$ case one has domain $\tilde{D} = \{\zeta \mid r > 0,\ = -\pi < \theta < 0\}$ where the ranges of $\sqrt{\zeta}$ are $R_I = \left\{w = \rho e^{i\phi} \mid \rho > 0,\ -\pi/2 < \phi < 0\right\}$ so that $\mathrm{Re}(\sqrt{\zeta}) > 0$ as before, and $R_{II} = \left\{w = \rho e^{i\phi} \mid \rho > 0,\ \pi/2 < \phi < \pi\right\}$ so that $\mathrm{Re}(\sqrt{\zeta}) < 0$.

In the limit of Ma $\downarrow 0$, the surfactant branch vanishes so $\gamma_R = 0$ and equation (80) implies $\mathrm{Re}(\sqrt{\zeta}) = \mathrm{Re}(F_1)$. Therefore, $sgn(\mathrm{Re}(\sqrt{\zeta})) = sgn(\mathrm{Re}(F_1))$ where sgn is the sign function. It is sufficient for the purposes of this dissertation to consider small wavenumbers $[0, \alpha_s]$ by choosing α_s such that $\alpha_s \ll 1$ where $\alpha_s \ll |\mathrm{Bo}|$. Then equation (A16) yields $sgn(\mathrm{Re}(F_1)) = sgn(\mathrm{Bo})$. It then follows that $sgn(\mathrm{Re}(\sqrt{\zeta})) = sgn(\mathrm{Bo})$. It was previously established that each branch has the same sign everywhere for all (α,Ma). Therefore, for the surfactant branch $sgn(\mathrm{Re}(\sqrt{\zeta})) = sgn(\mathrm{Bo})$ in the limit of $\alpha \downarrow 0$ as well. From equation (82) the $sgn(\gamma_R) = sgn(\mathrm{Re}(\sqrt{\zeta})$ and then $sgn(\gamma_R) = sgn(\mathrm{Bo})$. So the surfactant branch is

unstable for Bo > 0, $\gamma_R \propto +\alpha^{3/2}$ and stable for Bo < 0, $\gamma_R \propto -\alpha^{3/2}$. Consequently, the robust branch is stable (unstable) for Bo > 0 (Bo < 0).

In certain limits it is possible to find a longwave approximation to γ_R that captures the growth rate behavior in the neighborhood of the marginal wavenumber α_0. For Bo $\gg$ Ma and Ma/Bo$^2 \ll \alpha \ll 1$, equation (49) can be simplified to

$$\gamma_R \approx \frac{27}{4}\frac{(n-1)^2(n+1)^3 s^2 \mathrm{Ma}^2}{n^5 \mathrm{Bo}^3} - \frac{1}{4}\frac{n\mathrm{Ma}}{(n+1)}\alpha^2 \tag{84}$$

which is good for $\alpha \approx \alpha_0$. In Figure 10 the growth rate of the surfactant branch is plotted using (49) along with the asymptotic expression (84), which is valid for α near α_0. One can see the dashed line approximations approaches the full dispersion curve as $\alpha \uparrow \alpha_0$. The longwave γ_R approximation (82) is not plotted in figure 10 but for the same parameter values the error is less than 1% when $\alpha < 1.4 \times 10^{-9}$. An asymptotic expression for α_0 is obtained by solving $\gamma_R = 0$ for α from equation (84):

$$\alpha_0 \approx \frac{3s\,|n-1|\,(n+1)^2[3\mathrm{Ma}]^{1/2}}{n^3 \mathrm{Bo}^{3/2}}. \tag{85}$$

The above expression is also obtained from the longwave marginal wavenumber equation (69). This expression also suggests that gravity is not completely stabilizing since $\alpha_0 > 0$ at any positive finite value of Bo.

In figure 11, the impact of the viscosity ratio for values of m close to unity on the growth rate is shown for $n = 2$, $s = 1$, $M = 1$, Bo $= 1$. For $m \neq 1$, $\gamma_R \propto \alpha^2$ in the R (65) and S (66) sectors but for $m = 1$, $\gamma_R \propto \alpha^{3/2}$ (82) which was also found in FH and HF for Bo $= 0$. This can also be seen by noting the slope of the $m = 1$ curve shown in figure 11 is

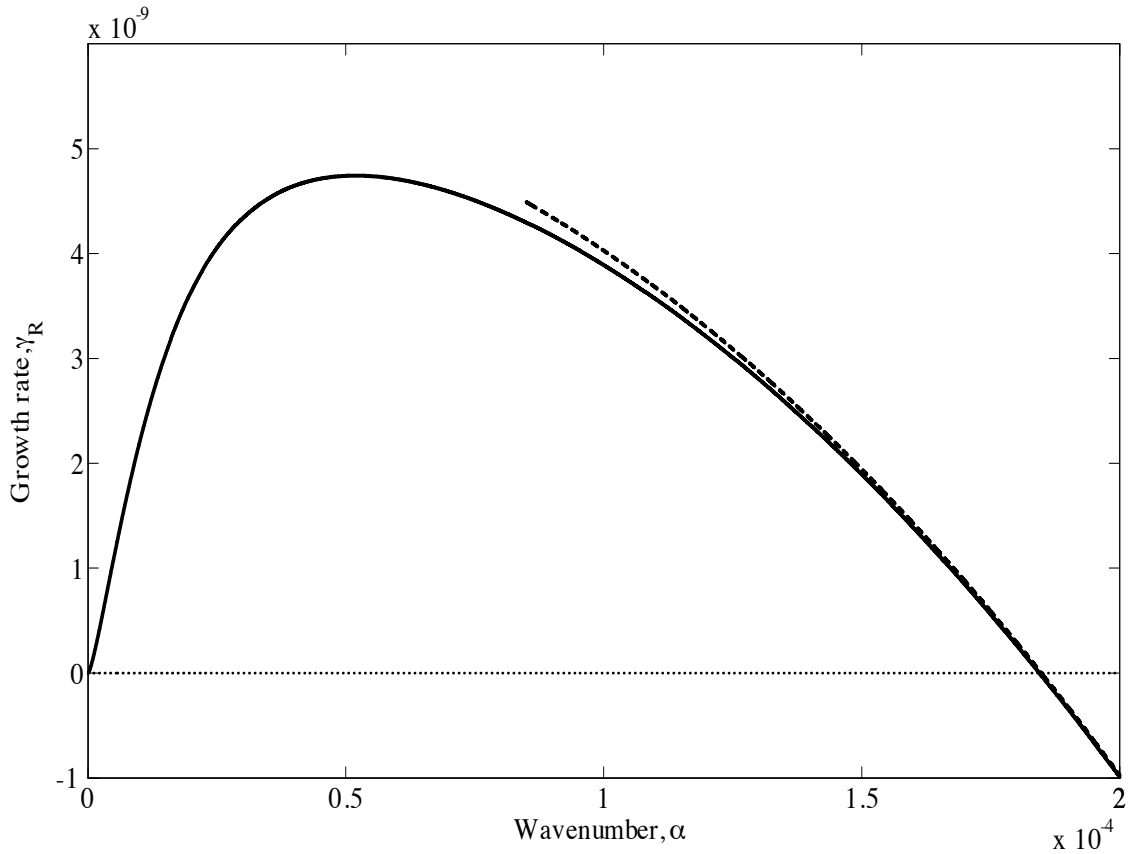

FIG. 10: The exact dispersion curve (49) (solid line) and the asymptotic expression of the growth rate around the marginal wavenumber (84) (dashed line) of γ_R for $m = 1$, $n = 2$, $s = 1$, $\mathrm{Ma} = 1$, and $\mathrm{Bo} = 1000$.

approximately $-1/2$.

Next, the border $n = 1$ with $m \neq 1$ is considered. Just like the $m = 1$ and $n \neq 1$ case, the imaginary part of the discriminant ζ, $\mathrm{Im}(\zeta) = 2\,\mathrm{Re}(F_1)\,\mathrm{Im}(F_1)$, is positive (or negative) for $m < 1$ (or $m > 1$) (50)-(55). The growth rate for the robust and surfactant branches are

$$\gamma_R \approx -\frac{(1+m)}{m^2 + 14\,m + 1}\left\{\mathrm{Ma} + \frac{1}{3}\mathrm{Bo}\right\}\alpha^2, \tag{86}$$

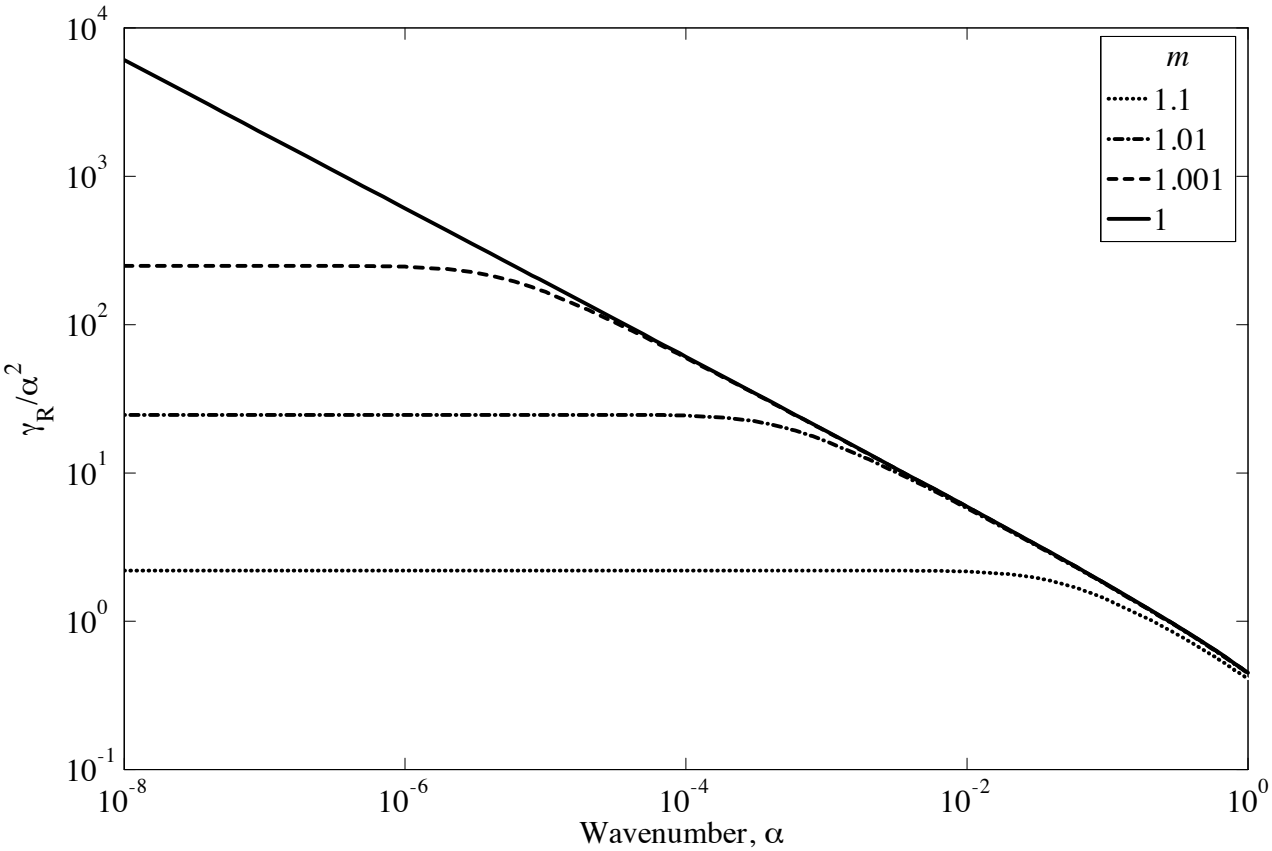

FIG. 11: Curves of γ_R/α^2 vs α for $n = 2$, $s = 1$, $M = 1$, Bo $= 1$, and different values of viscosity close to 1. The results are similar to equal viscosity case given in HF where gravity was neglected.

and

$$\gamma_R \approx -\frac{1}{192}\frac{(1+m)}{s^2\,(m-1)^2}\left\{\ \mathrm{Ma}+\frac{1}{3}\,\mathrm{Bo}\right\}\mathrm{Bo}\,\mathrm{Ma}\alpha^4\ -\frac{1}{192}\frac{(1+m)}{s^2\,(m-1)^2}\mathrm{Ma}^2\alpha^6. \qquad (87)$$

For this case both the robust and surfactant branches are longwave stable for Bo > 0. For Bo < 0 both branches are unstable if the magnitude of Bo is sufficiently large. This occurs when both leading term coefficients in (86) and (87) are positive, that is when Bo < -3Ma.

For the $m = n^2 \neq 1$ border, the growth rates for the robust and surfactant branches are

$$\gamma_R \approx -\left\{\frac{n\mathrm{Bo}}{12(n+1)}\right\}\alpha^2+\left\{\frac{n\,(2\mathrm{Ma}+n\mathrm{Bo}-5)}{60(n+1)}-\frac{n^2\mathrm{Ma}^2\,(3\mathrm{Ma}\ +n\mathrm{Bo})}{48s^2(n-1)^2(n+1)^3}\right\}\alpha^4, \qquad (88)$$

and

$$\gamma_R \approx -\left\{\frac{\mathrm{Ma}}{4(n+1)}\right\}\alpha^2, \tag{89}$$

Therefore the surfactant branch is always stable, and this is consistent with HF in the limit $\mathrm{Bo} \to 0$.

For the $m = 1$ and $n = 1$ case, the solutions to the dispersion equation (49) for arbitrary wavenumber are of the form

$$\gamma_R = \frac{-a\mathrm{Ma} - b(\mathrm{Bo} + \alpha^2) \pm [a\mathrm{Ma} - b(\mathrm{Bo} + \alpha^2)]}{2F_2\alpha^4}, \tag{90}$$

where

$$a = \alpha^2(s_\alpha^2 - \alpha^2)(c_\alpha s_\alpha + \alpha) \text{ and } b = (s_\alpha^2 - \alpha^2)(c_\alpha s_\alpha - \alpha)\,.$$

After substituting F_2, a, and b into (90), the growth rate for the robust branch is

$$\gamma_R = -\frac{(s_\alpha^2 - \alpha^2)(\mathrm{Bo} + \alpha^2)}{4\alpha(c_\alpha s_\alpha + \alpha)} \approx -\frac{1}{24}\left(\mathrm{Bo} + \alpha^2\right)\alpha^2 \text{ for } \alpha \ll 1,$$

and the growth rate for the surfactant branch is

$$\gamma_R = -\frac{\alpha(s_\alpha^2 - \alpha^2)\mathrm{Ma}}{4(c_\alpha s_\alpha - \alpha)} \approx -\frac{1}{8}\mathrm{Ma}\alpha^2 \text{ for } \alpha \ll 1.$$

Note that the surfactant branch is always stable but the robust branch is unstable if $\alpha^2 < -\mathrm{Bo}$. Obviously, this only occurs if $\mathrm{Bo} < 0$.

D. Arbitrary wavenumbers; mid-wave instability

In this section, results are given for arbitrary wavenumber, and comparisons are made across all sectors. First, the influence of gravity on the maximum growth rate $\gamma_{R\max}$, the corresponding wavenumber $\alpha_{\max}$ and the marginal wavenumber α_0 in the R, S, and Q sectors are considered for fixed values of the Marangoni number. Then similar results are given to show the influence of surfactant for fixed (positive and negative) values of Bond number. Also, many asymptotic results will be discussed.

The influence of Bo on $\gamma_{\max}$, the corresponding wavenumber $\alpha_{\max}$ and α_0 is examined first. Figure 12 shows plots of $\gamma_{\max}$, $\alpha_{\max}$ and α_0 for a representative (n, m) pair from each of the 6 sectors where panels (a, d, g), (b, e, h) and (c, f, i) represent the R, S and Q sectors, respectively. In the R sectors, panels (a, d, g) show that the system is unstable provided Bo does not exceed a finite positive value Bo_c and that $\gamma_{R\max}$, $\alpha_{\max}$, and α_0 all decrease to zero as $\mathrm{Bo} \downarrow \mathrm{Bo}_c$. These findings were also observed in the longwave limit (see section II C 2). Panels (b, e, h) show the surfactant branch is always unstable in the S sectors. The discontinuity in the graph of $\alpha_{\max}$ in panel (e) is discussed below with figure 13. In the Q sectors, gravity is completely stabilizing provided Bo exceeds some finite value Bo_c as shown in panels (c), (f) and (i). Note that $\mathrm{Bo}_c < 0$ according to the longwave analysis of section II C 4, see equation (77).

The discontinuity that can occur in the S sectors is highlighted in figure 13. Panel (a) shows that for negligible Bo one branch is longwave unstable and the other branch is stable. As the magnitude of Bo increases the previously stable branch becomes unstable ($\mathrm{Bo} = -1$) and at some point the branches cross ($\mathrm{Bo} = -1.5,\ -2.1$). Panel (b) shows that as $|\mathrm{Bo}|$ continues to increase the crossing eventually disappears and that one branch develops two

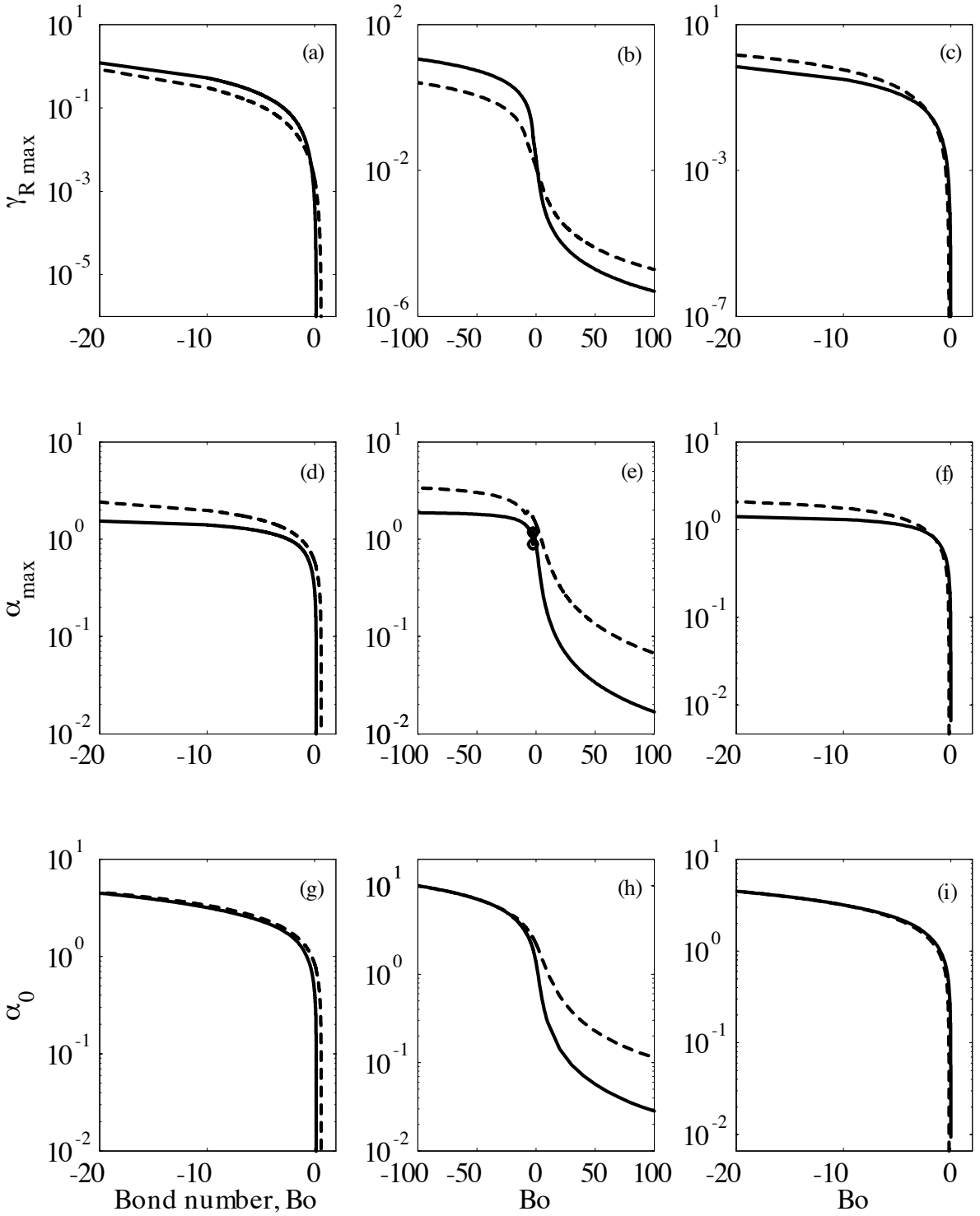

FIG. 12: The influence of the Bond number on the maximum growth rate $\gamma_{R\max}$, the corresponding wavenumber $\alpha_{\max}$, and the marginal wavenumber α_0 in the (a, d, g) R, (b, e, h) S, and (c, f, i) Q sectors. Here $s = 1$, Ma $= 0.1$ and the values of the (n, m) pairs for the R_1, R_2, S_1, S_2, Q_1, and Q_2 are $(2, 2)$, $(.5, .5)$, $(.5, 2)$, $(2, .5)$, $(2, 5)$, and $(.8, .4)$, respectively.

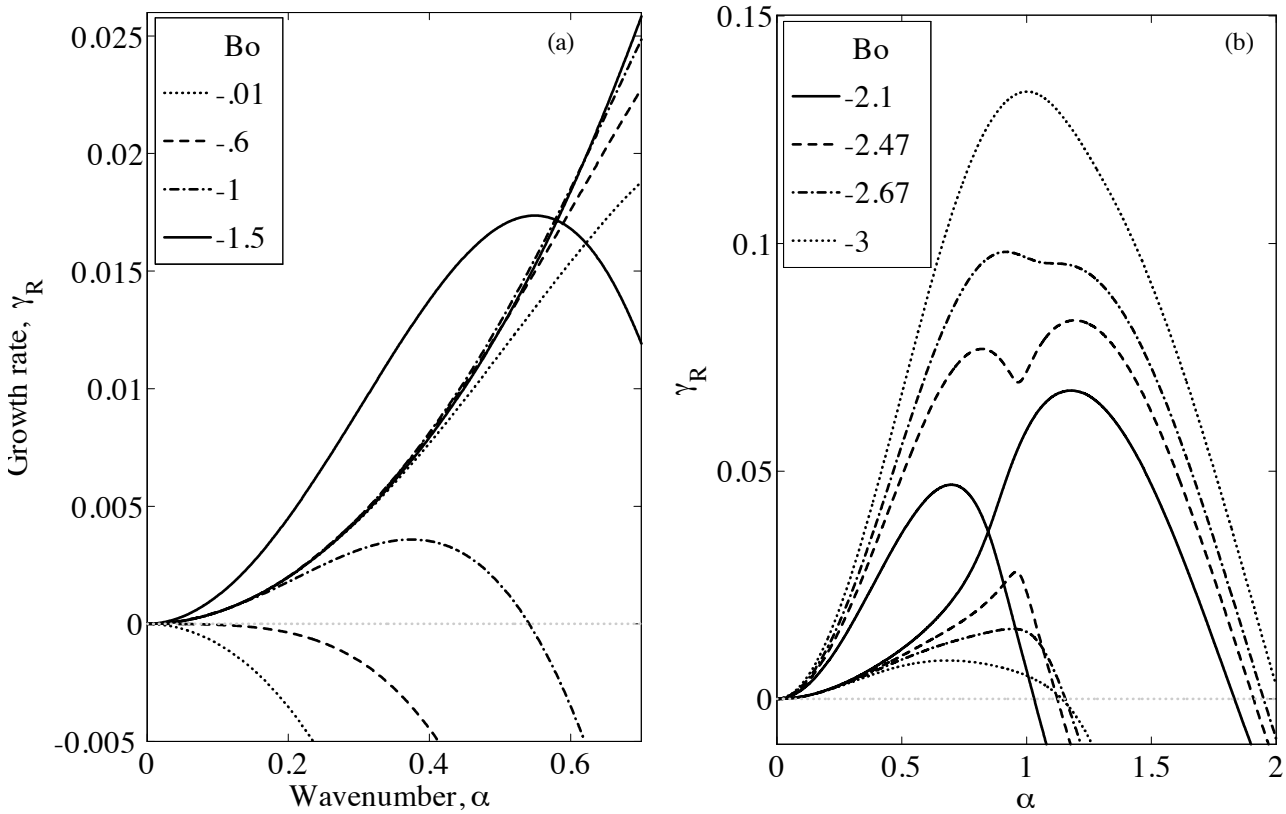

FIG. 13: Dispersion curves given by (49) in the S_1 sector ($n = 2$, $m = 0.5$) for selected values of Bond number showing it is possible to have two local maxima and a jump in the global maximum. Here $s = 1$ and Ma $= 0.1$.

local extrema. The global maximum shifts from the right local extremum (Bo $= -2.47$) to the left local extremum (Bo $= -2.67$). Finally, as Bo $\downarrow -\infty$, both branches are longwave unstable.

Next the influence of the Marangoni number Ma on the maximum growth rate $\gamma_{\max}$, the corresponding wavenumber $\alpha_{\max}$ and the marginal wavenumber α_0 is examined for a fixed value of Bo in the R and S sectors. The Q sectors are considered separately and will be discussed later (see figure 19), but one should note that both branches are stable for Bo > 0 and fixed Ma (see figure 12 panels (c), (f) and (i)).

Figures 14 (a) and (b) show that $\gamma_{R\max}$ attains a maximum at some Ma $= O(1)$ in the R

and S sectors respectively, and that $\gamma_{R\,\max} \downarrow 0$ as $\mathrm{Ma} \uparrow \infty$. The wavenumber corresponding to $\gamma_{R\,\max}$, $\alpha_{\max}$, and the marginal wavenumber α_0 also $\downarrow 0$ as $\mathrm{Ma} \uparrow \infty$. However, in the R sectors there is a critical Ma, Ma_{cL}, below which the flow is stable, while in the S sectors the flow is unstable for all $\mathrm{Ma} > 0$. Recall from the longwave results there is a direct relationship between Bo_c and Ma_{cL} (see equations (70) and (77)). In the S sectors, $\alpha_{\max}$ and α_0 approach some non-zero constant and $\gamma_{R\,\max} \downarrow 0$ showing no critical value of Ma that completely stabilizes the flow.

The small and large Ma asymptotics of α_0 are discussed next. Panels (e) and (f) suggest that $\alpha_0 \downarrow 0$ as $\mathrm{Ma} \uparrow \infty$. By substituting equations (A10) - (A14) into the marginal wavenumber equation (60) and keeping the dominant Ma terms the following expression is obtained,

$$\frac{n^2}{324}(n^3+m)^2\mathrm{BoMa}\alpha^2 + \frac{s^2}{108}\varphi(n-1)(n+1)^2(m-n^2) = 0. \tag{91}$$

Solving equation (91) for α gives,

$$\alpha_0 \approx \frac{s(n+1)\sqrt{3\varphi(n-1)(n^2-m)}}{n(n^3+m)}\mathrm{Bo}^{-1/2}\mathrm{Ma}^{-1/2} \tag{92}$$

which is consistent with the behavior for α_0 at large Ma. As $\mathrm{Ma} \downarrow 0$, it is clear from panel (f) that α_0 approaches some finite non-zero value. Therefore, by keeping only the (dominant) linear Ma terms, equation (60) reduces to

$$k_{11} + k_{13}\mathrm{B}^2 = 0 \tag{93}$$

where k_{11} and k_{13} are given by (A6) and (A9). However, this equation must be solved numerically for α_0 since α_0 is not necessarily small. The asymptotics for α_0 in the R sectors

were discussed above in the longwave section II C 3.

Panels (a), (b), (c) and (d) of figure 14 suggest that $\gamma_{R\,\max}$ and $\alpha_{\max} \downarrow 0$ as $\mathrm{Ma} \uparrow \infty$. In the longwave limit and for $\mathrm{M} \gg 1$, the linear and constant term of equation (58), whose coefficients are proportional to Ma^2 and Ma^3, are dominant, giving rise to the following simplified equation for γ_R:

$$\frac{1}{27}n^3(m+n^3)(n^2-m)\alpha^6\mathrm{Ma}\gamma_R - \frac{1}{108}(n-1)n^4(n^2-m)s^2\varphi\alpha^6\mathrm{Ma}^2 \approx 0 \tag{94}$$

The latter gives

$$\gamma_{R\,\max} \approx \frac{ns^2(n-1)(n+1)^2(m-n^2)\varphi}{4(n^3+m)^3}\mathrm{Ma}^{-1}. \tag{95}$$

Because α^6 appears in the simplified equation above, it is convenient when solving for $\alpha_{\max}$ to subtract α times equation (61) from 6 times equation (58) and obtain

$$\frac{8}{27}(m-1)^2n^5(n+1)^2(n^3+m)s^2\alpha^4\mathrm{Ma}\gamma_R - \frac{1}{162}n^6(n^3+m)^2\alpha^8\mathrm{BoMa}^3 \approx 0 \tag{96}$$

Solving for α yields

$$\alpha^4 \sim 48\frac{(m-1)^2(n+1)^2}{n(n^3+m)}s^2\mathrm{Ma}^{-3}\mathrm{Bo}^{-1}\gamma_R. \tag{97}$$

Equation (95) is substituted into (97), and the following asymptotic expression for $\alpha_{\max}$ is obtained:

$$\alpha_{\max} \approx \frac{[12\varphi(1-n)(m-n^2)]^{1/4}(m-1)^{1/2}s}{(n^3+m)}\mathrm{Ma}^{-3/4}\mathrm{Bo}^{-1/4}. \tag{98}$$

Panels (b) and (d) show that $\gamma_{R\,\max} \downarrow 0$ and $\alpha_{\max}$ approaches some non-zero constant as

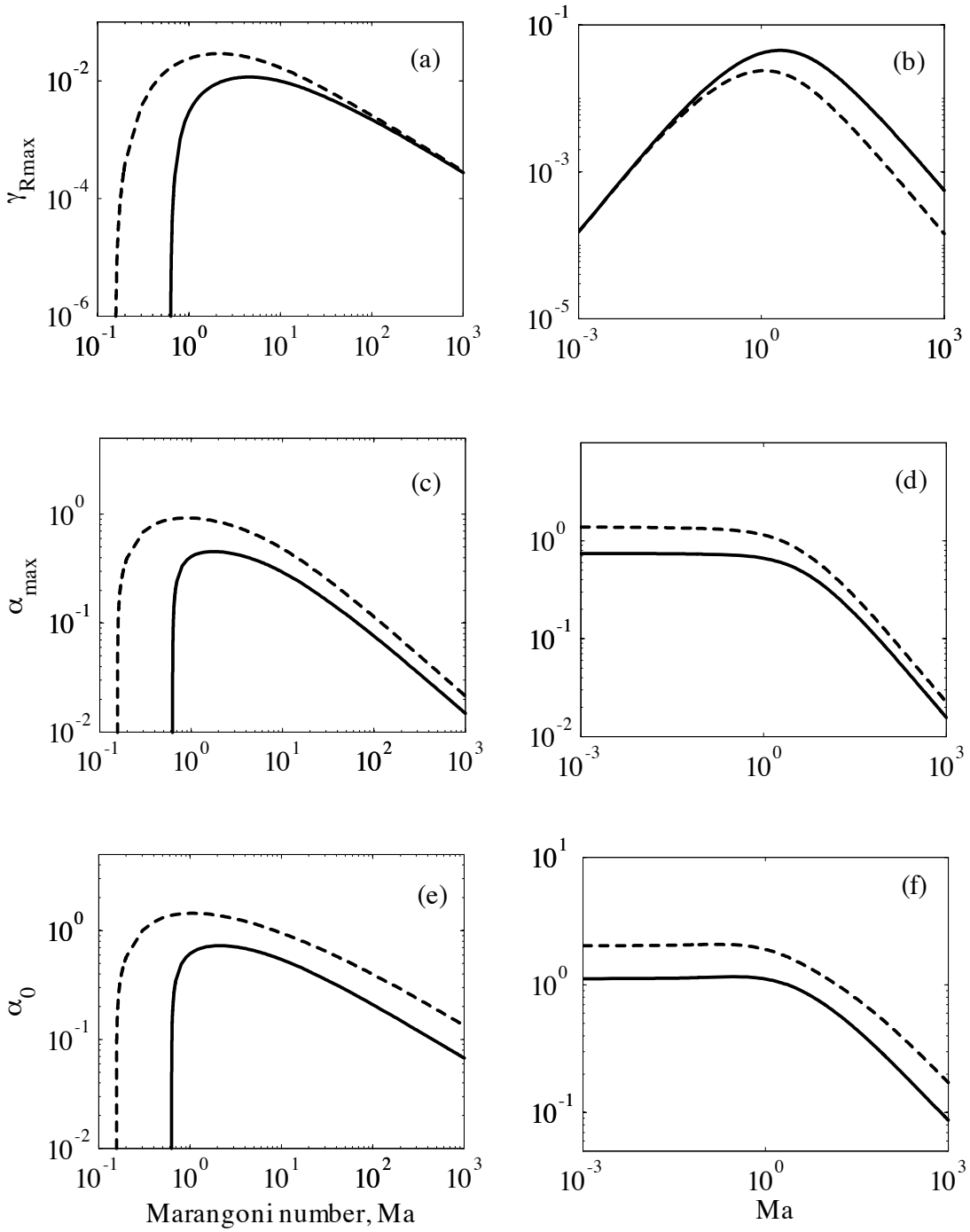

FIG. 14: (a,b) $\gamma_{R\max}$, (c,d) $\alpha_{\max}$ and (e,f) α_0 vs Marangoni number for Bo = 1.0 in the R sectors (a,c,e) and S sectors (b,d,f). Here $s = 1$ and the values of the (n, m) pairs for the sectors R_1, R_2, S_1 and S_2 are $(2, 2)$, $(.5, .5)$, $(2, .5)$ and $(.5, 2)$ respectively.

$\mathrm{Ma} \downarrow 0$. Therefore, equation (58) is approximately linear for $\gamma_R \ll 1$,

$$c_{10}\gamma_R \mathrm{Ma} + c_{01} \approx 0$$

so that

$$\gamma_R \approx -\frac{c_{01}}{c_{10}}\mathrm{Ma}^{-1} \tag{99}$$

where c_{ij} is independent of Ma. An equation for $\alpha_{\max}$ is obtained by differentiating (99) with respect to α and solving $d\gamma_R/d\alpha = 0$ numerically for α which is then substituted into equation (99) to obtain $\gamma_{R\max}$.

In contrast to the case shown in figure 14 for $\mathrm{Bo} > 0$, the flow is unstable for all Ma when $\mathrm{Bo} < 0$ in either the R or S sectors. Moreover, figures 15 (a) and (b) also show that $\gamma_{R\max}$ has a global maximum at $\mathrm{Ma} = O(1)$. However, in the S sectors $\gamma_{R\max}$ decreases with increasing Ma for sufficiently small Ma, up to $\mathrm{Ma} = \mathrm{Ma}_0$. At $\mathrm{Ma} = \mathrm{Ma}_0$ there is a jump in $\alpha_{\max}$. This behavior is due to the fact that the dispersion curves has two maxima and at this particular value of Ma there is a jump in the location of the global maximum, similar to that shown in figure 13. Figure 15 also shows that $\gamma_{R\max}$, $\alpha_{\max}$ and α_0 all approach some finite positive constant in the limits $\mathrm{Ma} \uparrow \infty$ and $\mathrm{Ma} \downarrow 0$ for both sectors.

The asymptotics of α_0 are discussed next. Panels (e) and (f) indicate that α_0 asymptotes to non-zero constants as $\mathrm{Ma} \uparrow 0$ and as $\mathrm{Ma} \downarrow 0$. For large Ma, the dominant term in equation (60) is the Ma^3 term, and since $k_{13} \neq 0$ this implies that

$$\alpha_0 \approx |\mathrm{Bo}|^{1/2} \tag{100}$$

For $\mathrm{Bo} = -1$, $a_0 \approx 1$ which is consistent with the numerical results shown in figures 15 (e)

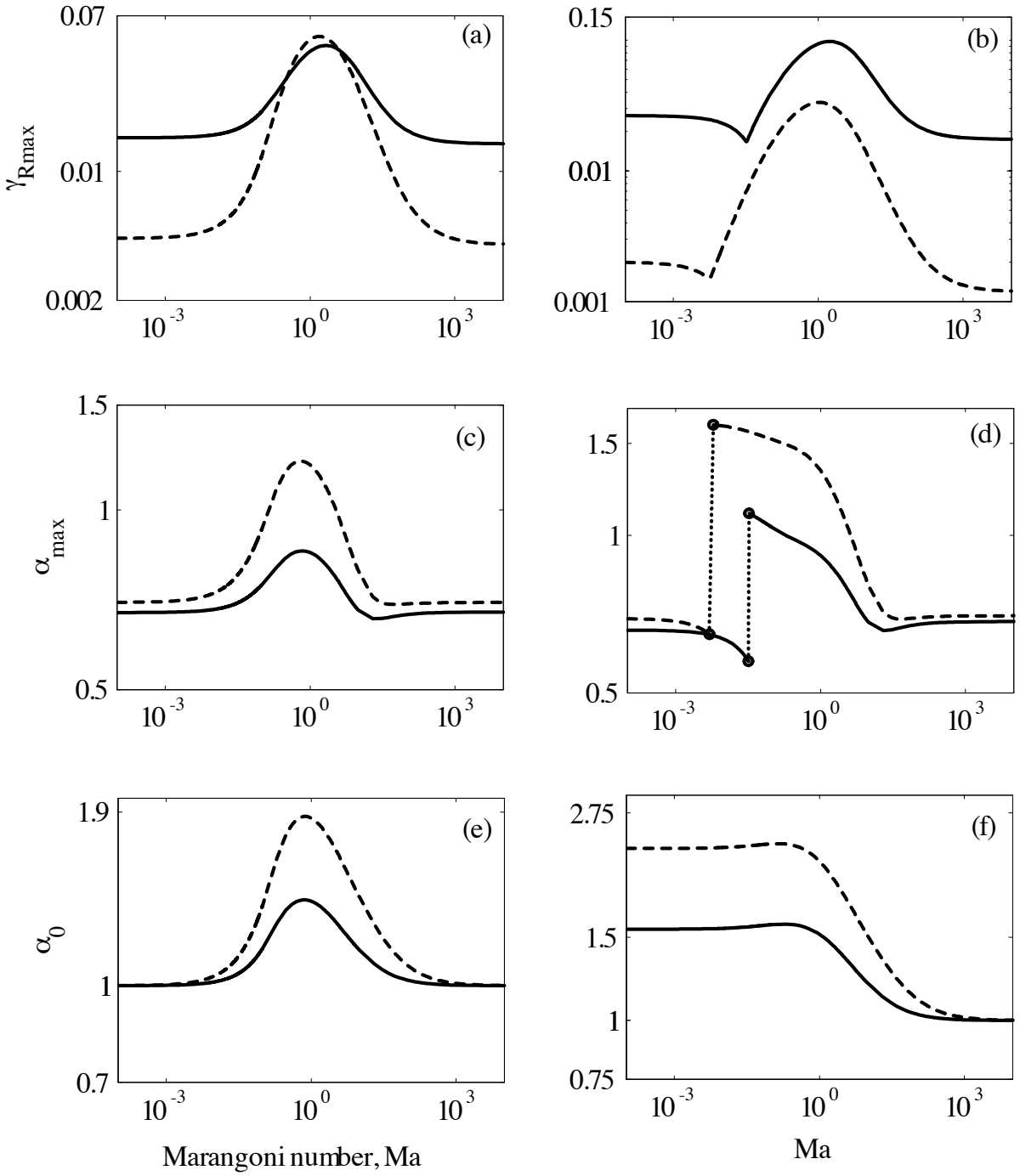

FIG. 15: (a,b) $\gamma_{R\max}$, (c,d) $\alpha_{\max}$ and (e,f) α_0 as functions of Marangoni number for Bo $= -1.0$ in the R sectors (a,c,e) and S sectors (b,d,f). Here $s = 1$ and the values of the (n, m) pairs for the sectors R_1, R_2, S_1 and S_2 are $(2, 2)$, $(.5, .5)$, $(2, .5)$ and $(.5, 2)$ respectively.

and (f). In the limit Ma $\downarrow 0$, equation (60) reduces to

$$\left(k_{11} + k_{13}\mathrm{B}^2\right) \mathrm{MaB} \approx 0. \tag{101}$$

In the R sectors, the solution $\alpha_0 \approx |\mathrm{Bo}|^{1/2}$ is again obtained because k_{11} and k_{13} are both positive. However, in the S sectors $k_{11} > 0$ and $k_{13} < 0$ and α is a solution of $k_{11} + k_{13}\mathrm{B}^2$ which is solved numerically for α. The solutions in the S_1 and S_2 sectors are approximately $\alpha_0 \approx 1.12$ and $a_0 \approx 2.01$ and agree with figure 15 (f).

Next the asymptotics of $\gamma_{R\,\max}$ and $\alpha_{\max}$ in the limit Ma $\uparrow \infty$, and then in the limit Ma $\downarrow 0$, (panels (a, b, c, d) of figure 15) are discussed. In this case, the terms proportional to Ma^3 in equation (58), yielding

$$c_{03} + c_{13}\gamma_R \approx 0 \tag{102}$$

where the coefficients c_{ij} correspond to the $\gamma_R^i \mathrm{Ma}^j$ terms in equation (58). Therefore,

$$\gamma_R \approx -\frac{c_{03}}{c_{13}} \approx -\frac{\left(s_\alpha^2 - \alpha^2\right)\left(s_{\alpha n}^2 - \alpha^2 n^2\right)\left(\mathrm{Bo} + \alpha^2\right)}{\alpha\left(s_\alpha^2 - \alpha^2\right)\left(s_{\alpha n}c_{\alpha n} + \alpha n\right)m + \alpha\left(s_{\alpha n}^2 - \alpha^2 n^2\right)\left(s_\alpha c_\alpha + \alpha\right)}. \tag{103}$$

Again, one must solve $d\gamma_R/d\alpha = 0$ numerically for $\alpha_{\max}$ which in turn is substituted into equation (103) to obtain $\gamma_{R\,\max}$.

The influence of n and m on $\alpha_{\max}$ and $\gamma_{R\,\max}$ shown in figure (16) for two values of Bo < 0 are found by solving these two simplified equations. For fixed n, $\gamma_{R\,\max} \downarrow 0$ as $m \uparrow$, while $\gamma_{R\,\max} \uparrow$ as $n \uparrow$ for fixed m, but a significant change is only observed at sufficiently large m. The corresponding wavenumber where the maximum growth rate occurs, $\alpha_{\max}$, is not strongly influenced by n or m for the smaller value of Bo, Bo $= -1$. Actually, $\alpha_{\max}$

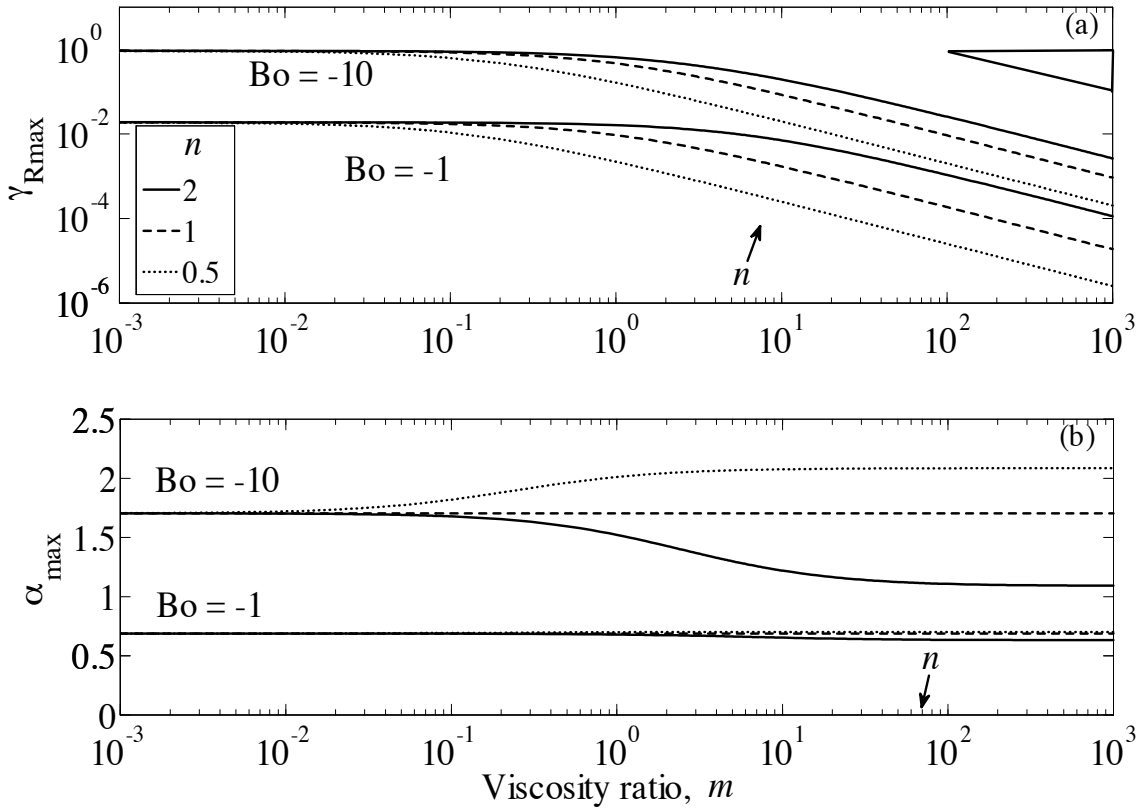

FIG. 16: (a) Maximum growth rate $\gamma_{R\max}$ and (b) the corresponding wavenumber $\alpha_{\max}$ vs viscosity ratio m in the limit Ma $\uparrow \infty$. For each Bond number (Bo $= -10$ and Bo $= -1$) there are three representative values of n where the arrow indicates the direction of increasing n for the pair of Bo. Here $s = 1$.

does not depend on m when $n = 1$ since equation (103) becomes

$$\gamma_R \approx -\frac{\left(s_\alpha^2 - \alpha^2\right)\left(\mathrm{Bo} + \alpha^2\right)}{2\alpha\left(m+1\right)\left(s_\alpha c_\alpha + \alpha\right)} \tag{104}$$

and is determined numerically by solving $d\gamma_R/d\alpha = 0$.

In the limit $m \uparrow \infty$, equation (61) is approximately

$$\gamma_R \sim -\frac{\left(s_{\alpha n}^2 - \alpha^2 n^2\right)\left(\mathrm{Bo} + \alpha^2\right)}{\alpha\left(s_{\alpha n} c_{\alpha n} + \alpha n\right)} m^{-1} \tag{105}$$

indicating that $\gamma_{R\max} \downarrow 0$. This is consistent with the results shown in panel (a) for large m. $a_{\max}$ is obtained by solving $d\gamma_R/d\alpha = 0$ using (105), and is thus dependent on n and Bo, as shown in panel (b). For $m \ll 1$, γ_R is approximately given by

$$\gamma_R \approx -\frac{(s_\alpha^2 - \alpha^2)(\mathrm{Bo} + \alpha^2)}{\alpha(s_\alpha c_\alpha + \alpha)}. \tag{106}$$

Thus both $\gamma_{R\max}$ and $\alpha_{\max}$ approach constants as $m \downarrow 0$ which depend only on the value of Bo. In the limit Bo $\downarrow -\infty$, $\alpha_{\max}$ satisfies $d\gamma_R/d\alpha = 0$ whose numerical solution is $\alpha_{\max} \sim 2.45$, and $\gamma_R \uparrow \infty$.

It is clear from equation (103) that the magnitude of $\gamma_{R\max}$ increases with the magnitude of Bo and it has been checked that $\alpha_{\max}$ approaches some non-zero constant (≈ 2.45) as Bo $\downarrow -\infty$.

For Ma $\ll 1$ equations (58) and (61) are approximately given by

$$c_{40}\gamma_R^4 + c_{30}\gamma_R^3 + c_{20}\gamma_R^2 + c_{10}\gamma_R \approx 0 \tag{107}$$

and

$$\gamma_R^4 \frac{d}{d\alpha}c_{40} + \gamma_R^3 \frac{d}{d\alpha}c_{30} + \gamma_R^2 \frac{d}{d\alpha}c_{20} + \gamma_R \frac{d}{d\alpha}c_{10} \approx 0. \tag{108}$$

Equations (107) and (108) are solved numerically for $\gamma_{R\max}$ and $\alpha_{\max}$ in the R and S sectors. Figure 17 shows the influence of m and n on $\gamma_{R\max}$ and $\alpha_{\max}$ for two negative values of Bo.

In the limit $m \uparrow \infty$, panels (a) and (b) suggest $\gamma_{R\max} \downarrow 0$ and $\alpha_{\max}$ approaches some non-zero constant dependent on the value of n and Bo. As $m \uparrow \infty$, the numerics suggest that $\gamma_R \sim m^{-1}$ which can be estimated by computing the slope of the triangle shown in panel (a). However, in the limit $m \downarrow 0$, both $\gamma_{R\max}$ and $\alpha_{\max}$ approach some positive

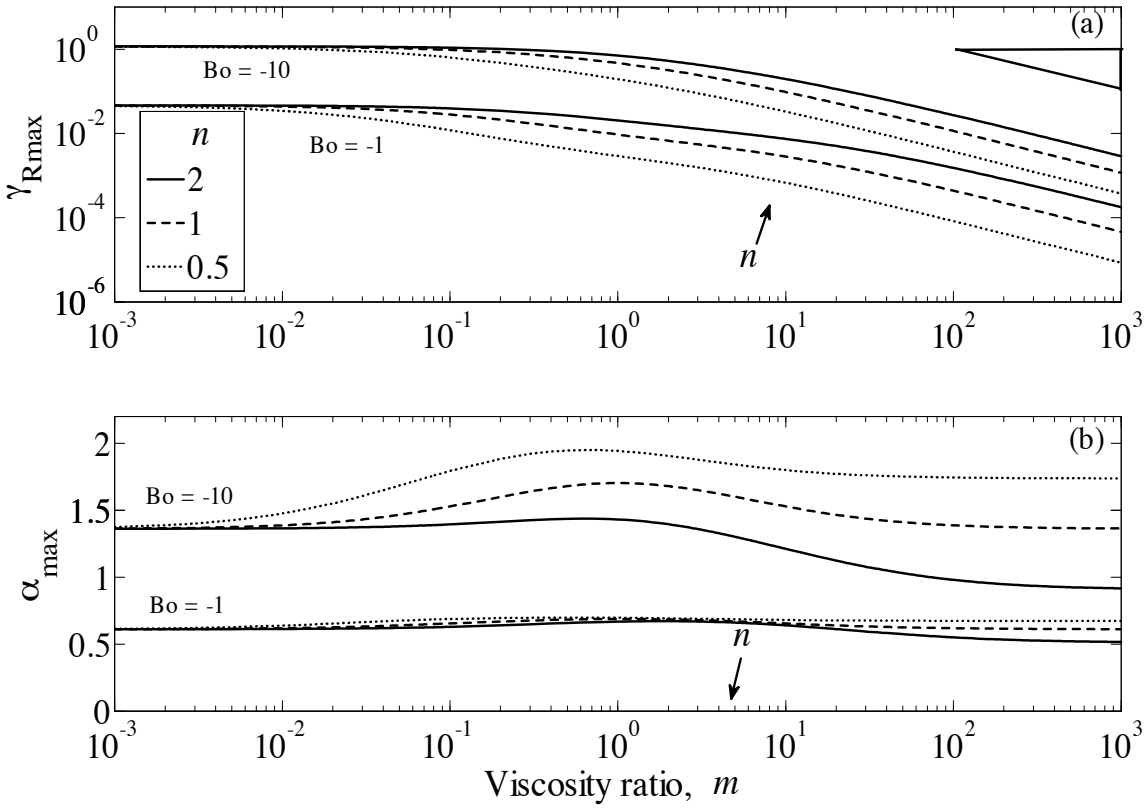

FIG. 17: (a) Maximum growth rate $\gamma_{R\max}$ and (b) the corresponding wavenumber $\alpha_{\max}$ vs viscosity ratio m in the limit Ma $\downarrow 0$. For each Bond number (Bo $= -10$ and Bo $= -1$) there are three representative values of n where the arrow indicates the direction of increasing n for the pair of Bo. Here $s = 1$.

non-zero constant dependent on only the value of Bo.

It was shown in HF (for zero Bond number) that the instability threshold $m \leq n^2$ applied if Ma $< 5/2$. For Ma $> 5/2$ and $m > n^2$ (Q_1 sector) HF found a midwave instability where $\gamma_R > 0$ for finite α-interval bounded away from $\alpha = 0$. In order to investigate this instability threshold more thoroughly, a critical Marangoni number, Ma_{cM}, is introduced which gives the onset (or end) of the midwave instability, and let α_{cM} be the corresponding wavenumber. Numerically, Ma_{cM} and α_{cM} are obtained by solving $\gamma_R = 0$ (49) and $\partial\gamma_R/\partial\alpha = 0$. In figure 18 the growth rate in the Q_1 sector (for $n = 2$ and $m = 5$) is plotted for three selected values

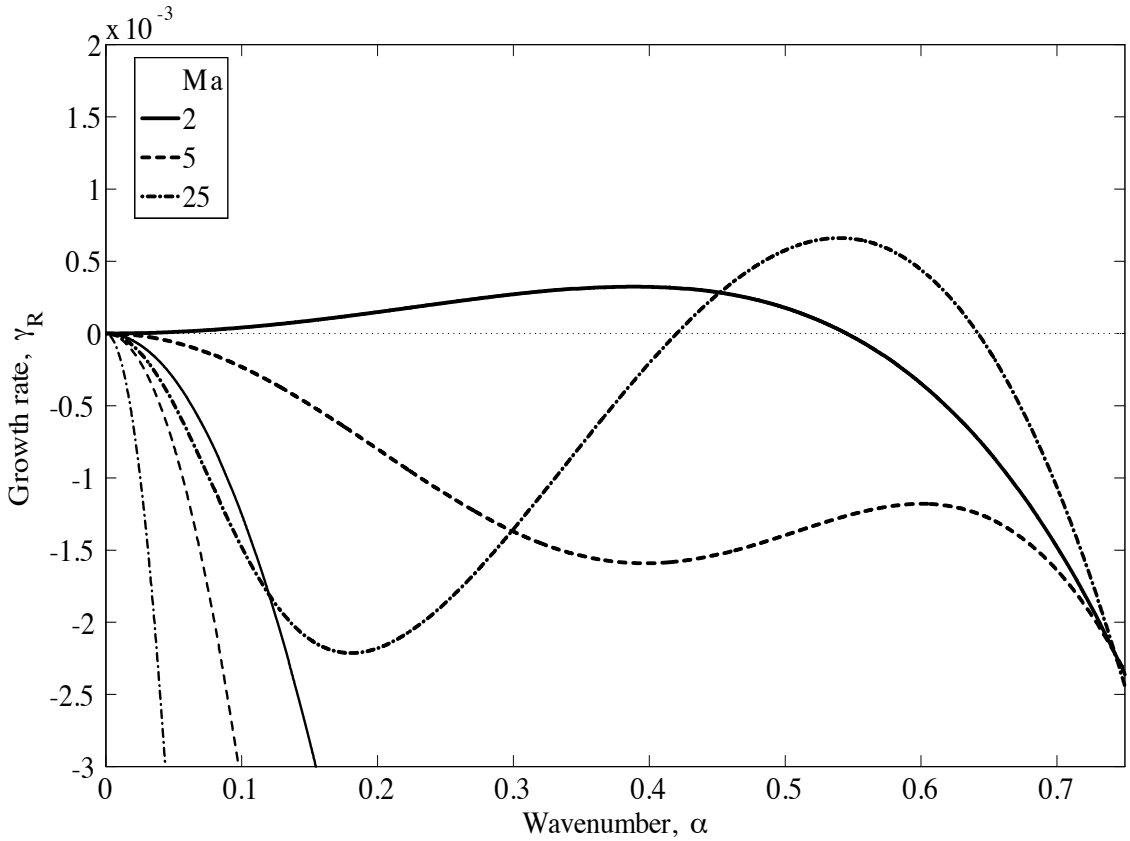

FIG. 18: Typical dispersion curves in the Q_1 sector ($n = 2$, $m = 5$) for $s = 1$, Bo $= -0.45$ and increasing values of Marangoni number depicting the transition of the dominant branch (thicker curves) from longwave unstable to longwave stable to midwave unstable. The corresponding more stable branch (thinner curves) are completely stable.

of Marangoni number. The instability is longwave provided Ma is less than Ma_{cL} (≈ 2.28). This is then followed by a region of stability when $\mathrm{Ma} \in [\mathrm{Ma}_{cL}, \mathrm{Ma}_{cM}]$ where $\mathrm{Ma}_{cM} \approx 15.6$. For $\mathrm{Ma}_{cL} < \mathrm{Ma} < \mathrm{Ma}_m$ (≈ 3.70), γ_R decreases monotonically with α. The growth rate γ_R develops a local maximum $\gamma_{R\,\max}$ at some $\alpha > 0$ provided $\mathrm{Ma} \geq \mathrm{Ma}_m$, and once Ma exceeds Ma_{cM}, γ_{Rm} becomes positive indicating the onset of a midwave instability. Therefore, Ma_m is the value of Marangoni number where $\gamma_{R\,\max}$ first develops. Note that when $\mathrm{Ma} > \mathrm{Ma}_{cM}$ there are two marginal wavenumbers, one on the left at $\alpha = \alpha_{0L}$ and another one on the right at $\alpha = \alpha_{0R}$.

In figure 19 $\gamma_{R\max}$, $\alpha_{\max}$, α_{0R}, and α_{0L} are plotted versus the Marangoni number Ma in the Q_1 sector for $n = 2$, $m = 5$, and $s = 1$, and four negative values of Bo. If Bo is sufficiently negative, as in figures 19 (a) and (c), $\gamma_R > 0$ for all Ma. For $\mathrm{Ma} < \mathrm{Ma}_{cL}$ the instability is longwave since $\alpha_{0L} = 0$. However, a midwave instability ensues when $\mathrm{Ma} > \mathrm{Ma}_{cL}$ and $\alpha_{0L} > 0$. When $\mathrm{Bo} = -0.52$, $\gamma_{R\max} < 0$ and consequently α_{0L} and α_{0R} are undefined for a range of Ma, $\mathrm{Ma}_{cL} < \mathrm{Ma} < \mathrm{Ma}_{cM}$, as shown in panels (e) and (f). In addition, $\alpha_{\max}$ is defined in this range of Ma because γ_R has a local maximum at a nonzero value of α. In panels (g) and (h) with $\mathrm{Bo} = -0.1$, $\gamma_{R\max}$, $\alpha_{\max}$, α_{0L}, and α_{0R} do not exist when $\mathrm{Ma} \in [\mathrm{Ma}_{cL}, \mathrm{Ma}_m]$ since $\gamma_R < 0$ and has no local maximum at some $\alpha > 0$.

A detailed discussion of the midwave instability follows by first considering what happens as the viscosity ratio is increased, starting from a value in the R_1 sector, then crossing the $m = n^2$ border, and finally reaching the Q_1 sector. In the R_1 sector ($1 < m < n^2$), the robust branch is longwave unstable provided $\mathrm{Ma} > \mathrm{Ma}_{cL}$ where Ma_{cL} is given by (77) and $\mathrm{Bo} > 0$. If $m < n^2$ and sufficiently far from the $m = n^2$ border, there exists one stability boundary delineated by $\mathrm{Ma} = \mathrm{Ma}_{cL}$ separating the longwave unstable and stable regions, as shown in figure 20 (a). As $m \uparrow n^2$, the onset of a midwave instability is observed. In panels (b) and (c) a midwave instability occurs provided $\mathrm{Ma}_{cM} < \mathrm{Ma} < \mathrm{Ma}_{cL}$ for $0 < \mathrm{Bo}_{LM1} < \mathrm{Bo} < \mathrm{Bo}_{LM2}$. The closed diamonds and squares denote the locations where Ma_{cL} and Ma_{cM} curves intersect each other at $\mathrm{Bo} = \mathrm{Bo}_{LM1}$ and $\mathrm{Bo} = \mathrm{Bo}_{LM2}$. When m is even closer to n^2 as shown in panel (d), the midwave instability boundary develops a "nose" and can be defined by two functions of Bo, $\mathrm{Ma} = \mathrm{Ma}_{cM1}$ for $\mathrm{Bo}_{LM1} < \mathrm{Bo} < \mathrm{Bo}_N$ (the lower branch) and $\mathrm{Ma} = \mathrm{Ma}_{cM2}$ for $\mathrm{Bo}_{LM2} < \mathrm{Bo} < \mathrm{Bo}_N$ (the upper branch). For fixed $\mathrm{Bo}_{LM2} < \mathrm{Bo} < \mathrm{Bo}_N$ there are four distinct regions: a region of stability for sufficiently small Ma, $0 < \mathrm{Ma} < \mathrm{Ma}_{cM1}$; a region of midwave instability, $\mathrm{Ma}_{cM1} < \mathrm{Ma} < \mathrm{Ma}_{cM2}$; another region of stability

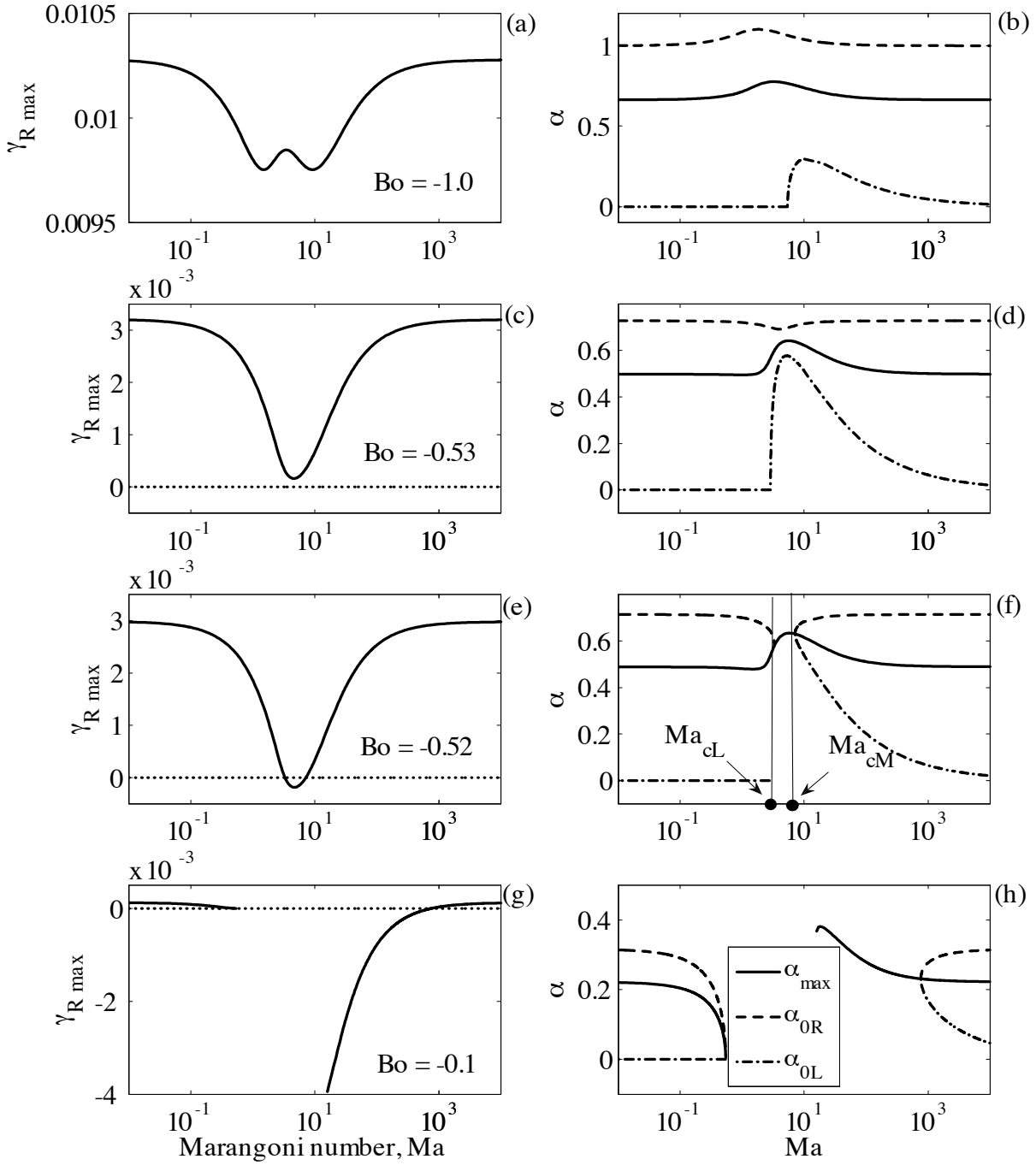

FIG. 19: Plots of $\gamma_{R\max}$, corresponding $\alpha_{\max}$, α_{0R}, and α_{0L} vs Ma in the Q_1 sector ($n = 2$, $m = 5$) for $s = 1$ and the four indicated values of Bo. Panel (g) shows the range $\mathrm{Ma}_{cL} < \mathrm{Ma} < \mathrm{Ma}_{cM}$ (Ma between the intersections of the $\gamma_{R\max} = 0$ dotted line) where $\gamma_{R\max} < 0$ and thus α_{0L} and α_{0R} do not exist in panel (h).

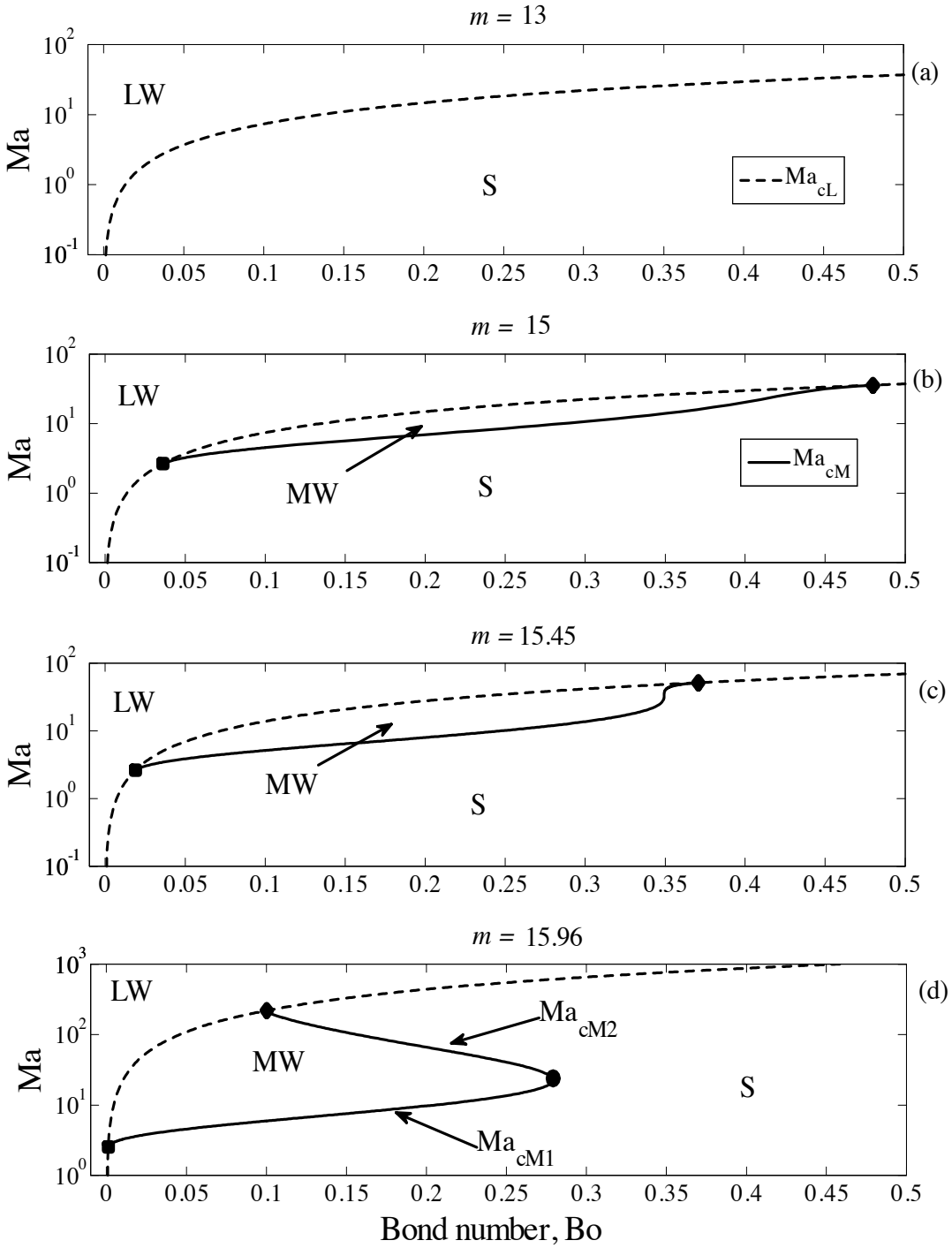

FIG. 20: Stability diagrams in the Bond-Marangoni plane showing the influence of the viscosity ratio m as $m \uparrow n^2$: (a) $m = 13$; (b) $m = 15$; (c) $m = 15.45$; and (d) $m = 15.96$. The $\mathrm{Ma} = \mathrm{Ma}_{cL}$ and $\mathrm{Ma} = \mathrm{Ma}_{cM}$ curves represent longwave and midwave instability boundaries where S, LW, and MW denote the stable, longwave unstable, and midwave unstable regions. Here $s = 1$ and $n = 4$. The closed diamonds and squares denote the locations where Ma_{cL} and Ma_{cM} curves intersect each other at $\mathrm{Bo} = \mathrm{Bo}_{LM1}$ and $\mathrm{Bo} = \mathrm{Bo}_{LM2}$. The solid circle denotes the location of the "nose."

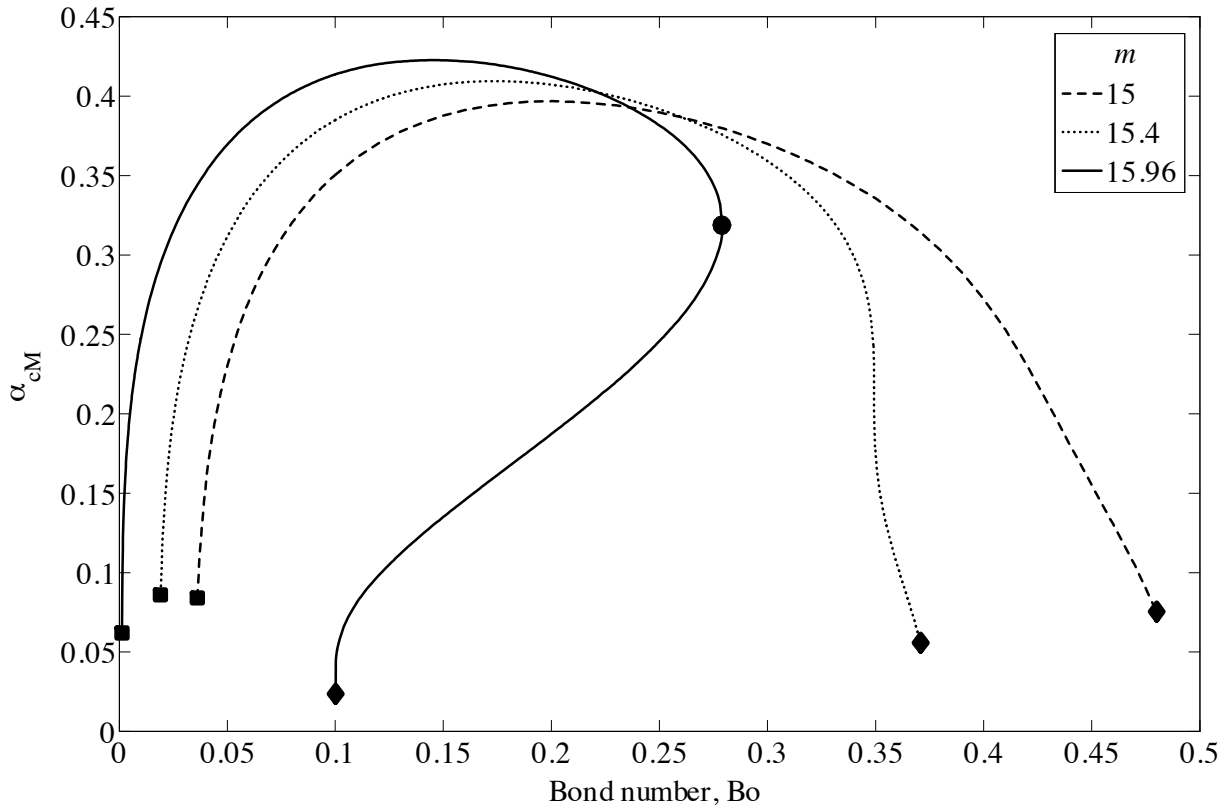

FIG. 21: The wavenumber α_{cM} that corresponds to Ma_{cM} given by figure (20) vs Bo for different viscosity ratios near the $m = n^2$ boundary. Here $n = 4$ and $s = 1$.

for $\mathrm{Ma}_{cM2} < \mathrm{Ma} < \mathrm{Ma}_{cL}$; and a region of longwave instability for $\mathrm{Ma} > \mathrm{Ma}_{cL}$. In figure (21) the wavenumber α_{cM} corresponding to Ma_{cM} is plotted versus Bo for the values of m in panels (b), (c), and (d) of figure (20). For all cases α_{cM} attains a maximum at some Bond number $\mathrm{Bo}_{LM1} < \mathrm{Bo} < \mathrm{Bo}_{LM2}$.

On the $m = n^2$ ($m = 16$) border, the robust branch is always longwave unstable for $\mathrm{Bo} < 0$ ($\mathrm{Ma}_{cL} = 0$), as shown in figure 22. Along the Ma axis ($\mathrm{Bo} = 0$) the stability results of HF that show the existence of a midwave instability for $\mathrm{Ma} > 5/2$ are recovered: $\mathrm{Ma}_{cM} \to 5/2$ and $\alpha_{cM} \to 0$ as $\mathrm{Bo}_{LM1} \to 0$, and $\mathrm{Ma}_{cM} \to \infty$ and $\alpha_{cM} \to 0$ as $\mathrm{Bo}_{LM2} \to 0$. For $0 < \mathrm{Bo} < \mathrm{Bo}_N$ there is a midwave instability when $\mathrm{Ma}_{cM1} < \mathrm{Ma} < \mathrm{Ma}_{cM2}$ and for Bo > 0 outside the midwave instability region the flow is always stable.

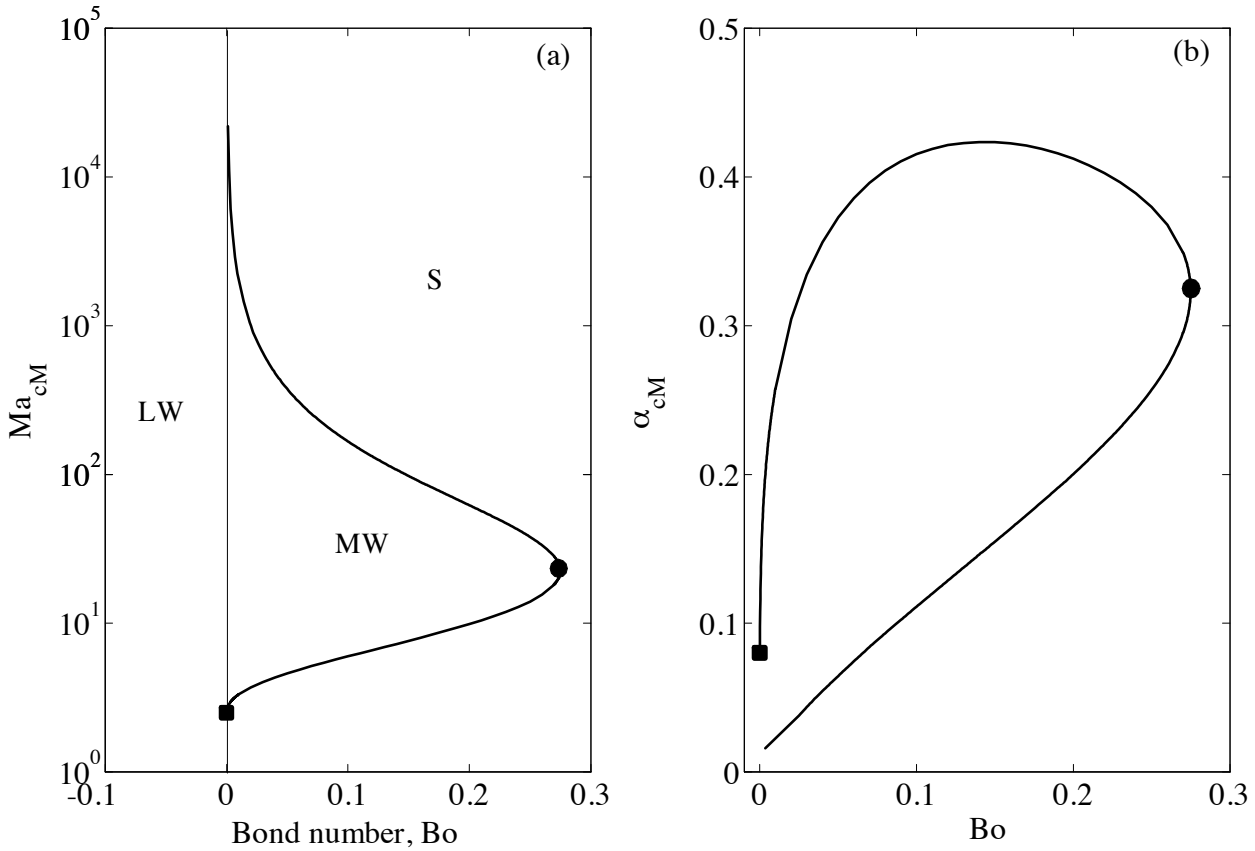

FIG. 22: (a) Stability diagram in the Bond-Marangoni plane similar to the ones shown in figure (20), for a case where $m = n^2$ ($m = 16$) and (b) the corresponding critical wavenumber, α_{cM}. Here $s = 1$.

The critical Marangoni number Ma_{cL}, which is given by equation (77), is positive for Bo < 0 in the Q sectors and two (left) noses appear in addition to the right nose as shown in figure 23. These two left noses occur at the same value of Bo, and as m increases all the noses move to the left but the single right nose moves faster than the two left noses. Eventually, at some sufficiently large m, the three noses merge into a single left nose.

Finally, in figure 24 the location of the noses are tracked as a function of Bo for values of viscosity ratio $m \geq 15.45$. Consistent with the stability diagrams shown in figures 20 and 22, there is only one nose when $m \leq 16$ (here $n = 4$). In the Q_1 sector, $m > 16$, there can be up to three noses for a certain range of parameter values. At some finite value of Bond

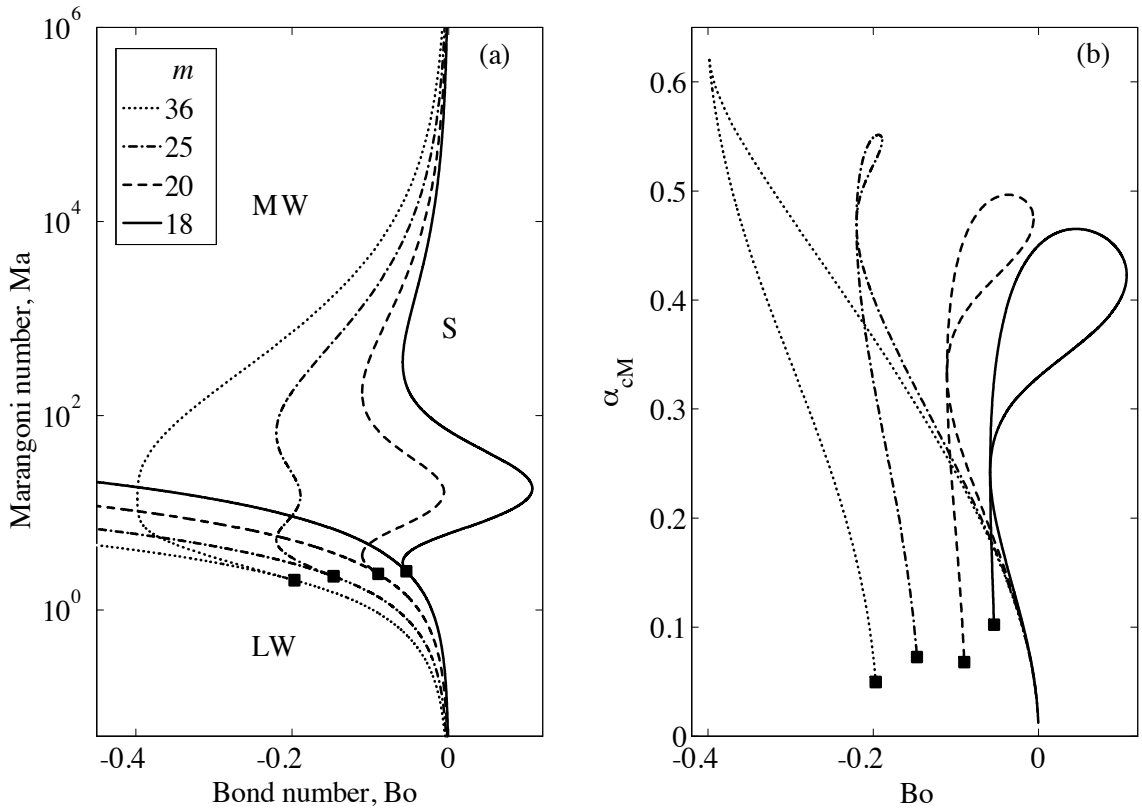

FIG. 23: (a) Stability diagram showing the regions of midwave and longwave instability and stability defined by the curves Ma_{cL} and Ma_{cM} as m increases in the Q_1 sector, and (b) the wavenumber corresponding to Ma_{cM} for the indicated values of m and $s = 1$.

number, Bo_N, the three noses collapse together to a single nose which remains through the Q_1 sector. The value of viscosity ratio (m_N) and corresponding Marangoni number (Ma_N), Bond number (Bo_N), and wavenumber (α_N) are obtained by solving: $\gamma_R(\alpha) = 0$, $\partial\gamma_R(\alpha)/\partial\alpha = 0$, $\partial\gamma_R(\alpha)/\partial\mathrm{Ma} = 0$, and $\zeta = 0$ simultaneously. When $n = 4$ and $s = 1$ then $m_N \approx 34.3$, $\mathrm{Ma}_N \approx 13.9$, $\mathrm{Bo}_N \approx -0.375$, and $\alpha_N \approx 0.613$, which is in agreement with the results in figure 24. For values of $m > m_N$ there is only a single left nose. Similar stability diagrams are also found when crossing the $m = n^2$ border going from the R_2 sector to the Q_2 sector for constant n while decreasing m.

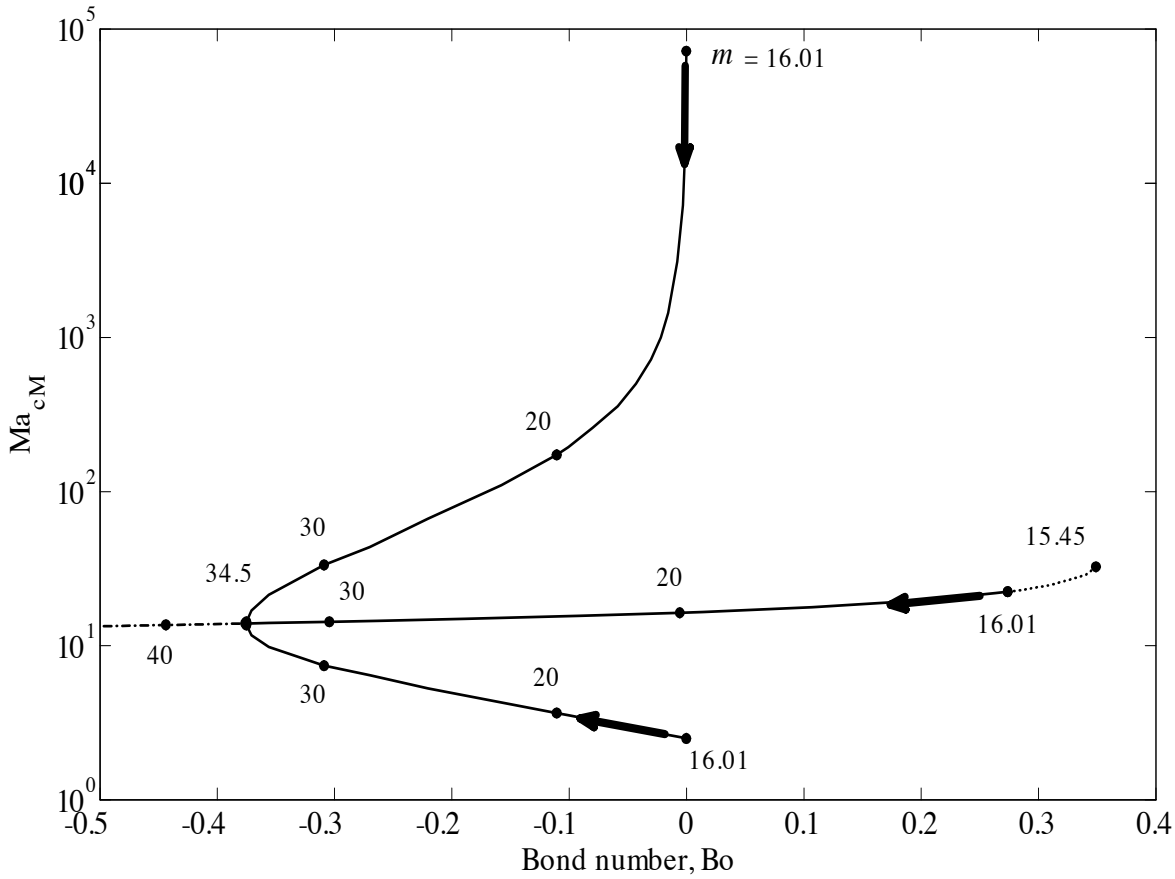

FIG. 24: The location of the noses in the Bo-Ma_{cM} plane where $n = 4$ and $s = 1$ for selected values of m starting R_1 sector and increasing through to the Q_1 sector.

III. SEMI-INFINITE GEOMETRY CASE

A. General stability properties

For an infinitely thick upper fluid layer, $n = \infty$, the perturbed velocity in the bottom layer $\hat{w}_1$ still satisfies (37) but in the upper layer the general solution of (27) for $\hat{w}_2$ that satisfies the no slip no penetration boundary conditions (28) is

$$\hat{w}_2(z) = e^{-\alpha z}(a_2 + b_2 z), \tag{109}$$

Similar to the finite n case the normalization $a_1 = 1$ is chosen. By using equations (41) and (42) and then applying the interfacial boundary conditions (32), (34) and (35) (which still apply here since they do not involve the upper layer) three equations involving b_1, b_2, and γ are obtained:

$$(s_\alpha^2 - \alpha^2)b_1 + b_2\alpha - \alpha^2 - \alpha - s_\alpha c_\alpha + \frac{si\alpha^2}{\gamma}\left(1 - \frac{1}{m}\right) = 0, \tag{110}$$

$$2\alpha m + \frac{\mathrm{Bo}}{\gamma} + \frac{\alpha^2}{\gamma} + 2b_1\alpha = 0, \tag{111}$$

$$\begin{aligned} &\left[\frac{\alpha \mathrm{Ma}}{\gamma}(s_\alpha^2 - \alpha^2) + 2(s_\alpha c_\alpha - \alpha)\right] b_1 - 2b_2\alpha m \\ &- 2c_\alpha^2 - \frac{\alpha \mathrm{Ma}}{\gamma}\left(\alpha + s_\alpha c_\alpha - \frac{is\alpha^2}{\gamma}\right) + 2\alpha^2(m-1) = 0. \end{aligned} \tag{112}$$

First an expression for b_1 is obtained from equation (111),

$$b_1 = -\frac{1}{2\alpha}\left(2\alpha m + \frac{\mathrm{Bo}}{\gamma} + \frac{\alpha^2}{\gamma}\right), \tag{113}$$

which is then substituted into (110) and (112). Equations (110) and (112) are written as a system of two linear equations of the form

$$\begin{bmatrix} B_{11} & B_{12} \\ B_{21} & B_{22} \end{bmatrix} \begin{bmatrix} b_2 \\ 1 \end{bmatrix} = \begin{bmatrix} 0 \\ 0 \end{bmatrix}, \tag{114}$$

where the coefficients B_{11}, B_{12}, B_{21}, and B_{22} are given in Appendix B 2. As before, the dispersion equation is quadratic in γ and given by equation (48). However, the coefficients are

$$\mathrm{Re}(F_2) = m^2\left(s_\alpha^2 - \alpha^2\right) + 2ms_\alpha c_\alpha + \left(c_\alpha^2 + \alpha^2\right) > 0, \tag{115}$$

$$\mathrm{Im}(F_2) = 0,$$

$$\begin{aligned} \mathrm{Re}(F_1) = \frac{1}{2\alpha}\Big\{ & m\mathrm{Ma}\left(s_\alpha^2 - \alpha^2\right)\alpha^2 + \mathrm{Ma}\left(\alpha + s_\alpha c_\alpha\right)\alpha^2 \\ & + m\left(s_\alpha^2 - \alpha^2\right)\left(\mathrm{Bo} + \alpha^2\right) \\ & + \left(s_\alpha c_\alpha - \alpha\right)\left(\mathrm{Bo} + \alpha^2\right)\Big\}, \end{aligned} \tag{116}$$

$$\mathrm{Im}(F_1) = (1-m)s\alpha^2, \tag{117}$$

$$\mathrm{Re}(F_0) = \frac{1}{4}(s_\alpha^2 - \alpha^2)\left(\mathrm{Bo} + \alpha^2\right)\mathrm{Ma}, \tag{118}$$

$$\mathrm{Im}(F_0) = -\frac{1}{2}s\mathrm{Ma}\alpha^3 < 0, \tag{119}$$

where the signs of the real and imaginary parts are determined as discussed for the finite n case. The zero gravity limit studied in HF is recovered by letting $\mathrm{Bo} = 0$, making the substitution $\gamma = -i\alpha c$ and then dividing (115)-(119) by α^3. As for the finite n case

discussion, the influence of the system parameters m, s, Ma and Bo have on the growth rate γ_R is investigated.

First the influence of the Marangoni number on the maximum growth rate $\gamma_{R\max}$, the corresponding wavenumber $\alpha_{\max}$ and the marginal wavenumber α_0 is examined. Here $\gamma_{R\max}$, $\alpha_{\max}$, and α_0 are found by substituting (115)-(119) into (58), (61) and (59). In figure 25 $\gamma_{R\max}$, $\alpha_{\max}$ and α_0 are plotted versus Ma for a representative sample of values of m and two values of Bo (one positive and one negative). Panels (a) and (b) show that as Ma increases from 0, $\gamma_{R\max}$ increases, attaining a maximum, $\max(\gamma_{R\max})$ at Ma = max(Ma), after which it decreases to 0 as Ma $\uparrow \infty$. Figure 26 shows more clearly the dependence of $\max(\gamma_{R\max})$ and max(Ma) on m. Both $\max(\gamma_{R\max})$ and max(Ma) approach some non-zero constants as $m \downarrow 0$, while in the limit $m \uparrow \infty$, $\max(\gamma_{R\max}) \downarrow 0$ and max(Ma) $\uparrow \infty$.

In the limit Ma $\uparrow \infty$ for Bo > 0, panels (a), (c) and (e) of figure 25 show $\gamma_{R\max} \downarrow 0$, $\alpha_{\max} \downarrow 0$, and $\alpha_0 \downarrow 0$ all of which are independent of m. Although it is not clear in panels (b) and (d), it will be shown below for Bo < 0, $\gamma_{R\max}$ and $\alpha_{\max}$ approach non-zero constants that depend on the value of m, while the marginal wavenumber α_0 approaches a constant that is independent of the value of m. In order to obtain the asymptotic behavior of α_0 it is convenient to write equation (60) as a polynomial in Ma and B (where B = Bo $+\alpha^2$)

$$\begin{aligned}
&\{(m-1)(s_\alpha c_\alpha + \alpha + m\left(s_\alpha^2 - \alpha^2\right)) - (c_\alpha + \alpha^2 + 2ms_\alpha c_\alpha + m^2\left(s_\alpha^2 - \alpha^2\right))\}4s^2\alpha^6\mathrm{Ma}^2 \\
&+4s^2\alpha^4(m-1)(s_\alpha c_\alpha - \alpha + m\left(s_\alpha^2 - \alpha^2\right))\mathrm{MaB} \\
&+\left(s_\alpha c_\alpha - \alpha + m\left(s_\alpha^2 - \alpha^2\right)\right)^2\left(s_\alpha^2 - \alpha^2\right)\alpha^{-2}\mathrm{MaB}^3 \\
&+2\left(s_\alpha c_\alpha - \alpha + m\left(s_\alpha^2 - \alpha^2\right)\right)\left(s_\alpha c_\alpha + \alpha + m\left(s_\alpha^2 - \alpha^2\right)\right)\left(s_\alpha^2 - \alpha^2\right)\mathrm{Ma}^2\mathrm{B}^2 \\
&+\left(s_\alpha c_\alpha + \alpha + m\left(s_\alpha^2 - \alpha^2\right)\right)^2\left(s_\alpha^2 - \alpha^2\right)\alpha^2\mathrm{Ma}^3\mathrm{B} = 0. \qquad (120)
\end{aligned}$$

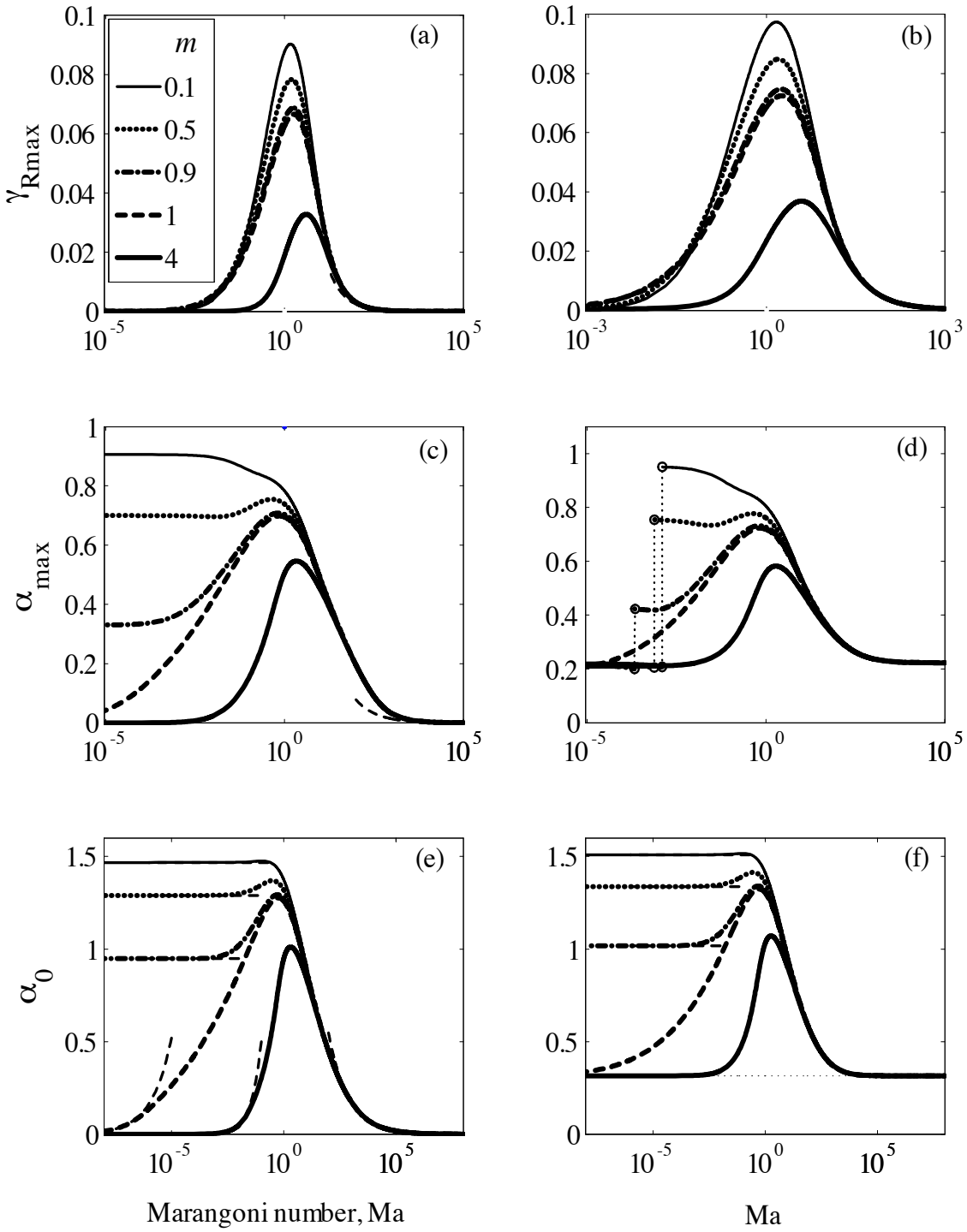

FIG. 25: (a,b) $\alpha_{\max}$, (c,d) $\gamma_{R\max}$ and (e,f) α_0 vs Ma for Bo = 0.1 (a,c,e) and Bo = −0.1 (b,d,f) and the five indicated values of m and $s = 1$. In panels (a), (c), (e) and (f) certain asymptotic expressions are also plotted.

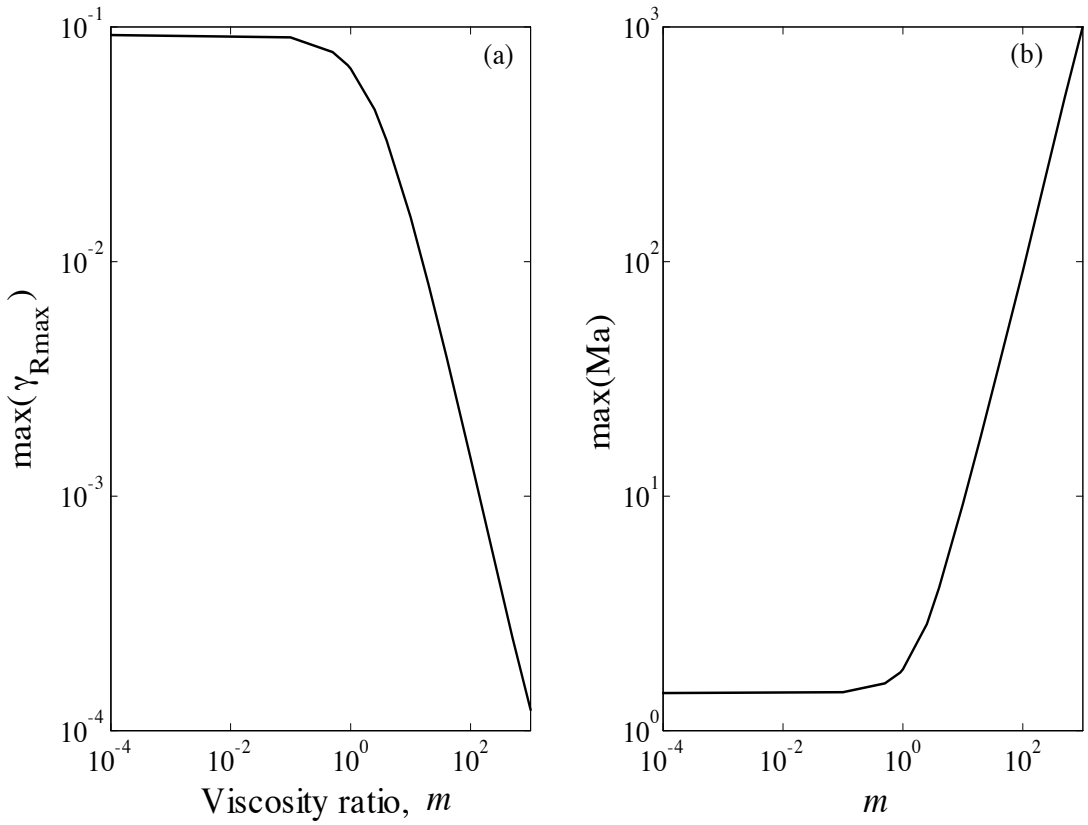

FIG. 26: (a) $\max(\gamma_{R\max})$ and (b) max(Ma) vs m for Bo $= 0.1$ and $s = 1$.

In the limit Ma $\uparrow \infty$, the Ma^{3}B term in equation (120) dominates all other terms. So, to leading order B ≈ 0 and thus $\alpha_0 \approx |\mathrm{Bo}|^{1/2}$, which is good for Bo < 0 only. This is consistent with the numerical results shown in panel (f) of figure 25 for Ma $\gg 1$. The error of this approximation is less than 1% for Ma $> 2.53 \times 10^4$. For Bo > 0, the numerics suggest that $\alpha_0 \downarrow 0$ independent of the value of m, and consequently it is convenient to substitute the longwave coefficients F_2, F_1 and F_0 (B5)-(B9) into (59). The following equation for α_0 is obtained

$$\frac{1}{108}\mathrm{Bo}^3\alpha^2 - \frac{1}{4}s^2\mathrm{Ma} + \frac{1}{6}\left(m-1\right)s^2\,\mathrm{Bo}\alpha + \frac{1}{12}\mathrm{Ma}^2\mathrm{Bo}\alpha^2 = 0. \tag{121}$$

The α_0 approximation is found from the balance of the second and fourth terms in (121), yielding

$$\alpha_0 \approx s\sqrt{3}\mathrm{Ma}^{-1/2}\mathrm{Bo}^{-1/2}. \tag{122}$$

Note that the other terms in (121) are important below when the case $m \geq 1$ and Bo < 0 is considered. This approximation converges to the numerical solution obtained by solving equation (59) in panel (e) of figure 25, with the error being less than 1% for Ma $> 2.7 \times 10^5$.

Next, the asymptotics of $\alpha_{\max}$ and $\gamma_{\max}$ are discussed. Since $\alpha_{\max} \downarrow 0$ as Ma $\uparrow \infty$ for Bo > 0, a longwave approximation can be used. The γ_R coefficients are found by substituting (B5)-(B9) into (58). However, the correction term to equation (B5), $2m\alpha$, is kept so the γ_R^4 term in (61),$\frac{d}{d\alpha}C_4(\alpha)$, does not disappear. In this limit equations (58) and (61) are approximately given by

$$4\gamma_R^4 + 8\mathrm{Ma}\alpha^2\gamma_R^3 + 5\mathrm{Ma}^2\alpha^4\gamma_R^2 + \mathrm{Ma}^3\alpha^6\gamma_R + \frac{1}{12}\mathrm{Ma}^3\mathrm{Bo}\alpha^8 - \frac{1}{4}\mathrm{Ma}^2 s^2\alpha^6 \approx 0 \tag{123}$$

and

$$24m\gamma_R^4 + 16\mathrm{Ma}\alpha\gamma_R^3 + 20\mathrm{Ma}^2\alpha^3\gamma_R^2 + 6\mathrm{Ma}^3\alpha^5\gamma_R + \frac{2}{3}\mathrm{Ma}^3\mathrm{Bo}\alpha^7 - \frac{3}{2}\mathrm{Ma}^2 s^2\alpha^5 \approx 0. \tag{124}$$

It is helpful to multiply equation (124) by $-\alpha/6$ and then add it to equation (123) to eliminate the γ_R term and one of the constant (in γ_R) terms to obtain

$$4\gamma_R^4 + \frac{16}{3}\mathrm{Ma}\alpha^2\gamma_R^3 + \frac{5}{3}\mathrm{Ma}^2\alpha^4\gamma_R^2 - \frac{1}{36}\mathrm{Ma}^3\mathrm{Bo}\alpha^8 = 0. \tag{125}$$

The behavior of $\gamma_{R\max}$ is found by balancing the two dominant terms in (123) which are the

fourth and last terms, yielding

$$\gamma_{R\max} \approx \frac{1}{4} s^2 \mathrm{Ma}^{-1}. \tag{126}$$

In (125) the dominant terms are the last two, and by substituting (126) into (125) the following approximation for $\alpha_{\max}$ is obtained

$$\alpha_{\max} \approx s \left(\frac{15}{4\mathrm{Bo}} \right)^{1/4} \mathrm{Ma}^{-3/4}. \tag{127}$$

Expressions (126) and (127) converge to the solutions obtained by solving the original equations (59) and (61) for large values of Ma as shown in panels (a) and (c) of figure 25. Note that these two expressions are independent of m. The errors in using these approximations for $\alpha_{\max}$ and $\gamma_{R\max}$ are less than 1% when $\mathrm{Ma} > 8.61 \times 10^9$ and $\mathrm{Ma} > 2.66 \times 10^3$, respectively.

When $\mathrm{Bo} < 0$, the longwave approximations cannot be used. The asymptotics for $\alpha_{\max}$ and $\gamma_{\max}$ are found by first retaining the dominant cubic terms in Ma which appear in the coefficient of the linear term and the constant term in γ_R in equation (58). The growth rate γ_R can then be readily written in terms of α

$$\gamma_R \approx -\frac{(s_\alpha^2 - \alpha^2)(\mathrm{Bo} + \alpha^2)}{2\alpha(m(s_\alpha^2 - \alpha^2) + \alpha + s_\alpha c_\alpha)}. \tag{128}$$

The maximum wavenumber, $\alpha_{\max}$, is found by solving $d\gamma_R/d\alpha = 0$ or simply

$$\begin{gathered} \left(\mathrm{Bo} - \alpha^2\right)\left(s_\alpha^2 - \alpha^2\right)^2 m - \left(\alpha^3(1 + 2s_\alpha^2) + \alpha^2 s_\alpha c_\alpha - 2\alpha s_\alpha^2 - s_\alpha^3 c_\alpha\right)\mathrm{Bo} \\ \alpha^5(1 - 2s_\alpha^2) + \alpha^4 s_\alpha c_\alpha + \alpha^3 s_\alpha^2(s_\alpha^2 - c_\alpha^2) - \alpha^2 s_\alpha^3 c_\alpha = 0 \end{gathered} \tag{129}$$

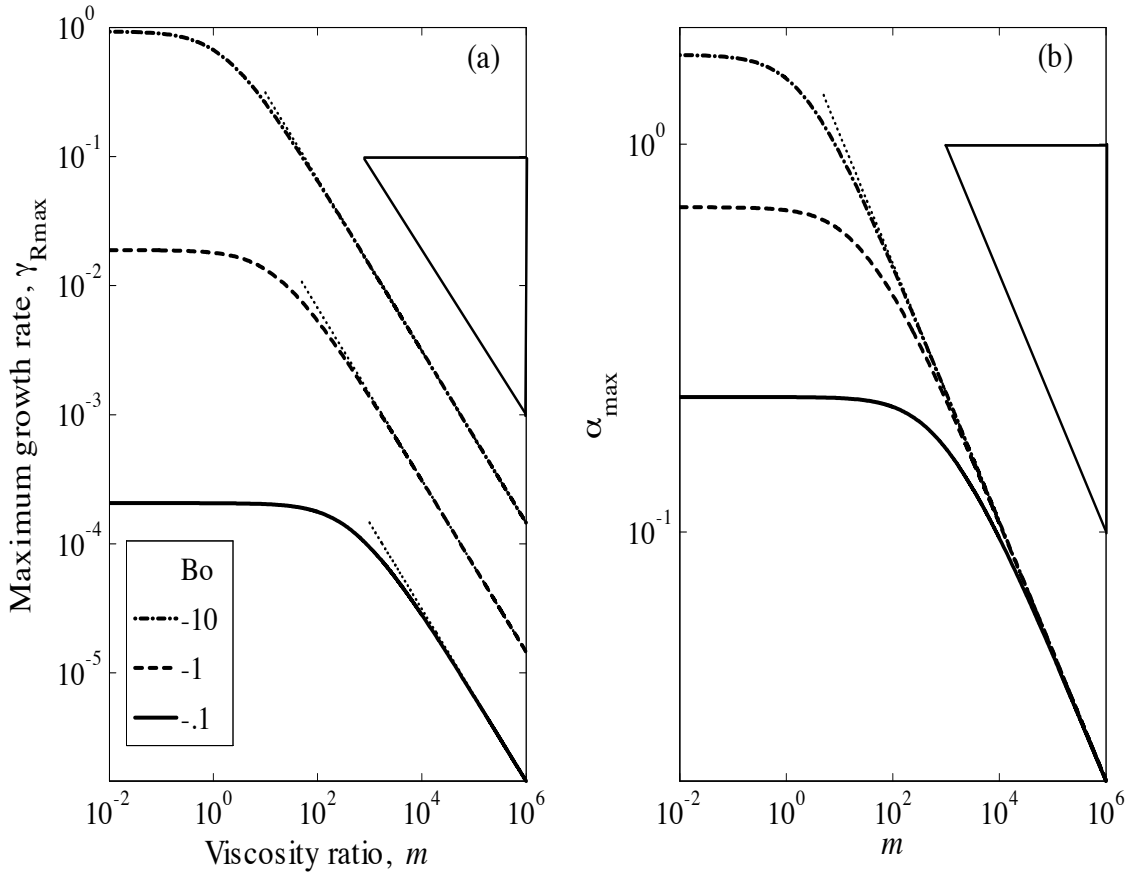

FIG. 27: (a) $\gamma_{R\max}$ and (b) $\alpha_{\max}$ vs m in the limit of infinitely large Ma for the indicated values of Bo and $s = 1$. The thin lines correspond to the large m asymptotics described by equations (130) and (131).

for $\alpha_{\max}$ which is substituted into (128) to obtain $\gamma_{R\max}$. It is also clear from equation (128) that $(\alpha_{\max}, \gamma_{R\max})$ depends on the viscosity ratio and the Bond number which is not quite evident from figures 25 (b) and (d). The dependence of $\gamma_{R\max}$ and $\alpha_{\max}$ on m is shown in figure 27 for the three indicated values of Bo.

It is also possible to find the asymptotic behavior of $\gamma_{R\max}$ and $\alpha_{\max}$ for $m \gg 1$ since $\alpha_{\max} \downarrow 0$ and $\gamma_R \downarrow 0$ as $m \uparrow \infty$ as shown in figures 27 (a) and(b). A Taylor series about $\alpha = 0$ of equation (129) yields

$$-12\mathrm{Bo} + m\mathrm{Bo}\alpha^3 \approx 0$$

to leading order in Ma. Thus

$$\alpha_{\max} \approx 12^{1/3} m^{-1/3}. \tag{130}$$

The maximum growth rate $\gamma_{R\max}$ is obtained by approximating (128) for small α and substituting (130), so that

$$\gamma_{R\max} \approx -\frac{12^{2/3}}{36} \mathrm{Bo} m^{-2/3}. \tag{131}$$

It is clear from figure 27 (a) and the approximation (131) that $\gamma_{R\max}$ depends linearly on Bo. However, as shown in figure 27 (b), $\alpha_{\max}$ is independent of Bo in the limit Ma $\uparrow \infty$ and $m \uparrow \infty$, which is consistent with (130). The approximations are quite good for sufficiently large m. For the values of Bo $= -0.1, -1$ and -10 used in figure 27 the error in $\alpha_{\max}$ is less than 1% when $m > 3.74 \times 10^5, 1.19 \times 10^4$ and 384, respectively, and the error in $\gamma_{R\max}$ is less than 1% when $m > 3.84 \times 10^5, 1.33 \times 10^4$ and 824 .

In the limit $m \downarrow 0$, figure 27 clearly shows that $\gamma_{R\max}$ and $\alpha_{\max}$ both approach some positive constants that depend on Bo. For $m \ll 1$, equations (128) and (129) are approximately given by

$$\gamma_R \approx -\frac{(s_\alpha^2 - \alpha^2)(\mathrm{Bo} + \alpha^2)}{2\alpha(\alpha + s_\alpha c_\alpha)} \tag{132}$$

and

$$\begin{aligned} &-\left(\alpha^3(1+2s_\alpha^2) + \alpha^2 s_\alpha c_\alpha - 2\alpha s_\alpha^2 - s_\alpha^3 c_\alpha\right)\mathrm{Bo} \\ &\alpha^5(1-2s_\alpha^2) + \alpha^4 s_\alpha c_\alpha + \alpha^3 s_\alpha^2(s_\alpha^2 - c_\alpha^2) - \alpha^2 s_\alpha^3 c_\alpha = 0. \end{aligned} \tag{133}$$

The values of $\gamma_{R\max}$ and $\alpha_{\max}$ are found by solving (133) and (132) numerically when Bo $= -10$, -1, and -0.1, and are $(1.7, .936)$, $(.689, 1.89\times10^{-2})$, $(.223, 2.06\times10^{-4})$, respectively. These solutions agree with the exact values used in figure 27 in the limit $m \downarrow 0$.

As Ma $\downarrow$ 0, figure 25 (c) clearly indicates that $\alpha_{\max}$ approaches a non-zero constant dependent on the value of m for $m < 1$ for Bo > 0. When Bo is sufficiently negative there is a jump in $\alpha_{\max}$ as shown in figure 25 (d). This is a consequence of the crossing of the two branches and is discussed later, see figure 32. The α_0 behavior is similar to $\alpha_{\max}$ in the limit Ma $\downarrow$ 0.

The marginal wavenumber equation (120) is approximately

$$c_1(m-1)\mathrm{MaB} + c_2\mathrm{MaB}^3 \approx 0 \tag{134}$$

in the limit Ma $\downarrow$ 0, where the coefficients $c_i(\alpha, s, m)$ $(i = 1, 2)$ are positive. For $m \geq 1$ the only solution is B ≈ 0, which implies that $\alpha_0 \approx |\mathrm{Bo}|^{1/2}$ and is only valid for Bo < 0. This result agrees with panel (f) of figure 25 as Ma $\downarrow$ 0 for $m \geq 1$. The error is less than 1% when Ma $< 1.09 \times 10^{-3}$ for $m = 4$ and Ma $< 2.3 \times 10^{-11}$ for $m = 1$. (When $m = 1$, it is generally required that Ma be very small for the error to be less than 1%.) In panels (e) and (f) the thin dashed lines for $m < 1$ were obtained by solving (134) numerically. These approximations are quite good for Ma $\downarrow$ 0, for example, when $m = 0.9, 0.5$ and 0.1 the asymptotic solution to equation (134) has an error less than 1% when Ma $< 1.1 \times 10^{-3}, 1.47 \times 10^{-2}$ and .378 for Bo $= -0.1$ and for Bo $= 0.1$ when Ma $< 1.02 \times 10^{-3}, 1.42 \times 10^{-2}$ and .392.

When $m \geq 1$ and Bo > 0 the marginal wavenumber $\alpha_0 \downarrow 0$ and thus the longwave approximation can be used. For $m > 1$, the α_0 approximation is found from the balance of the second and third terms in equation (121), yielding

$$\alpha_0 \approx \frac{3}{2(m-1)}\mathrm{MaBo}^{-1}, \tag{135}$$

and for $m = 1$ the first two terms in equation (121) yield the dominant balance, and so

$$\alpha_0 \approx 3s\,[3\mathrm{Ma}]^{1/2}\,\mathrm{Bo}^{-3/2}. \tag{136}$$

Both approximations (135) and (136) converge to the numerically obtained solutions. The error is less than 1% when $\mathrm{Ma} < 7.05 \times 10^{-3}$ for $m = 4$ and $\mathrm{Ma} < 8.5 \times 10^{-8}$ for $m = 1$ which again is not as good when $m = 4$. Again recall that when $m < 1$ and $\mathrm{Bo} > 0$ equation (134) is solved numerically.

The dependence of $(\alpha_{\max}, \gamma_{R\max})$ on m is investigated next for $\mathrm{Bo} > 0$ and $m < 1$. Since figure 25 (a) shows that $\gamma_{R\max} \downarrow 0$ as $\mathrm{Ma} \downarrow 0$, it is not difficult to ascertain that equation (58) can be approximated by a linear equation in γ_R,

$$c_{10}(\alpha, s, m, \mathrm{Bo})\gamma_R + c_{01}(\alpha, s, m, \mathrm{Bo})\mathrm{Ma} \approx 0,$$

whose solution is

$$\gamma_R = -\frac{c_{01}(\alpha, s, m, \mathrm{Bo})}{c_{10}(\alpha, s, m, \mathrm{Bo})}\mathrm{Ma}. \tag{137}$$

$\alpha_{\max}$ is found by solving $d\gamma_R/d\alpha = 0$ numerically and $\gamma_{R\max}$ is obtained by substituting $\alpha_{\max}$ into (137). The $(\alpha_{\max}, \gamma_{R\max})$ solutions obtained for $m = 0.9, 0.5$ and 0.1 are approximately $(0.330, 9.80 \times 10^{-7})$, $(0.699, 5.36 \times 10^{-7})$, and $(0.906, 4.00 \times 10^{-7})$. These agree with the results shown in panel (c).

For $m \geq 1$, figure 25 (c) shows that $\alpha_{\max} \downarrow 0$ as $\mathrm{Ma} \downarrow 0$. In the longwave limit for Ma

$\ll 1$, equations (58) and (61) are approximately given by

$$1296\gamma_R^4 + 864\mathrm{Bo}\alpha^2\gamma_R^3 + 36\left(5\mathrm{Bo}^2 + 9s^2(m-1)^2\right)\alpha^4\gamma_R^2$$
$$+\left(12\mathrm{Bo}^2 + 108s^2(m-1)^2\right)\mathrm{Bo}\alpha^6\gamma_R + 54(m-1)s^2\mathrm{BoMa}\alpha^7 - 81s^2\mathrm{Ma}^2\alpha^6 \approx 0 \qquad (138)$$

and

$$1296m\gamma_R^4 + 288\mathrm{Bo}\alpha\gamma_R^3 + \left(120\mathrm{Bo}^2 + 54s^2(m-1)^2\right)\alpha^3\gamma_R^2$$
$$+\left(12\mathrm{Bo}^2 + 108s^2(m-1)^2\right)\mathrm{Bo}\alpha^5\gamma_R + 63(m-1)s^2\mathrm{BoMa}\alpha^6 - 81s^2\mathrm{Ma}^2\alpha^5 \approx 0. \qquad (139)$$

The numerics suggest that $\alpha_{\max} \sim k_1\mathrm{Ma}$ and $\gamma_{R\max} \sim k_2\mathrm{Ma}^2$ for $m > 1$, and consequently no terms in (138) and (139) can be neglected since all terms in equation (138) are of the same order. Equations (138) and (139) are solved numerically for the coefficients k_1 and k_2 which depend on the value of m. For $m = 4$, $k_1 \approx 0.208$, and $k_2 \approx 2.5$, and the errors in $\alpha_{\max}$ and $\gamma_{R\max}$ are less than 1% when $\mathrm{Ma} < 1.34\times10^{-3}$ and $\mathrm{Ma} < 6.6\times10^{-4}$, respectively.

Equations (138) and (139) can be simplified for $m = 1$ case,

$$1296\gamma_R^4 + 864\mathrm{Bo}\alpha^2\gamma_R^3 + 180\mathrm{Bo}^2\alpha^4\gamma_R^2 + 12\mathrm{Bo}^3\alpha^6\gamma_R + 3\mathrm{Bo}^3\mathrm{Ma}\alpha^8 - 81s^2\mathrm{Ma}^2\alpha^6 = 0 \qquad (140)$$

and

$$1296m\gamma_R^4 + 288\mathrm{Bo}\alpha\gamma_R^3 + 120\mathrm{Bo}^2\alpha^3\gamma_R^2 + 12\mathrm{Bo}^3\alpha^5\gamma_R + 4\mathrm{Bo}^3\mathrm{Ma}\alpha^7 - 81s^2\mathrm{Ma}^2\alpha^5 = 0. \qquad (141)$$

Equation (141) is multiplied by α and subtracted from equation (140) in order to eliminate

the α^6 terms, yielding the following equation

$$1296\gamma_R^4 + 576\mathrm{Bo}\alpha^2\gamma_R^3 + 60\mathrm{Bo}^2\alpha^4\gamma_R^2 - \mathrm{Bo}^3\mathrm{Ma}\alpha^8 = 0. \tag{142}$$

The correct balance is between the last two terms in (142), which yields

$$\gamma_R \approx \frac{\sqrt{15}}{30}\mathrm{Bo}^{1/2}\mathrm{Ma}^{1/2}\alpha^2. \tag{143}$$

Substituting (143) into (140) and keeping the dominant terms, the linear term in γ_R and the last term yields

$$\alpha_{\max} \approx \frac{1}{2}3^{7/4}5^{1/4}2^{1/2}s\mathrm{Bo}^{-7/4}\mathrm{Ma}^{3/4}, \tag{144}$$

and therefore

$$\gamma_{R\max} \approx \frac{27}{4}s^2\mathrm{Bo}^{-3}\mathrm{Ma}^2. \tag{145}$$

The errors in using expressions (144) and (145) are less than 1% when $\mathrm{Ma} < 3 \times 10^{-11}$ and $\mathrm{Ma} < 8.9 \times 10^{-7}$, respectively.

Next the dependence of $(\alpha_{\max}, \gamma_{R\max})$ on m for $\mathrm{Bo} < 0$ is investigated in the limit $\mathrm{Ma} \downarrow 0$. It is sufficient to retain the dominant (constant) Ma terms in equations (58) and (61). These terms appear in all γ_R terms except the constant term. Equations (58) and (61) are approximately given by

$$c_{40}(\alpha)\gamma_R^4 + c_{30}(\alpha)\gamma_R^3 + c_{20}(\alpha)\gamma_R^2 + c_{10}(\alpha)\gamma_R \approx 0 \tag{146}$$

and

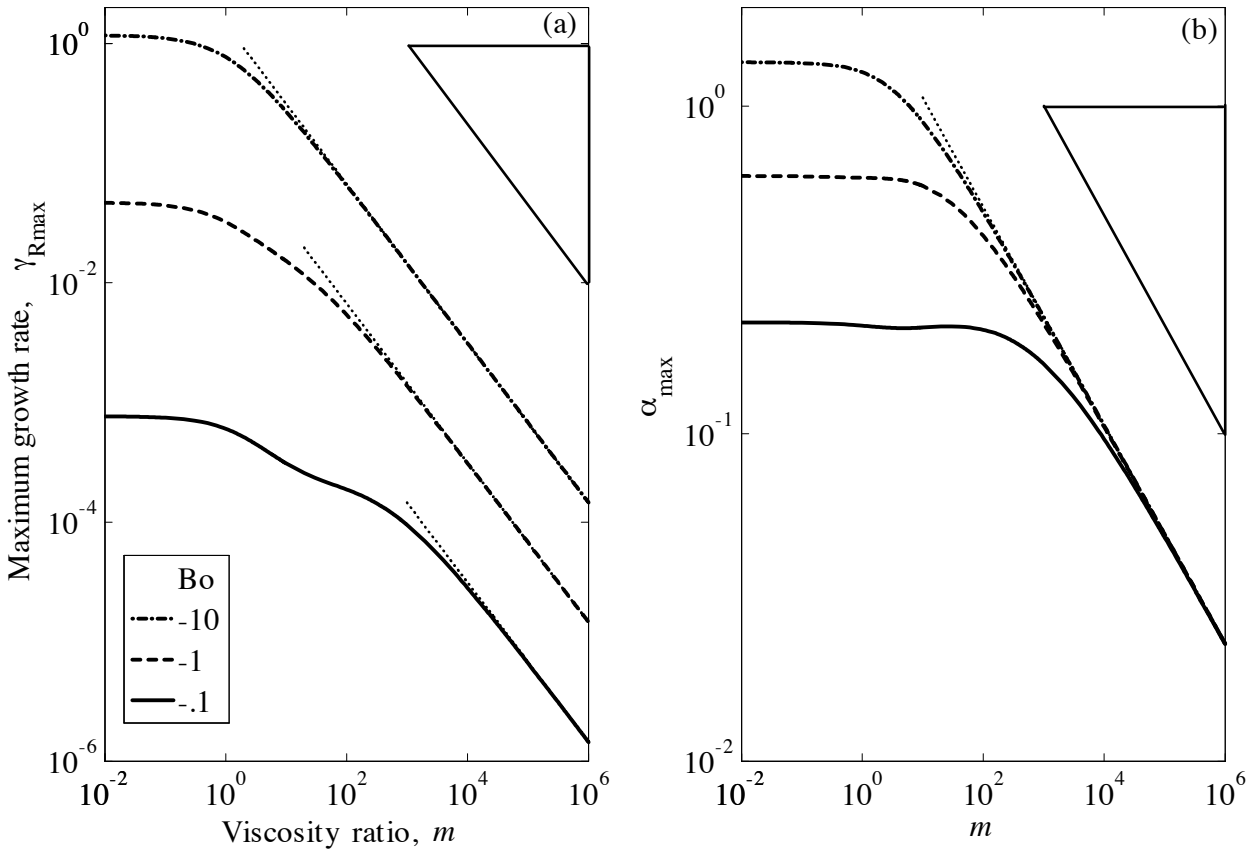

FIG. 28: (a) $\gamma_{R\max}$ and (b) $\alpha_{\max}$ vs m in the limit Ma $\downarrow 0$, for the indicated values of Bo, and $s = 1$. The thin lines correspond to the large m asymptotics described by equations (153) and (152).

$$\gamma_R^4 \frac{d}{d\alpha} c_{40}(\alpha) + \gamma_R^3 \frac{d}{d\alpha} c_{30}(\alpha) + \gamma_R^2 \frac{d}{d\alpha} c_{20}(\alpha) + \gamma_R \frac{d}{d\alpha} c_{10}(\alpha) \approx 0 \tag{147}$$

where $c_{i0}(\alpha, s, m, \mathrm{Bo})$ $(i = 1, 4)$. In figure 28 $\gamma_{R\max}$ and $\alpha_{\max}$ are plotted versus m for the three indicated values of Bo by solving equations (146) and (147) numerically. Both $\gamma_{R\max}$ and $\alpha_{\max}$ approach a non-zero constant (dependent on the value of Bo) as $m \downarrow 0$. However, in the limit $m \uparrow \infty$, both $\gamma_{R\max}$ and $\alpha_{\max}$ decrease to zero, and $\alpha_{\max}$ is independent of Bo.

Since $\gamma_{R\max} \downarrow 0$ as $m \uparrow \infty$ the quartic and cubic terms in γ_R in equation (146) can be

neglected, so that

$$c_{10}(\alpha)\gamma_R + c_{20}(\alpha)\gamma_R^2 \approx 0.$$

Therefore,

$$\gamma_R \approx -\frac{c_{10}(\alpha)}{c_{20}(\alpha)}. \tag{148}$$

Again, $\alpha_{\max}$ is found by solving $d\gamma_R/d\alpha = 0$ or

$$-c_{20}\frac{dc_{10}}{d\alpha} + c_{10}\frac{dc_{20}}{d\alpha} = 0 \tag{149}$$

and $\gamma_{R\max}$ is found by substituting $\alpha_{\max}$ into (148). The longwave approximation can be used to obtain the asymptotic behavior of $(\gamma_{R\max}, \alpha_{\max})$ since $\alpha_{\max} \downarrow 0$. After performing a Taylor series expansion of c_{10} and c_{20} about $\alpha = 0$ and keeping the dominant m terms, equations (148) and (149) become to leading order

$$\gamma_R \approx -\frac{\mathrm{Bo}\alpha^2}{12 + 2m\alpha^3} \tag{150}$$

and

$$m^3\alpha^5 - 12m^2\alpha^2 - 21m\alpha - 12 = 0. \tag{151}$$

The correct balance is between the first and second terms in (151), yielding

$$\alpha_{\max} \approx 12^{1/3}m^{-1/3}. \tag{152}$$

Then $\gamma_{R\max}$ is obtained by substituting (152) into (150) yielding

$$\gamma_{R\max} \approx -\frac{12^{2/3}}{36}\mathrm{Bo}m^{-2/3}. \tag{153}$$

For the values of Bo $= -0.1, -1$ and -10, the errors in $\alpha_{\max}$ and $\gamma_{R\max}$ are less than 1% when $m > 3.78\times10^5, 1.3\times10^4$ and 870 and $m > 3.81\times10^5, 1.25\times10^4$ and 540 , respectively.

In the limit as $m \downarrow 0$, additional terms can be dropped from equations (146) and (147) whose solutions depend on s and Bo. However, not much insight is gained in displaying these equations since their solutions are obtained numerically.

Next, the influence of the Bond number on the maximum growth rate $\gamma_{\max}$, the corresponding wavenumber $\alpha_{\max}$ and the marginal wavenumber α_0 is investigated. In figure 29 $\gamma_{R\max}$, $\alpha_{\max}$ and α_0 are plotted versus Bo. As for the finite n case in the S sectors (see figure 12b), figure 29 shows that the dominant branch is always longwave unstable, and there can be a discontinuity in the graph of $\alpha_{\max}$ (see figure 32 discussion).

In the limit as Bo $\downarrow -\infty$, figure 29 (c) suggests that $\alpha_0 \uparrow \infty$. Note that as $\alpha \uparrow \infty$, $s_\alpha \sim e^\alpha$ and $c_\alpha \sim e^\alpha$ and therefore $s_\alpha, c_\alpha \gg \alpha$. Using these approximations the marginal wavenumber equation (120) becomes to leading order

$$k_1\alpha^6\mathrm{Ma}^2 + k_2\alpha^4\mathrm{MaB} + k_3e^{4\alpha}\alpha^{-2}\mathrm{B}^3\mathrm{Ma} + k_4e^{4\alpha}\mathrm{Ma}^2\mathrm{B}^2 + k_5e^{4\alpha}\alpha^2\mathrm{Ma}^3\mathrm{B} \approx 0, \tag{154}$$

where the coefficients k_i $(i = 1, 5)$ depend on m and s. Assuming that Ma and B are not large, the first term dominates the second term, and the last term is much larger than the third and fourth terms in equation (154). Balancing the first and last terms of (154) yields

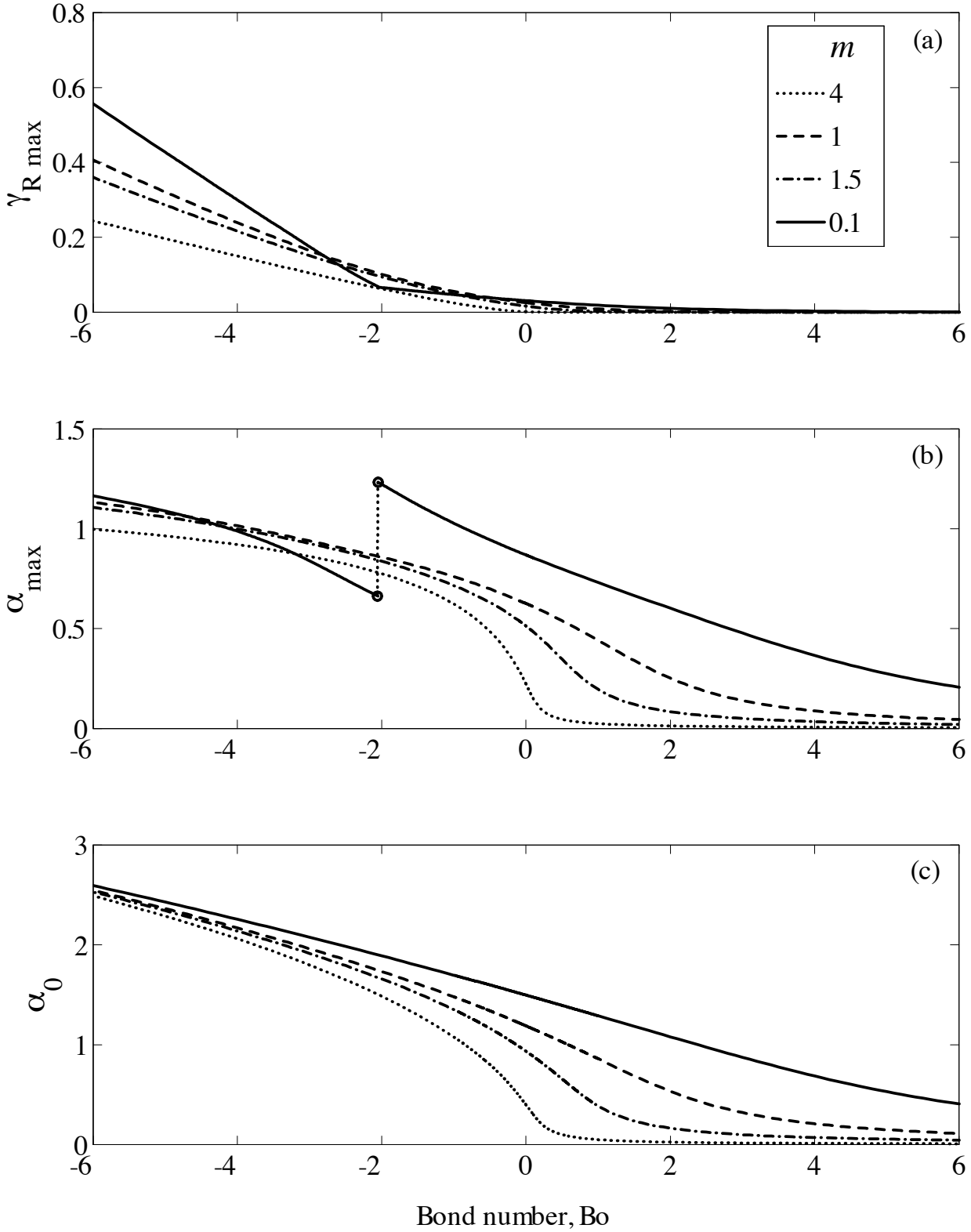

FIG. 29: (a) $\gamma_{R\,\max}$, (b) $\alpha_{\max}$ and (c) α_0 are plotted vs Bo for Ma = 0.1, $s = 1.0$, and four different values of m given in the legend.

the following expression for B:

$$\mathrm{B} \sim -\frac{k_1}{k_5}\alpha^4 e^{-4\alpha}\mathrm{Ma}^{-1}.$$

Thus the Bond number is given by

$$\mathrm{Bo} \sim -\alpha^2 + \frac{4s^2(2m+1)}{(m+1)^2}\alpha^4 e^{-4\alpha}\mathrm{Ma}^{-1}. \tag{155}$$

The marginal wavenumber α_0 is expressed as an infinite series by solving (155) for α in terms of Bo as $\alpha \uparrow \infty$. The first two terms are

$$\alpha_0 \approx |\mathrm{Bo}|^{1/2} + \frac{2s^2(2m+1)}{(m+1)^2}e^{-4|\mathrm{Bo}|^{1/2}}\mathrm{Ma}^{-1}\,|\mathrm{Bo}|^{3/2}. \tag{156}$$

This asymptotic formula agrees very well with the numerical results shown in figure 29 (c) even when |Bo| is not large for sufficiently large viscosity ratios. The the error is found to be less than 1% for $m = 0.1, 1.0, 1.5$ and 4.0 when $\mathrm{Bo} < -10.5, -9.31, -8.86$ and -7.28, respectively.

Next, the asymptotic behavior of α_0 in the limit $\mathrm{Bo} \uparrow \infty$ is examined. A longwave analysis can be used for this case since, figure 29(c) shows that $\alpha_0 \downarrow 0$ as $\mathrm{Bo} \uparrow \infty$. In order to obtain an expression for α_0, the longwave coefficients F_2, F_1 and F_0 (B5)-(B9) are substituted into (59), and to leading order the equation for α is

$$\frac{1}{108}\mathrm{Bo}^3\alpha^2 - \frac{1}{4}s^2\mathrm{Ma} + \frac{1}{6}(m-1)\,s^2\,\mathrm{Bo}\alpha + \frac{1}{18}\mathrm{MaBo}^2\alpha^2 \approx 0. \tag{157}$$

Here, the dominant balance is between the first two terms which gives

$$\alpha_0 \approx \alpha_{00} = 3s\,[3\mathrm{Ma}]^{1/2}\,\mathrm{Bo}^{-3/2}. \tag{158}$$

Corrections to α_{00}, are determined by expressing α_0 as a power series in fractional powers of Bo

$$\alpha_0 = \alpha_{00} + \alpha_{01}\mathrm{Bo}^{-2} + \alpha_{02}\mathrm{Bo}^{-5/2} + ... \tag{159}$$

and substituting this series into (157) to obtain

$$\alpha_{01} = 9s^2(1-m) \text{ and } \alpha_{02} = \frac{9\sqrt{3}}{2}s(s^2(1-m)^2 - 2\mathrm{Ma}^2)\mathrm{Ma}^{-1/2}. \tag{160}$$

The asymptotics indicate that for fixed but large Bo, α_0 decreases with increasing m, as shown in figure 29. All three terms in (160) were used to approximate α_0 and the error of these approximations are less than 1% for $m = 0.1, 1.0, 1.5$ and 4.0 when Bo $> 66.6, 19.2, 13.8$ and 1130, respectively.

A small $\alpha_{\max}$ and $\gamma_{R\max}$ analysis can also be carried out in the limit as Bo $\uparrow \infty$, see figures 29 (a) and (b). In this limit, equations (58) and (61) are approximately

$$\begin{aligned} &1296\gamma_R^4 + 864\mathrm{Bo}\alpha^2\gamma_R^3 + 108\mathrm{Bo}^2\alpha^4\gamma_R^2 + 12\mathrm{Bo}^3\alpha^6\gamma_R \\ &+3\mathrm{Bo}^3\mathrm{Ma}\alpha^8 + 54(m-1)s^2\mathrm{BoMa}\alpha^7 - 81s^2\mathrm{Ma}^2\alpha^6 \approx 0 \end{aligned} \tag{161}$$

and

$$1296m\gamma_R^4 + 288\mathrm{Bo}\alpha\gamma_R^3 + 120\mathrm{Bo}^2\alpha^3\gamma_R^2 + 12\mathrm{Bo}^3\alpha^5\gamma_R$$
$$+4\mathrm{Bo}^3\mathrm{Ma}\alpha^7 + 63(m-1)s^2\mathrm{BoMa}\alpha^6 - 81s^2\mathrm{Ma}^2\alpha^5 \approx 0. \tag{162}$$

Equation (162) multiplied by α and subtracted from equation (161) in order to eliminate the terms proportional to α^6 in (161). This operation yields

$$1296\gamma_R^4 + 576\mathrm{Bo}\alpha^2\gamma_R^3 + 60\mathrm{Bo}^2\alpha^4\gamma_R^2 - 9(m-1)s^2\mathrm{MaBo}\alpha^7 - \mathrm{Bo}^3\mathrm{Ma}\alpha^8 \approx 0. \tag{163}$$

When $m < 1$ the only negative term in (163) is the last one, which is balanced with the second to last term yielding

$$\alpha_{\max} \approx 9(1-m)s^2\mathrm{Bo}^{-2}. \tag{164}$$

Equation (161) can be further simplified since $\alpha_{\max} \sim \mathrm{Bo}^{-2}$, and thus the constant terms in γ_R proportional to $\mathrm{Bo}^3\alpha^8$ and $\mathrm{Bo}\alpha^7$ can be dropped. It now becomes

$$1296\gamma_R^4 + 864\mathrm{Bo}\alpha^2\gamma_R^3 + 108\mathrm{Bo}^2\alpha^4\gamma_R^2 + 12\mathrm{Bo}^3\alpha^6\gamma_R - 81s^2\mathrm{Ma}^2\alpha^6 \approx 0. \tag{165}$$

It turns out that all the terms in (165) are of the same size, with $\gamma_{R\max} \sim k_1\mathrm{Bo}^{-3}$. The coefficient k_1 is obtained by numerically solving a polynomial in k_2 when $m < 1$. For $m > 1$, the proper balance is between the last term and the γ_R^2 term in equation (163), which yields

$$\gamma_R \approx \left(\frac{\mathrm{MaBo}}{60}\right)^{1/2}\alpha^2. \tag{166}$$

With the aid of equation (166), equation (161) can be further simplified by dropping terms smaller than $\mathrm{Bo}^3\alpha^8$. Substituting this into equation (161) allows terms to be neglected and reduces to

$$12\mathrm{Bo}^3\alpha^6\gamma_R - 81s^2\mathrm{Ma}^2\alpha^6 \approx 0 \tag{167}$$

yielding

$$\gamma_{R\max} \approx \frac{27}{4}s^2\mathrm{Bo}^{-3}\mathrm{Ma}^2. \tag{168}$$

Equating equations (166) and (168) gives

$$\alpha_{\max} \approx \frac{1}{2}3^{7/4}5^{1/4}2^{1/2}s\mathrm{Bo}^{-7/4}\mathrm{Ma}^{3/4}. \tag{169}$$

The error in the $\gamma_{R\max}$ approximation is less than 1% for $m = 0.1, 1.0, 1.5$ and 4.0 when $\mathrm{Bo} > 1.08 \times 10^3, 1.6 \times 10^4, 2.5 \times 10^4$ and 6.9×10^4, respectively, while the error of the $\alpha_{\max}$ approximation is less than 1% for $m = 0.1, 1.0, 1.5$ and 4.0 when $\mathrm{Bo} > 6.23 \times 10^8, 2.73 \times 10^3, 5.91 \times 10^7$ and 7.5×10^{10}, respectively.

In the limit $\mathrm{Bo} \downarrow -\infty$, the numerics suggest that $\gamma_{R\max} \sim k\mathrm{Bo}$, and that $\alpha_{\max}$ approaches some non zero constant. Under such assumptions, equation (58) becomes

$$\begin{aligned}
&4\left(m^2\left(s_\alpha^2-\alpha^2\right)+2ms_\alpha c_\alpha+\alpha^2+c_\alpha^2\right)^3k^3\\
&+\frac{4}{\alpha}\left(m^2\left(s_\alpha^2-\alpha^2\right)+2ms_\alpha c_\alpha+\alpha^2+c_\alpha^2\right)^2\left(m\left(s_\alpha^2-\alpha^2\right)+s_\alpha c_\alpha-\alpha\right)k^2\\
&+\frac{5}{4\alpha^2}\left(m^2\left(s_\alpha^2-\alpha^2\right)+2ms_\alpha c_\alpha+\alpha^2+c_\alpha^2\right)\left(m\left(s_\alpha^2-\alpha^2\right)+s_\alpha c_\alpha-\alpha\right)^2k\\
&+\frac{1}{8\alpha^3}\left(m\left(s_\alpha^2-\alpha^2\right)+s_\alpha c_\alpha-\alpha\right)^3=0.
\end{aligned} \tag{170}$$

The second equation, (61), is too lengthy to give here. However, these two equations for

$\alpha_{\max}$ and k must be solved numerically. In figure 30, $\alpha_{\max}$ and $-k$ are plotted versus m along with the asymptotic expressions that are valid for $m \uparrow \infty$, which are derived next. The numerics suggests that $\alpha \sim am^{-1/3}$ and $k \sim bm^{-2/3}$ for $m \gg 1$, which when substituted into (58) and (61) yield

$$\begin{aligned}&\frac{4}{27}a^9b^3 + \frac{8}{3}a^6b^3 + \frac{4}{27}a^8b^2 + \frac{5}{108}a^7b + 16a^3b^3\\&+\frac{16}{9}a^5b^2 + \frac{5}{18}a^4b + 32b^3 + \frac{16}{3}a^2b^2 + \frac{1}{216}a^6 = 0\end{aligned} \tag{171}$$

and

$$\begin{aligned}&\frac{16}{9}a^9b^3 + 24a^6b^3 + \frac{44}{27}a^8b^2 + \frac{25}{54}a^7b + 96a^3b^3\\&+\frac{128}{9}a^5b^2 + \frac{35}{18}a^4b + 96b^3 + \frac{80}{3}a^2b^2 + \frac{1}{24}a^6 = 0.\end{aligned} \tag{172}$$

The numerically computed values for a and b are $a \approx 2.28$ and $b \approx -0.145$. These expressions are plotted in figure 30 as dashed lines next to the solutions obtained by solving equation (170) and the equation obtained by differentiating equation (170) with respect to α and setting $d\gamma_R/d\alpha = 0$. The errors of these two approximations are less than 1% when $m > 190$ and $m > 70$, respectively.

In the limit $m \downarrow 0$, figure 30 shows $\alpha_{\max}$ and k approach some non-zero constant. In this case, to leading order, only the terms independent of m in equation (170) are kept,

$$\begin{aligned}&4\left(\alpha^2 + c_\alpha^2\right)^3 k^3 + \frac{4}{\alpha}\left(\alpha^2 + c_\alpha^2\right)^2 \left(s_\alpha c_\alpha - \alpha\right) k^2\\&+\frac{5}{4\alpha^2}\left(\alpha^2 + c_\alpha^2\right)\left(s_\alpha c_\alpha - \alpha\right)^2 k + \frac{1}{8\alpha^3}\left(s_\alpha c_\alpha - \alpha\right)^3 \approx 0.\end{aligned} \tag{173}$$

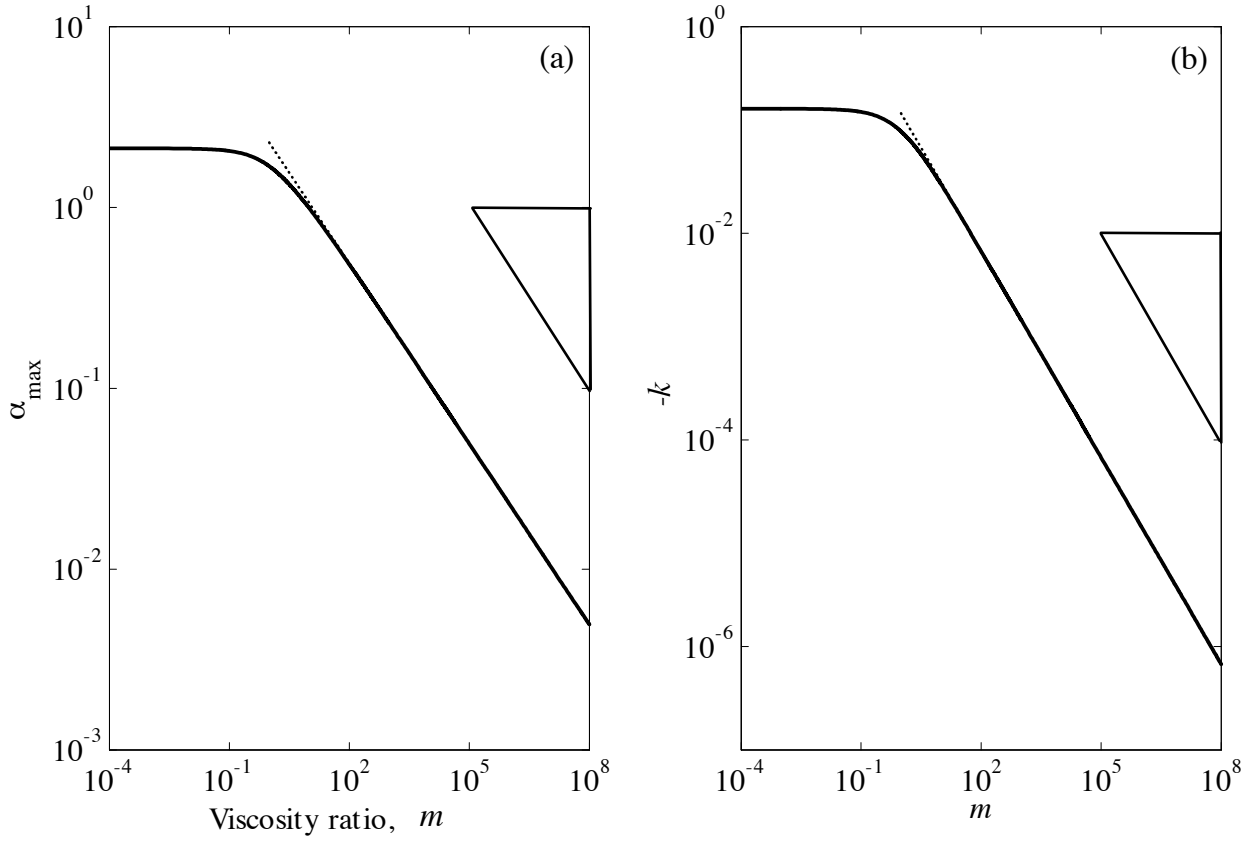

FIG. 30: (a) $\alpha_{\max}$ and (b) $-k$ for Bo $= -\infty$ vs m. The dashed lines are the approximations $\alpha_{\max} \approx 2.28m^{-1/3}$ and $k \approx -0.145m^{-2/3}$. Here $s = 1$.

The numerical solution of equation (173) and the derivative of equation (173) with respect to α (too large to display here) yields $\alpha_{\max} \approx 2.12$ and $k \approx -.161$. These values agree with the results shown in figure 30 as $m \downarrow 0$.

The zero gravity case studied in FH and HF did not mention the possible crossing of the two dispersion curves. Figure 31 shows dispersion curves of both branches for increasing values of Marangoni number when Bo $= 0$. In panel (a) the surfactant branch (dashed curve) disappears when Ma $= 0$ since $\gamma_R = 0$ and the robust branch (solid curve) is stable when Ma $= 0$. As Ma increases, the surfactant branch becomes unstable for small values of k and the two branches cross each other (panels (b)-(e)). When Ma is sufficiently large (Ma

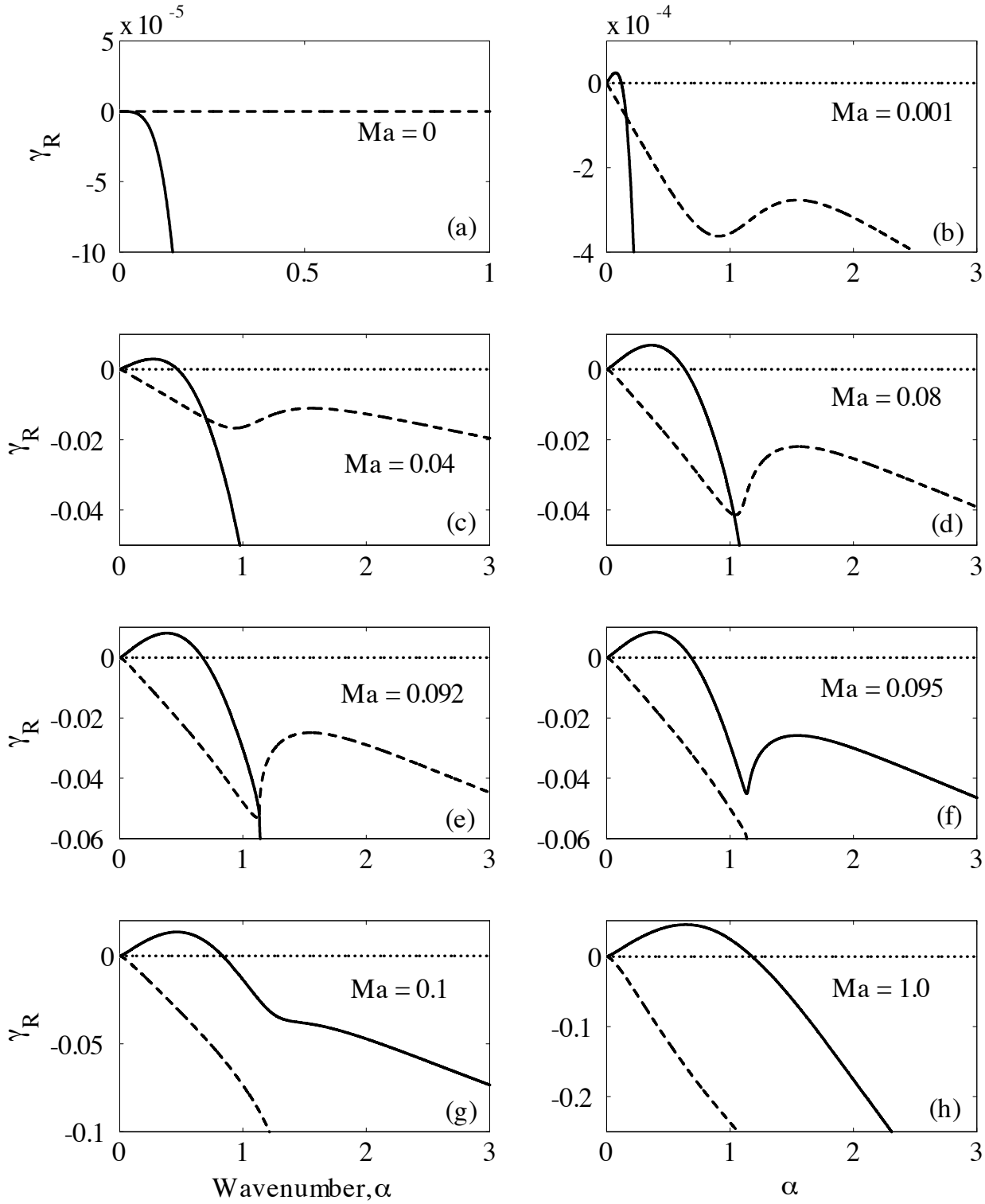

FIG. 31: Dispersion curves depicting the evolution of the two branches as Ma increases for the zero gravity case. Here $m = 2$ and $s = 1$.

> 0.092) the branches split (panels (f)-(h)). As Ma increases from 0, the robust branch becomes longwave unstable and the surfactant branch appears and develops local minima and maxima but remains stable (panel (b)). The crossing of the two branches moves toward the local minima of the surfactant branch (panels (c)-(d)) and they eventually meet (panel (e)). Panel (f) shows there is a reconnection of the surfactant and robust branches since the two stable local extrema now belong to the robust branch and not the surfactant branch. As Ma continues to increase the local extrema flatten out (panel (g)) until the robust branch is longwave unstable and the surfactant branch is stable (panel (h)).

Evidence has shown the midwave instability can occur for $n = \infty$ provided $m < 1$. Figure 32 shows dispersion curves of both branches for negative values of Bo in increasing order of magnitude. Here the surfactant branch and the robust branch are represented by dashed and solid curves, respectively. For $\alpha \ll 1$ the robust branch is unstable and the surfactant branch is stable. In panel (a) the surfactant branch has a local maximum and the robust branch is longwave unstable. As |Bo| increases the surfactant branch local maximum rises above the $\gamma_R = 0$ line and becomes midwave unstable (panel (b)). A further increase in |Bo| shows the dispersion curves can exhibit a midwave instability and branch crossing simultaneously which was not seen for finite n (see figure 18) as shown in panel (c). At some point there is a jump in the global maximum from the longwave unstable robust branch maximum to the midwave unstable surfactant branch maximum (panel (d)). Eventually these two regions disappear one by one with further increase in |Bo|, and one should note the change of the branch curve style from panel (d) to panel (e). The second separation is easier to see in panel (f). Panel (g) shows the midwave unstable surfactant branch develops one local minimum between two local maximums that separates two regions of midwave instability. As |Bo| continues to increase the right most local maximum drops

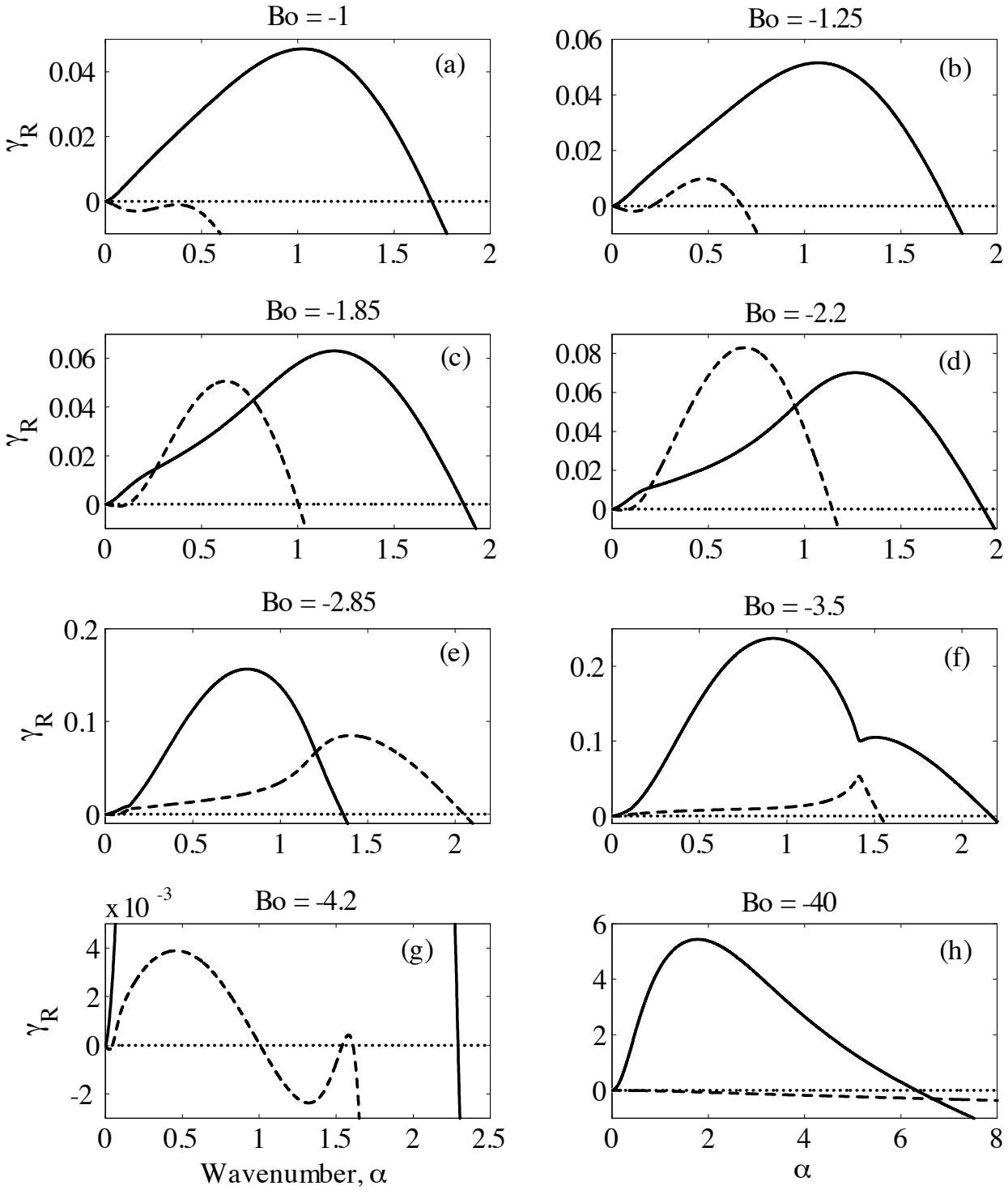

FIG. 32: Dispersion curves depicting the evolution of the two branches as the magnitude of Bo increases. Here $m = 0.1$, $s = 1$, and Ma $= 0.1$.

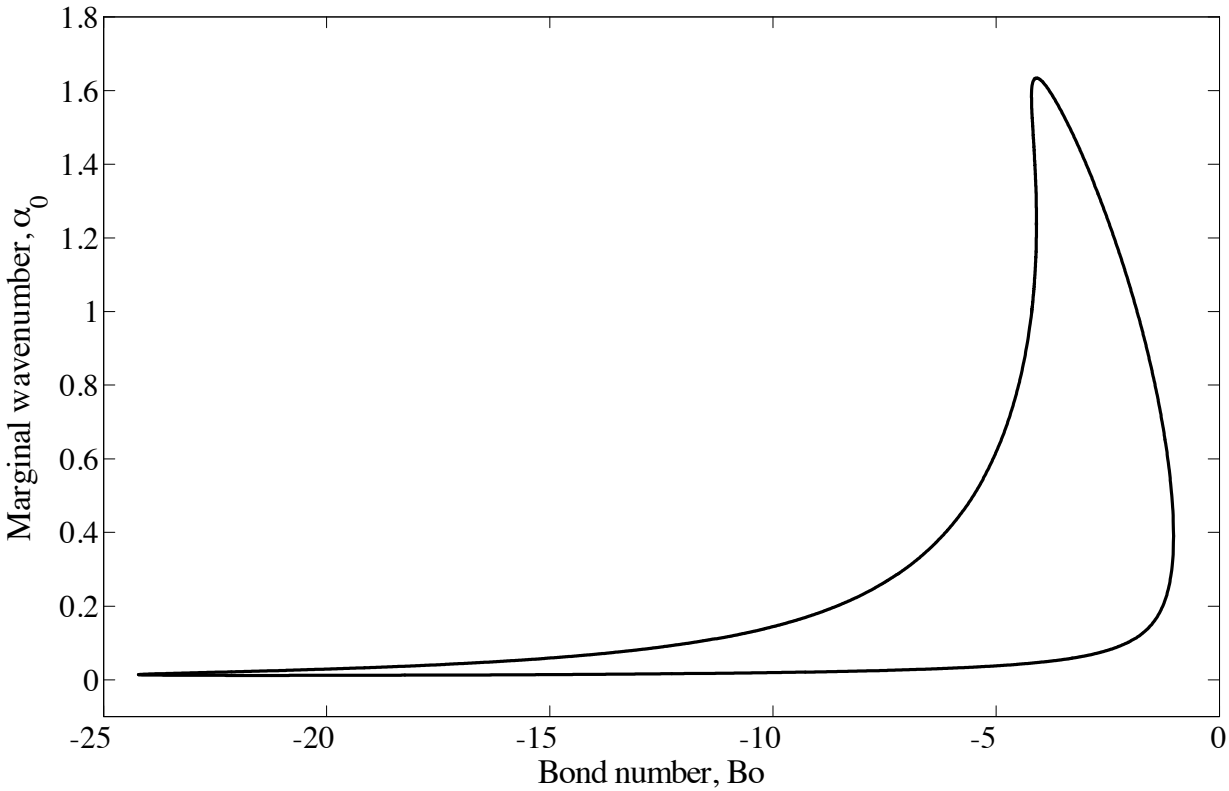

FIG. 33: The multiple marginal wavenumbers of the less dominant branch corresponding to the midwave instability shown in figure 32.

below the $\gamma_R = 0$ line leaving a single region of midwave stability until the left most local maximum also drops below the $\gamma_R = 0$ line and the surfactant branch becomes stable for Bo $\downarrow -\infty$ while the robust branch remains longwave unstable (panel h).

The multiple surfactant branch α_0 locations (up to four) yielding the midwave unstable region(s) are tracked and shown in figure 33. Although it is hard to see, the four α_0 values shown in figure 32 panel (g) for Bo $= -4.2$ are also shown in figure 33. The rightmost α_0 in figure 32 corresponds to the (solid line) α_0 in figure 29(c).

Again, it is possible for the discriminant to equal zero, note the branch crossings in figure 32. The branches are defined to be continuous in α which are depicted by the continuous solid and dashed dispersion curves in figures 31 and 32. However, the gaps in figure 31(f)

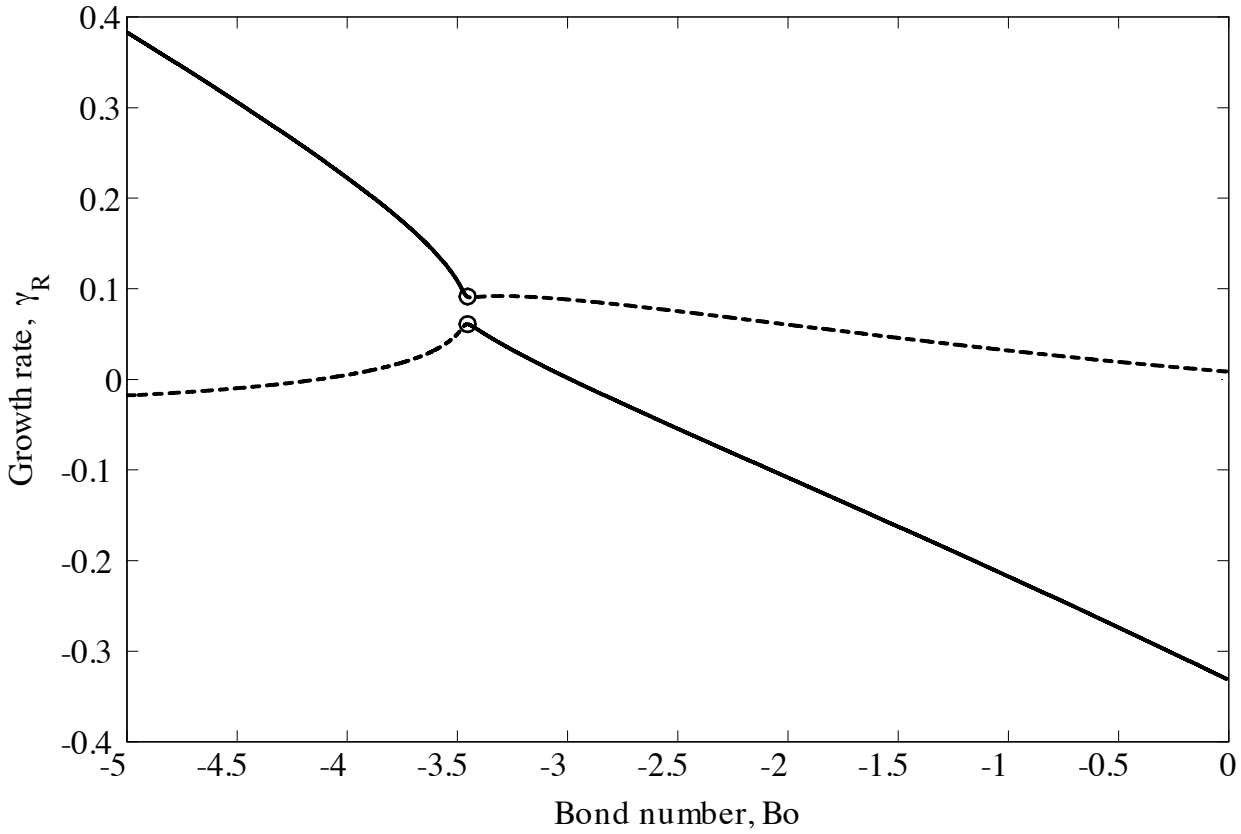

FIG. 34: The growth rate of the robust branch and surfactant branch vs Bo for fixed wavenumber. Here $\alpha = 1.4$, $m = 0.1$, $s = 1$ and Ma $= 0.1$.

and figure 32(e) and (f) suggest a discontinuity in Ma and Bo, respectively. This feature is explained by first noting the rightmost gap in figure 32(f) occurs at $\alpha \approx 1.4$ for Bo $= -3.5$. In figure 34 γ_R is plotted as a function of Bo for $\alpha = 1.4$. By tracking the branches (continuous in α) in figure 32 to those in figure 34 the branches clearly have a discontinuity in Bo at Bo ≈ -3.5. Similarly, the branches in figure 31 are always continuous in α but possibly discontinuous in Ma.

Even though the robust branch is always longwave unstable, a stability diagram of the surfactant midwave unstable branch is discussed. Equation (59) and the derivative of (59) are solved for the critical midwave Marangoni number Ma_{cM} and corresponding wavenumber

α_{cM}. In figure 35 (a) Ma_{cM} and (b) α_{cM} are plotted versus Bond number for the indicated values of m to obtain a midwave stability diagram. Note that for the selected values of m the surfactant branch is midwave unstable for $\mathrm{Ma} < \mathrm{Ma}_{cM}$ and is stable for $\mathrm{Ma} > \mathrm{Ma}_{cM}$. For example, when $m = 0.5$ there is midwave instability for values of Ma below the solid curve in panel (a).

Figure 35 shows that both Ma_{cM} and α_{cM} approach 0 in the limit $\mathrm{Bo} \downarrow -\infty$ and in the limit $\mathrm{Bo} \uparrow 0^-$. To obtain these asymptotics it is easier to first substitute the longwave expressions (B5)-(B9) into equation (59) and the derivative of equation (59) with respect to α. In the limit $\mathrm{Ma} \downarrow 0$, (59) and the derivative with respect to α are approximately

$$18(m-1)s^2\alpha^3 + \mathrm{Bo}^3\alpha^2 + 18(m-1)s^2\mathrm{Bo}\alpha - 27\mathrm{Ma}s^2 \approx 0 \tag{174}$$

and

$$81(m-1)s^2\alpha^3 + 4\mathrm{Bo}^3\alpha^2 + 63(m-1)s^2\mathrm{Bo}\alpha - 81\mathrm{Ma}s^2 \approx 0. \tag{175}$$

Note that equation (175) has been multiplied by a factor of α. As $|\mathrm{Bo}| \downarrow 0$ equations (174) and (175) simplify to

$$2(m-1)\alpha^3 + 2(m-1)\mathrm{Bo}\alpha - 3\mathrm{Ma} \approx 0 \tag{176}$$

and

$$9(m-1)\alpha^3 + 7(m-1)\mathrm{Bo}\alpha - 9\mathrm{Ma} \approx 0. \tag{177}$$

An expression for α_{cM} in terms of Bo is obtained by eliminating Ma from the above equations,

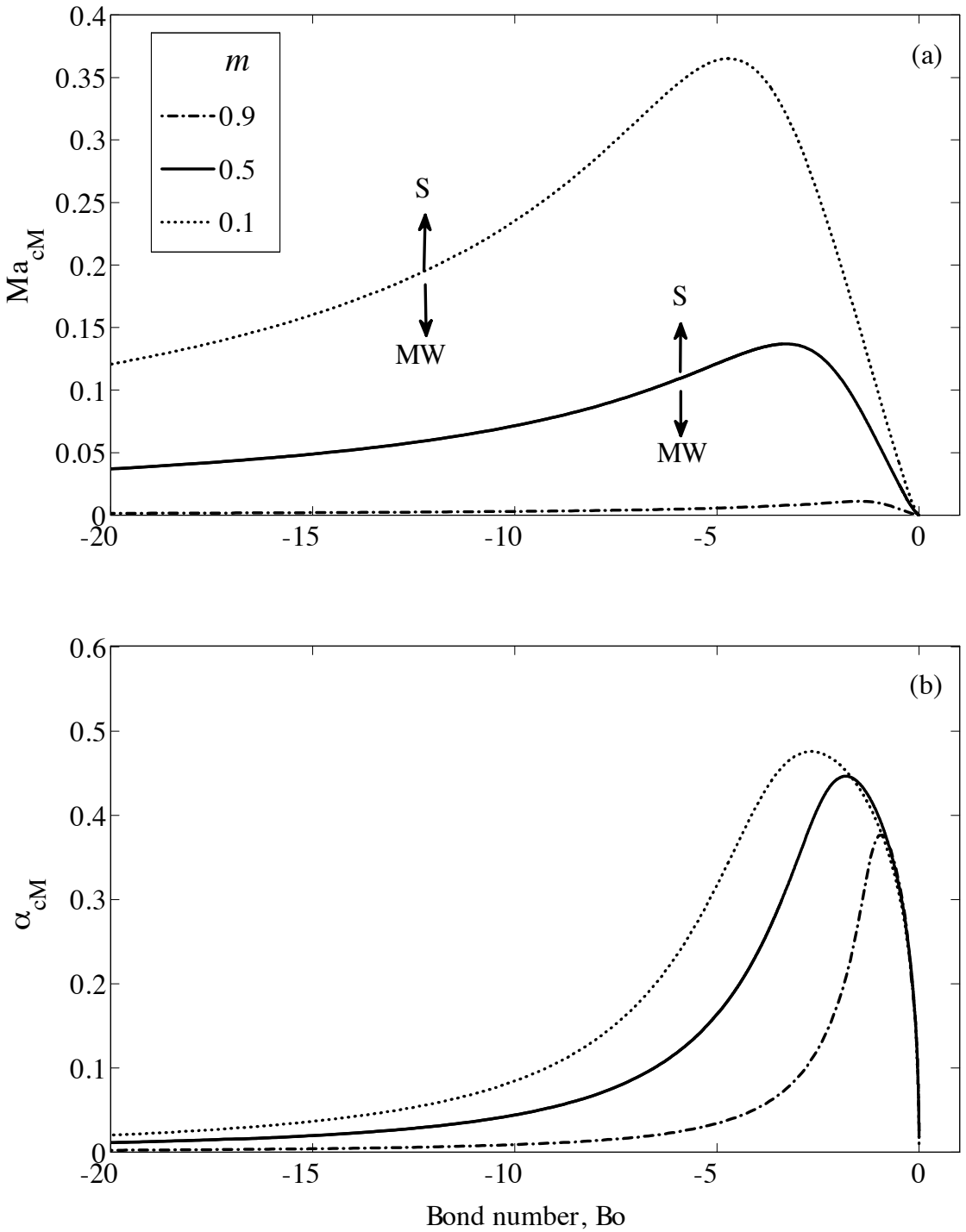

FIG. 35: (a) A stability diagram of Ma_{cM} and (b) corresponding α_{cM} as vs Bond number for the indicated values of m. The arrows indicate the stability or midwave instability for values of Ma above or below the Ma_{cM} curves. Here $s = 1$.

and is given by

$$\alpha_{cM} \approx \frac{\sqrt{3}}{3}\left(-\mathrm{Bo}\right)^{1/2}. \tag{178}$$

Substituting (178) into (176) and solving for the Marangoni number yields,

$$\mathrm{Ma}_{cM} \approx \frac{4\sqrt{3}}{27}(1-m)\left(-\mathrm{Bo}\right)^{3/2}. \tag{179}$$

The error of the α_{cM} approximation given by (178) is less than 1% for $m = 0.1, 0.5$ and 0.9 when $\mathrm{Bo} < -7.0 \times 10^{-5}$, -9.0×10^{-5}, and -1.2×10^{-4}, respectively, while the error of the Ma_{cM} approximation given by (179) is less than 1% when $\mathrm{Bo} < -6.0 \times 10^{-4}$, -8.0×10^{-4}, and -1.0×10^{-3}, respectively.

In the limit $\mathrm{Bo} \downarrow -\infty$, equations (174) and (175) reduce to

$$\mathrm{Bo}^3\alpha^2 + 18(m-1)s^2\mathrm{Bo}\alpha - 27\mathrm{Ma}s^2 \approx 0 \tag{180}$$

and

$$4\mathrm{Bo}^3\alpha^2 + 63(m-1)s^2\mathrm{Bo}\alpha - 81\mathrm{Ma}s^2 \approx 0. \tag{181}$$

Eliminating the Marangoni terms from the last two equations yields the following expression for α_{cM},

$$\alpha_{cM} \approx 9s^2(1-m)\left(-\mathrm{Bo}\right)^{-2}. \tag{182}$$

The critical Marangoni number, Ma_{cM}, is found by substituting (182) into (180), yielding

$$\mathrm{Ma}_{cM} \approx 3(1-m)^2 s^2\left(-\mathrm{Bo}\right)^{-1}. \tag{183}$$

These approximation are quite good even when Bo is not so large: the error of α_{cM} is less than 1% for $m = 0.1$, 0.5, and 0.9 when Bo < -24.1, -12.0, and -10.7, respectively, while the error of the Ma_{cM} approximation is less than 1% when Bo < -15.2, -21.5, and -12.8, respectively.

B. The conundrum of the Surfactant and Robust Branches

In this section details of which branch is the surfactant branch and which branch is the robust branch are given. The conundrum occurs from the difficulties in defining the branches under certain parameter values. Here is it sufficient to consider the longwave approximation in order to establish which branch is which.

In the limit of $\alpha \downarrow 0$, similar to the finite thickness $m = 1$ case, $|{F_1}^2| \ll |F_2 F_0|$ since $|(F_1)^2| \sim \alpha^4$ and $|F_2 F_0| \approx \mathrm{Im}(F_2 F_0) \sim \alpha^3$, which are also given in Appendix B 2. Therefore, the increment, equation (49), is approximated by (79) and the growth rates of the two branches (80) to leading order in α are

$$\gamma_R \approx \frac{\mathrm{Re}(\zeta^{1/2})}{2F_2} = \pm\frac{1}{2}\,(s\mathrm{Ma})^{1/2}\,\alpha^{3/2}. \tag{184}$$

It is clear that one branch is stable and the other is unstable. However, from the definition of the surfactant branch, $\gamma_R \to 0$ as $\mathrm{Ma} \downarrow 0$, it is not immediately clear whether the unstable branch in (184) is the surfactant or the robust branch.

The definition of continuous branches of the growth rate is more problematic here than in the finite thickness case with $m = 1$. Recall that the two distinct analytic branches of the function $\sqrt{\zeta}$ exist in any simply connected domain in the complex plane that does not contain the origin ($\zeta = 0$). For infinite n it is shown that $\zeta = 0$ for some values of α, Ma

and the other parameters. The imaginary part of ζ (81) is

$$\begin{aligned}\mathrm{Im}(\zeta) = \mathrm{Ma}s\alpha^3 \big\{ & m^2(s_\alpha^2 - \alpha^2) + m\left(s_\alpha^2 - \alpha^2 + s_\alpha c_\alpha - \alpha\right) \\ & + 2(c_\alpha^2 + \alpha^2) + s_\alpha c_\alpha(2m+1) + \alpha \big\} \\ & - s\alpha(\mathrm{Bo} + \alpha^2)\,(m-1)\left(m(s_\alpha^2 - \alpha^2) + s_\alpha c_\alpha - \alpha\right). \end{aligned} \tag{185}$$

Solving $\mathrm{Im}(\zeta) = 0$ for Marangoni number, yields

$$\mathrm{Ma} = \frac{(\mathrm{Bo} + \alpha^2)\,(m-1)\,(m(s_\alpha^2 - \alpha^2) + s_\alpha c_\alpha - \alpha)}{\alpha^2\left\{m^2(s_\alpha^2 - \alpha^2) + m(s_\alpha^2 - \alpha^2 + s_\alpha c_\alpha - \alpha) + 2(c_\alpha^2 + \alpha^2) + s_\alpha c_\alpha(2m+1) + \alpha\right\}}. \tag{186}$$

Note that not all values of (Bo,m) are appropriate here because Ma must be positive. The denominator of (186) and the factor $(m(s_\alpha^2 - \alpha^2) + s_\alpha c_\alpha - \alpha)$ are clearly positive, and thus the quantity $(\mathrm{Bo} + \alpha^2)\,(m-1)$ in the numerator must be positive. (Note that for $\alpha^2 \ll |\mathrm{Bo}|$ this means that either $\mathrm{Bo} > 0$ with $m > 1$ or $\mathrm{Bo} < 0$ with $m < 1$.)

To solve the system $\mathrm{Re}(\zeta) = 0$ and $\mathrm{Im}(\zeta) = 0$ for Ma and Bo (186) is substituted into $\mathrm{Re}(\zeta)$ which yields

$$\mathrm{Re}(\zeta) = A\mathrm{B}^2 + C \tag{187}$$

where $\mathrm{B} = \mathrm{Bo} + \alpha^2$, and A and C do not depend on Ma (see equations (B17) and (B18) in Appendix B 2). Therefore, $\mathrm{Bo} = \mathrm{Bo}(\alpha)$ where

$$\mathrm{Bo}(\alpha) = -\alpha^2 \pm \sqrt{-\frac{C}{A}}. \tag{188}$$

Substituting (188) for Bo into equation (186) yields Ma such that $\zeta = 0$ for a given α. Again only the values $\mathrm{Bo} = \mathrm{Bo}_m(\alpha)$ that yields $\mathrm{Ma} = \mathrm{Ma}_m(\alpha) > 0$ are valid. In figures 36(a) and (b) curves $\mathrm{Bo} = \mathrm{Bo}_m(\alpha)$ and $\mathrm{Ma} = \mathrm{Ma}_m(\alpha)$ are plotted for various values of m. If, for example, $m = 2$ and $\mathrm{Bo} = 2$ then the corresponding value of α is approximately 0.3 (see light dashed line figure 36(a)). With this value of α, $\mathrm{Ma}_2 \approx 0.14$ (see 36(b)). Thus for Bo $= 2$, $\zeta = 0$ at the point $(0.3, 0.14)$ in the αMa-plane.

Next it is shown that there is always a strip $\mathcal{D}_s = \{0 < \alpha < \alpha_s \ , \ \mathrm{Ma} > 0\}$ where $\zeta \neq 0$. Indeed, it appears in figure 36(a) that any horizontal line $\mathrm{Bo} = \mathrm{Bo}_f$ (constant) intersects any of the graphs of $\mathrm{Bo} = \mathrm{Bo}_m(\alpha)$ at no more than three points. If there are no intersections then the value of α_s is chosen completely arbitrarily. Otherwise, α_s must be smaller than the smallest α of the intersection points. For the purpose of this dissertation, the existence of $\mathcal{D}_s$ (and thus of the two branches of the growth rate) is sufficient with any small but finite α_s. The existence of α_s is shown analytically for small values of α.

Considering again figure 36(a), it is clear that the points $\zeta = 0$ correspond to zeros of the function $f(\alpha) = \mathrm{Bo}_m(\alpha) - \mathrm{Bo}_f$. Thus it suffices to show that $f(\alpha)$ has no zeros in some strip $\mathcal{D}_s$. Here one must allow for complex values of α and consider the complex valued function $f(\alpha) = \mathrm{Bo}_m(\alpha) - \mathrm{Bo}_f$ where $\mathrm{Bo}_m(\alpha)$ and $f(\alpha)$ are analytic continuations of the real functions from the real axis of the complex α-plane. In particular,

$$\mathrm{Bo}_m(\alpha) = -\alpha^2 + \sqrt{-\frac{C}{A}} \tag{189}$$

where α is complex (so that for example $\sinh \alpha$ in the expressions C and A given by equations (B17) and (B18) in Appendix B 2 are understood to be a function of a complex variable α).

First the $m = 1$ case is considered. The discriminant $D(\alpha) \neq 0$ for all α (see Appendix

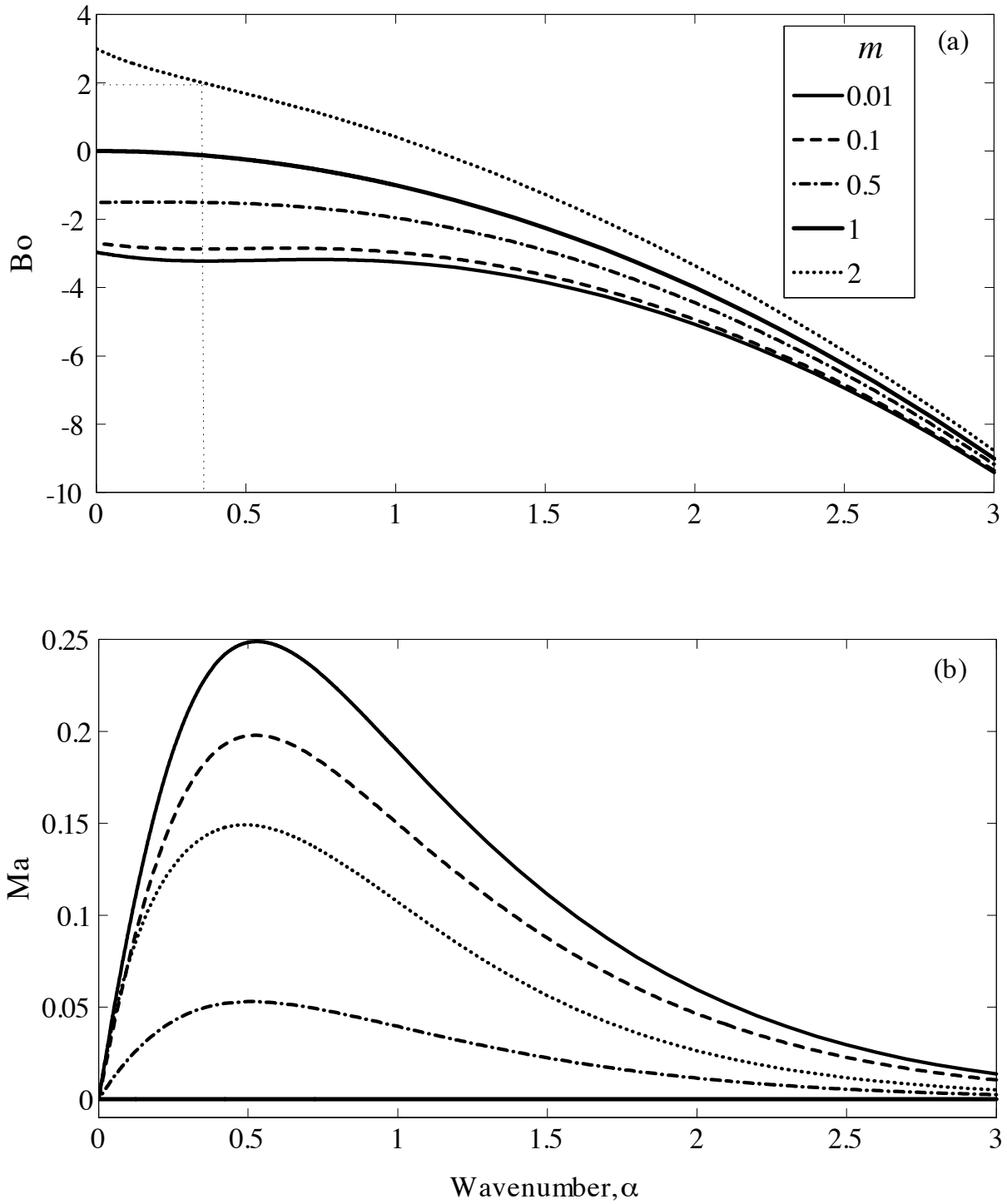

FIG. 36: (a) Curves $\mathrm{Bo} = \mathrm{Bo}_m(\alpha)$ and (b) $\mathrm{Ma} = \mathrm{Ma}_m(\alpha)$ vs α for select values of m.

B 2), and $f(\alpha) = -\alpha^2 - \mathrm{Bo}_f$. Clearly if $\mathrm{Bo}_f \geq 0$ then $f(\alpha)$ has no zeros except the one at the origin when $\mathrm{Bo}_f = 0$, and if $\mathrm{Bo}_f < 0$ then $f(\alpha)$ has a single zero at $\alpha_s = \sqrt{-\mathrm{Bo}_f}$ and thus $f(\alpha)$ has no zeros in the strip $\mathcal{D}_s$.

Next the case $m \neq 1$ is examined. In the limit $\alpha \downarrow 0$ the discriminant $D(\alpha) = -C(\alpha)/A(\alpha) \approx 9s^2(m-1)^2$. By defining $D(0) = 9s^2(m-1)^2$ the analytic function $D(\alpha) \neq 0$ in some disc $|\alpha| < \alpha_f$ (since $D(\alpha)$ is continuous and non-zero at $\alpha = 0$). Therefore, $\sqrt{D(\alpha)}$ has two analytic branches in the disc $|\alpha| < \alpha_f$. Consequently, $\mathrm{Bo}_m(\alpha)$, and then $f(\alpha)$, has two analytic branches in this disc. One should choose the branch $f_m(\alpha)$ that corresponds to the positive Ma_m for the real values of α in this disc. It is shown below that $f_m(\alpha)$ has no zeros in the punctured disc $0 < |\alpha| < \alpha_s$. (Then of course it follows that the real function $f(\alpha)$ has no zeros in the interval $0 < \alpha < \alpha_s$ and therefore for Bo fixed at Bo_f, $\zeta \neq 0$ in the strip $\mathcal{D}_s$ of the αMa-plane.) For this a well-known fact from complex analysis is used. In Churchill et al. [11] it is stated: "*If f is analytic at the point α_c then there is a punctured disc about α_c in which f has no zeros unless f is identically zero in a neighborhood of α_c.*"

Clearly in the present case, $\alpha_c = 0$, and also f_m is not identically zero, which is seen by considering its Maclaurin series. It follows then that there is a punctured disc about zero, $0 < |\alpha| < \alpha_s$, in which f_m has no zeros. So the argument is now complete.

Unlike the finite thickness $m = 1$ case, it is possible to have $\mathrm{Ma} = \mathrm{Ma}_{\mathrm{Bo}}(\alpha)$ satisfying $\mathrm{Im}(\zeta) = 0$ (equation 185) and thus $\mathrm{Re}(\sqrt{\zeta}) = 0$ for fixed Bo that starts at $\alpha = 0$ (see figure 37). It remains to identify the surfactant and robust branches in the strip $\mathcal{D}_s$. Figure 37 shows examples of the curves $\mathrm{Ma} = \mathrm{Ma}_{\mathrm{Bo}}(\alpha)$ (equation 186) and the three possible pairs of m and Bo. For $m > (<) 1$ and $\mathrm{Bo} > (<) 0$ $\mathrm{Ma}_{\mathrm{Bo}}$ starts at $\alpha = 0$ but $\mathrm{Ma}_{\mathrm{Bo}}$ is not defined for $\alpha > \sqrt{-\mathrm{Bo}}$ in the $(<)$ case. When $m > 1$ and $\mathrm{Bo} < 0$, $\mathrm{Ma}_{\mathrm{Bo}}$ is only defined for $\alpha > \sqrt{-\mathrm{Bo}}$, and thus does not start at the origin.

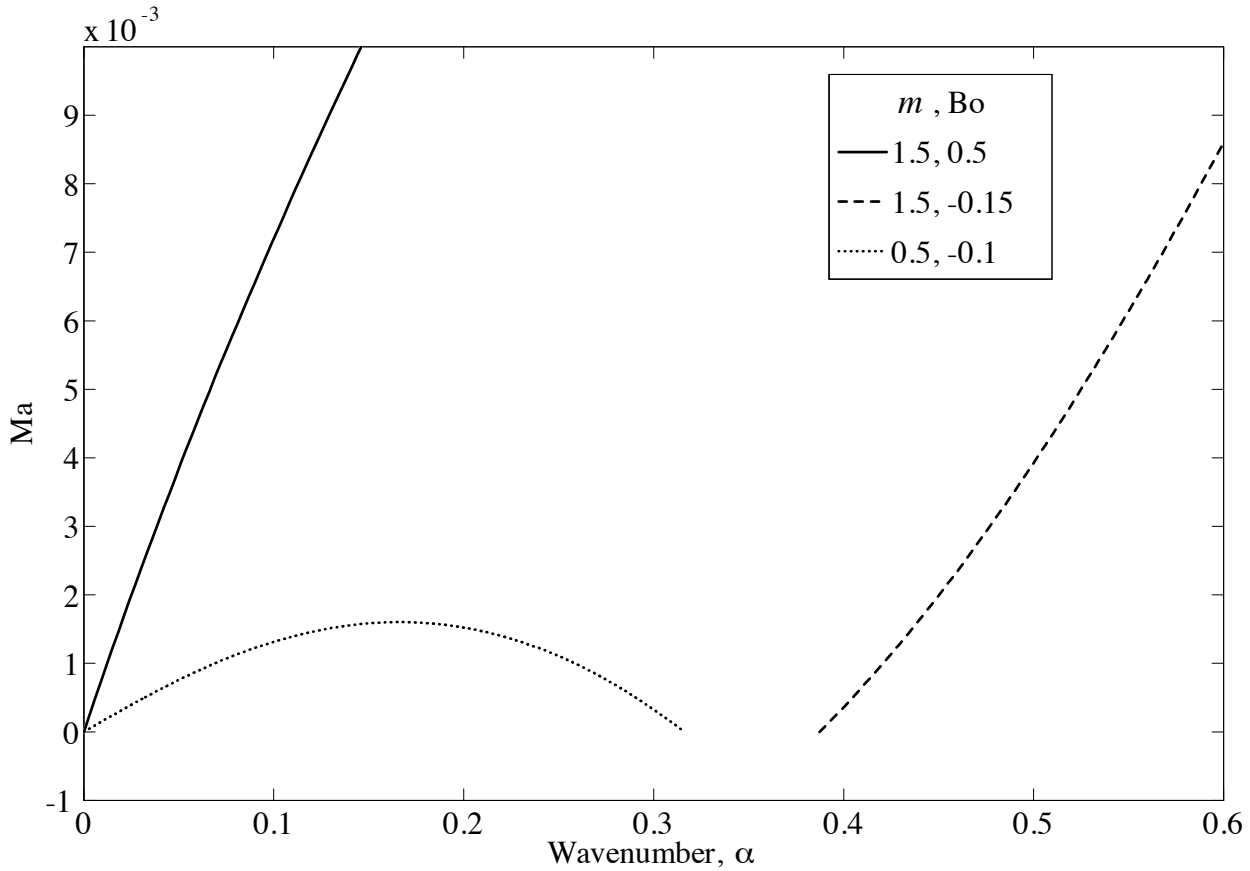

FIG. 37: Curves $\mathrm{Ma} = \mathrm{Ma}_{\mathrm{Bo}}(\alpha)$ for select values of m and Bo.

Just as in the finite thickness $m = 1$ case, $sgn(\mathrm{Re}(\sqrt{\zeta})) = sgn(\mathrm{Re}(F_1))$ in the limit of $\mathrm{Ma} \downarrow 0$, and from equation (B6) $sgn(\mathrm{Re}(F_1)) = sgn(\mathrm{Bo})$ for $0 < \alpha < \alpha_s$. Therefore, $sgn(\mathrm{Re}(\sqrt{\zeta})) = sgn(\mathrm{Bo})$. Next it is shown that $\mathrm{Re}\sqrt{\zeta}$ changes sign as Ma increases through Ma_0 for any fixed α.

To establish the behavior of $\mathrm{Re}(\sqrt{\zeta})$ as Ma increases through Ma_0, recall the fact that $\mathrm{Im}(\sqrt{\zeta})$ is continuous at Ma_0 and (in view of $\mathrm{Re}(\sqrt{\zeta}) = 0$) $\mathrm{Im}(\sqrt{\zeta}) \neq 0$, provided $\zeta \neq 0$, which implies $\sqrt{\zeta} \neq 0$. Therefore $\mathrm{Im}(\sqrt{\zeta})$ keeps the sign (for each branch) as Marangoni number increases through $\mathrm{Ma}_{\mathrm{Bo}}$. The condition determining $\mathrm{Ma}_{\mathrm{Bo}}$, that is $\mathrm{Re}(\sqrt{\zeta}) = 0$, in

view of

$$\mathrm{Im}(\zeta) = 2\,\mathrm{Re}(\sqrt{\zeta})\,\mathrm{Im}(\sqrt{\zeta}), \tag{190}$$

is equivalent to $\mathrm{Im}(\zeta) = 0$, provided $\mathrm{Im}(\sqrt{\zeta}) \neq 0$ i.e., $\zeta \neq 0$. The imaginary part of the discriminant (185) is clearly linear in Ma, and $\mathrm{Im}(\zeta) = 0$ at $\mathrm{Ma}_{\mathrm{Bo}}$. Hence, $\mathrm{Im}(\zeta)$ and $\mathrm{Re}(\sqrt{\zeta})$ change sign as Ma increases through $\mathrm{Ma}_{\mathrm{Bo}}$ since it has already been established that $\mathrm{Im}(\sqrt{\zeta})$ does not change sign.

If $\alpha < \alpha_s$, $\mathrm{Ma}_{\mathrm{Bo}}$ does not exist for $m > (<)1$ and $\mathrm{Bo} < (>)0$. Therefore, $sgn(\mathrm{Re}(\sqrt{\zeta}))$ does not change sign and the branches are determined exactly as in the finite thickness $m = 1$ case. One can also infer from equation (184) that when $\mathrm{Bo} < (>)0$ the surfactant branch is stable (unstable). For the cases $m > (<)1$ and $\mathrm{Bo} > (<)0$ the surfactant branch that has a positive (negative) $sgn(\mathrm{Re}(\sqrt{\zeta}))$ for $\mathrm{Ma} < \mathrm{Ma}_{\mathrm{Bo}}$ continues with a negative (positive) $sgn(\mathrm{Re}(\sqrt{\zeta}))$ for $\mathrm{Ma} > \mathrm{Ma}_{\mathrm{Bo}}$. Therefore, by (184), the surfactant branch (robust branch) is unstable (stable) for $\mathrm{Ma} < \mathrm{Ma}_{\mathrm{Bo}}$ and stable (unstable) for $\mathrm{Ma} > \mathrm{Ma}_{\mathrm{Bo}}$.

When $\mathrm{Ma} \ll |\mathrm{B}|$ where $\mathrm{B} = \mathrm{Bo} + \alpha^2$ and $m \ll 1$ equations (115)-(119) simplify such that the surfactant and robust branch are approximated by,

$$\gamma_R \approx -\frac{(s_\alpha^2 - \alpha^2)\alpha\mathrm{Ma}}{2(s_\alpha c_\alpha - \alpha)} \tag{191}$$

$$\gamma_R \approx -\frac{(s_\alpha c_\alpha - \alpha)\,\alpha\mathrm{B}}{2\,(\alpha^2 + c_\alpha^2)} + \frac{(s_\alpha^2 - \alpha^2)\mathrm{Ma}}{2(s_\alpha c_\alpha - \alpha)} \tag{192}$$

where the surfactant branch takes the $+$ in the $\pm$ in (62). In figure 32(h) one can see that the robust branch (192) (surfactant branch (191)) is unstable (stable) for $\alpha \ll 1$ and is more (less) negative for $\alpha \gg 1$.

IV. CONCLUSIONS AND DISCUSSION

In this dissertation, the linear stability of two immiscible fluid layers between two parallel plates that move steadily with respect to each other was investigated. In particular, the effects of an insoluble surfactant monolayer along the interface between the two fluids and gravity were examined. A normal mode analysis was used to derive an eigenvalue problem consisting of two Orr-Sommerfeld equations and several homogenous boundary conditions at the plates and the interface. Non trivial solutions were found provided the increment γ, the complex "growth rate," satisfied a quadratic equation with lengthy coefficients that are functions of the wavenumber, the Marangoni number, the Bond number, the viscosity ratio, the aspect ratio, and the interfacial shear. The dispersion equation was solved for two increment branches, and the real part of the growth rate was analyzed to make conclusions on the stability of the flow. One of the branches was identified as the "robust" branch, which was present even when $\mathrm{Ma} = 0$, and the other one was defined to be the "surfactant" branch that disappeared as $\mathrm{Ma} \downarrow 0$.

Based on the longwave analysis performed by FH, six sectors in the aspect ratio-viscosity ratio plane that characterize the stability of the system without gravity ($\mathrm{Bo} = 0$) were identified: the Q-sectors, Q_1 ($1 < n^2 < m$) and Q_2 ($m < n^2 < 1$), where both modes are stable; the R-sectors, R_1 ($1 < m < n^2$) and R_2 ($n^2 < m < 1$), where only the robust branch is unstable; the S-sectors, S_1 ($1 < n < \infty$ and $0 < m < 1$) and S_2 ($0 < n < 1$ and $1 < m < \infty$), where only the surfactant mode is unstable. The same longwave sectors were found for non-zero Bo. In the S sectors, the surfactant mode remained unstable for all Bo, while in the R sectors the growth rate of the robust branch was found to be unstable provided $\mathrm{Bo} < \mathrm{Bo}_c$. In the Q sectors, both branches remain stable for $\mathrm{Bo} \geq 0$, but the

growth rate of the robust branch can be longwave unstable for small values of Ma or midwave unstable for large values of Ma when Bo < 0 in certain sectors.

Also, some interesting behavior for arbitrary wavenumbers was found in the R sectors. Both branches were found to be unstable for negative values of Bond number, and eventually for sufficiently large $|\mathrm{Bo}|$ the robust branch became the dominant branch. This allowed for both unstable branches to cross and split causing one branch to have two local maxima and thus the possibility for a jump in the global maximum as shown in figure 13.

The change in character of the instability between the R_1 and Q_1 sectors by increasing the viscosity ratio but keeping the aspect ratio fixed was also investigated. When in the R_1 sector close to the $m = n^2$ border, the flow was found to be longwave unstable provided $\mathrm{Bo} < \mathrm{Bo}_c$ (equation 65) or stable. However, a new region of midwave instability away from $\alpha = 0$ was observed in the R_1 sectors close to the $m = n^2$ border and continued vertically through the Q_1 sector. In some instances the flow instability could switch from being unstable to stable, and also from longwave to midwave unstable (see stability diagrams in figures 20, 23, 22, and 24).

The infinitely thick upper layer, $n = \infty$, case was also considered. For the longwave limit, the growth rate branches were found to be proportional to $\mathrm{Ma}\alpha^{3/2}$ (see equation (184)) which caused difficulty in determining which branch was the surfactant branch since again the surfactant was defined to be the one that disappears as $\mathrm{Ma} \downarrow 0$. The branches were distinguished by looking at the asymptotic behavior for small values of Ma to determine which branch takes the $+$ sign and which branch takes the $-$ sign in equation (184). It was found that the robust branch was the stable branch if $m > 1$ and the surfactant branch was unstable if $m < 1$, however, this was for the less dominant branch. Similar to the S sectors, the branches exhibited crossings but for the $n = \infty$ case it was possible for

$\mathrm{Im}(\sqrt{\zeta}) = 0$ and $\mathrm{Re}(\sqrt{\zeta}) = 0$, simultaneously. Therefore, dispersion curves were shown to exhibit discontinuities in Bond number (or Marangoni number), since dispersion curves were always defined to be continuous in wavenumber.

Many effects were neglected in this dissertation which allows for the possibility of future investigation, such as, the effects of inertia, surfactant diffusion, and allowing for porosity of the plates. To estimate the importance of inertia consider an oil/water system that has $\mu_2 = 10$cP (oil), $\mu_1 = 1$cP (water), $\rho_2 = 0.8$g/cm^3, and $\rho_1 = 1$g/cm^3. Assume that $\sigma_0 = 10$dyn/cm and that the bottom plate is $d_1 = 10\mu$m then $\mathrm{Re}_1 = 100$ indicating that for such a system the effect of inertia should be considered. However, if water is replaced by a more viscous motor oil with $\mu_1 = 100$cP inertia can be neglected since $\mathrm{Re}_1 = 0.01$. Then according to Wei and Rumschitzki [49], the Marangoni number ranges from 25 to 250 (and thus Γ_0 ranges from 10^{-10} to 10^{-10}mol/cm) which is within the range of the current study. In this dissertation a linear stability analysis was carried out which only allowed for small amplitude disturbances. Therefore, only insight about the initial development of instability was obtained. To determine if one of the layers may rupture or if instability is saturated a non-linear stability analysis must be carried out.

REFERENCES

[1] Anshus, B. E. and A. Acrivos (1967). The effect of surface active agents on the stability characteristics of falling liquid films. *Chemical Engineering Science 22*, 389–393.

[2] Arnett, W. D., J. N. Bahcall, R. P. Kirshner, and S. E. Woosley (1989). Supernova 1987a. *Annual Review of Astronomy and Astrophysics 27*, 629–700.

[3] Bassom, A. P., M. G. Blyth, and D. T. Papageorgiou (2010). Nonlinear development of two-layer couette-poiseuille flow in the presence of surfactant. *Physics of Fluids 22*(10), 102102.

[4] Bassom, A. P., M. G. Blyth, and D. T. Papageorgiou (2012). Using surfactants to stabilize two-phase pipe flows of core-annular type. *Journal of Fluid Mechanics 704*, 333–359.

[5] Blyth, M. G. and A. P. Bassom (2013). Stability of surfactant-laden core-annular flow and rod-annular flow to non-axisymmetric modes. *Journal of Fluid Mechanics 716*, R13.

[6] Blyth, M. G., H. Luo, and C. Pozrikidis (2006). Stability of axisymmetric core-annular flow in the presence of an insoluble surfactant. *Journal of Fluid Mechanics 548*, 207–235.

[7] Blyth, M. G. and C. Pozrikidis (2004a). Effect of inertia on the Marangoni instability of two-layer channel flow, Part II: normal-mode analysis. *Journal of Engineering Mathematics 50*(2-3), 329–341.

[8] Blyth, M. G. and C. Pozrikidis (2004b). Effect of surfactant on the stability of film flow down an inclined plane. *Journal of Fluid Mechanics 521*, 241–250.

[9] Blyth, M. G. and C. Pozrikidis (2004c). Effect of surfactants on the stability of two-layer channel flow. *Journal of Fluid Mechanics 505*, 59–86.

[10] Chandrasekhar, S. (1961). *Hydrodynamics and Hydromagnetic Stability.* Dover Publications.

[11] Churchill, R., J. Brown, and R. Verhey (1974). *Complex Variables and Applications* (3rd ed.). McGrawHill.

[12] Craster, R. V. and O. K. Matar (2009). Dynamics and stability of thin liquid films. *Reviews of Modern Physics 81*(3), 1131–1198.

[13] De Wit, A., D. Gallez, and C. I. Christov (1994). Nonlinear evolution equations for thin liquid films with insoluble surfactants. *Physics of Fluids 6*, 3256–3266.

[14] Frenkel, A. L. and D. Halpern (2002). Stokes-flow instability due to interfacial surfactant. *Physics of Fluids 14(7)*, L45–L48.

[15] Frenkel, A. L. and D. Halpern (2005). Effect of inertia on the insoluble-surfactant instability of a shear flow. *Physics Review E 71*(1), 016302.

[16] Frenkel, A. L. and D. Halpern (2006). Strongly nonlinear nature of interfacial-surfactant instability of couette flow. *International Journal of Pure and Applied Mathematics 29*, 205–224.

[17] Gao, G. P. and X. Y. Lu (2006). Effect of surfactants on the long-wave stability of oscillatory film flow. *Journal of Fluid Mechanics 562*, 345–354.

[18] Gao, P. and X.-Y. Lu (2007). Effect of surfactants on the inertialess instability of a two-layer film flow. *Journal of Fluid Mechanics 591*, 495–507.

[19] Halpern, D. and A. L. Frenkel (2003). Destabilization of a creeping flow by interfacial surfactant: Linear theory extended to all wavenumbers. *Journal of Fluid Mechanics 485*, 191–220.

[20] Halpern, D. and A. L. Frenkel (2008). Nonlinear evolution, travelling waves, and secondary instability of sheared-film flows with insoluble surfactants. *Journal of Fluid Mechanics 594*, 125–156.

[21] Halpern, D. and J. B. Grotberg (1993). Surfactant effects on fluid elastic instabilities of liquid lined flexible tubes: a model of airway closure. *Journal of Biomedical Engineering 115*, 271–277.

[22] Hinds, W. C., A. Ashley, N. J. Kennedy, and P. Bucknam (2002, December). Conditions for cloud settling and rayleigh-taylor instability. *Aerosol Science and Technology 36*(12), 1128–1138.

[23] Joseph, D. D. and Y. Renardy (1993). *Fundamentals of Two-Fluid Dynamics, vol I: Mathematical Theory and Applications; vol II: Lubricated Transport, Drops and Miscible Liquids.* Springer.

[24] Kistler, S. and P. Schweizer (1997). *Liquid Film Coating.* Chapman Hall.

[25] Kull, H. J. (1991, August). Theory of the rayleigh-taylor instability. *Physics Reports-review Section of Physics Letters 206*(5), 197–325.

[26] Kwak, S. and C. Pozrikidis (2001). Effect of surfactants on the instability of a liquid thread or annular layer. Part I: Quiescent fluids. *International Journal of Multiphase Flow 27*, 1–37.

[27] Levy, R. and M. Shearer (2006). The motion of a thin liquid film driven by surfactant and gravity. *SIAM Journal on Applied Mathematics 66*(5), 1588–1609.

[28] Lin, S. P. (1970). Stabilizing effects of surface-active agents on a film flow. *AIChE Journal 16*, 375.

[29] Lindl, J. D., R. L. McCrorey, and E. M. Campbell (1992). Progress toward ignition and burn propagation in inertial confinement fusion. *Physics Today 45*, 32–40.

[30] Oron, A., S. H. Davis, and S. G. Bankoff (1997). Long–scale evolution of thin liquid films. *Reviews of Modern Physics 69*, 931–980.

[31] Orr, W. (1907). The stability or instability of the steady state motions of a perfect liquid and of a viscous liquid. *Proceedings of the Royal Irish Academy A. 27*, 9–138.

[32] Otis, D. R., M. Johnson, T. J. Pedley, and R. D. Kamm (1993). Role of pulmonary surfactant in airway closure: a computational study. *Journal of Applied Physiology 75*, 1323–1333.

[33] Peng, J. and K.-Q. Zhu (2010). Linear instability of two-fluid taylor-couette flow in the presence of surfactant. *Journal of Fluid Mechanics 651*, 357–385.

[34] Pozrikidis, C. (1997). *An Introduction to Theoretical and Computational Fluid Dynamics*. Oxford.

[35] Pozrikidis, C. (2003). Effect of surfactants on film flow down a periodic wall. *Journal of Fluid Mechanics 496*, 105–127.

[36] Pozrikidis, C. (2004). Effect of inertia on the Marangoni instability of two-layer channel flow, Part I: numerical simulations. *Journal of Engineering M 50*(2-3), 311–327.

[37] Pozrikidis, C. and A. I. Hill (2011). Surfactant-induced instability of a sheared liquid layer. *Ima Journal of Applied Mathematics 76*(6), 859–875.

[38] Rayleigh, L. (1883). Investigation of the character of the equilibrium of an incompressible heavy fluid of variable density. *Proceedings of the London Mathematical Society 14*, 170–197.

[39] Rubinstein, B. Y. and S. G. Bankoff (2001). Dynamics of thin liquid films on a coated solid surface with insoluble surfactants: weakly nonlinear analysis. *Langmuir 17*, 1306–1307.

[40] Rudraiah, N., K. B. Chavaraddi, and I. S. Shivakumara (2011). Non-linear study of electrohydrodynamic rayleigh-taylor instability in a composite fluid-porous layer. *International Journal of Non-linear Mechanics 46*(8), 1009–1016.

[41] Slattery, J. C. (1974). Interfacial effects in the entrapment and displacement of residual oil. *AIChE Journal 20*, 1145–1154.

[42] Sommerfeld, A. (1908). Ein beitrag zur hydrodynamischen erklärung der turbulenten flüssigkeitsbewegungen. *Proceedings 4th International Congress of Mathematicians III*, 116–124.

[43] Suman, B. and S. Kumar (2008). Surfactant- and elasticity-induced inertialess instabilities in vertically vibrated liquids. *Journal of Fluid Mechanics 610*, 407–423.

[44] Taylor, G. I. (1950). The instability of liquid surfaces when accelerated in a direction perpendicular to their planes. *Proceedings of the Royal Society of London A: Mathematical and Physical Sciences 201*, 192–196.

[45] Wei, H. H. (2005a). Effect of surfactant on the long-wave instability of a shear-imposed liquid flow down an inclined plane. *Physics of Fluids 17*(1), 012103.

[46] Wei, H. H. (2005b). Marangoni destabilization on a core-annular film flow due to the presence of surfactant. *Physics of Fluids 17*(2), 027101.

[47] Wei, H. H. (2005c). On the flow-induced Marangoni instability due to the presence of surfactant. *Journal of Fluid Mechanics 544*, 173–200.

[48] Wei, H. H. (2007). Role of base flows on surfactant-driven interfacial instabilities. *Physics Review E 75*(3), 036306.

[49] Wei, H. H. and D. S. Rumschitzki (2005). The effects of insoluble surfactants on the linear stability of a core-annular flow. *Journal of Fluid Mechanics 541*, 115–142.

[50] Whitaker, S. (1964). Effect of surface active agents on the stability of falling liquid films. *Industrial and Engineering Chemistry Fundamentals 3*, 132.

[51] Whitaker, S. and L. O. Jones (1966). Stability of falling liquid films. Effect of interface and interfacial mass transport. *AIChE Journal 12*, 421–431.

[52] Whitehead, J. A. and D. S. Luther (1975). Dynamics of laboratory diapir and plume models. *Journal of Geophysical Research 80*(5), 705–717.

[53] Yiantsios, G. and G. Higgins (1988). Linear stability of plane Poiseuille flow of two superposed fluids. *Physics of Fluids 31*, 3225–3238.

[54] Yih, C. S. (1966). Instability of laminar flows due to a film of adsorption. *Journal of Fluid Mechanics 28*, 493–500.

[55] Yih, C. S. (1967). Instability due to viscosity stratification. *Journal of Fluid Mechanics 27*, 337–352.

APPENDICES

APPENDIX A: FINITE ASPECT RATIO DETAILS

1. Expressions for coefficients A_{ij}

The coefficients A_{11}, A_{12}, A_{21}, and A_{22} from 47 in section II B are:

$$A_{11} = \left(\frac{s_{\alpha n}^2 - \alpha^2 n^2}{m n^2 \alpha} - \frac{1}{\alpha} \left(s_\alpha^2 - \alpha^2 \right) \right) \tag{A1}$$

$$\begin{aligned} A_{12} = & \frac{1}{n^2 \alpha} \left(s_{\alpha n} c_{\alpha n} + \alpha\, n + n^2 \left(\alpha + s_\alpha c_\alpha \right) \right) - \frac{i \alpha\, s}{\gamma\, m} (m-1) \\ & + \frac{1}{2 m n^2 \alpha^2 \gamma} \left(\mathrm{Bo} + \alpha^2 \right) \left(s_{\alpha n}^2 - \alpha^2 n^2 \right) \end{aligned} \tag{A2}$$

$$A_{21} = \left(\frac{2}{n^2} \left(s_{\alpha n} c_{\alpha n} - \alpha n \right) + 2 \left(s_\alpha c_\alpha - \alpha \right) + \frac{\alpha}{\gamma} \left(s_\alpha^2 - \alpha^2 \right) \mathrm{Ma} \right) \tag{A3}$$

$$\begin{aligned} A_{22} = & \frac{1}{n^2 \alpha \gamma} \left(s_{\alpha n} c_{\alpha n} - n \alpha \right) \left(\mathrm{Bo} + \alpha^2 \right) - \frac{\alpha}{\gamma} \mathrm{Ma} \left(\alpha + s_\alpha c_\alpha \right) \\ & \frac{2}{n^2} \left(m \left(\alpha^2 n^2 + c_{\alpha n}^2 \right) - n^2 \left(\alpha^2 + c_\alpha^2 \right) \right) + \frac{1}{\gamma^2} i s \alpha^3 \mathrm{Ma} \end{aligned} \tag{A4}$$

The coefficients k_{20}, k_{11}, k_{31}, k_{22} and k_{13} that appear in equation (60) are

$$
\begin{aligned}
k_{20} = & -\frac{s^2}{4\alpha^3}\left[(m-1)\left(s_{\alpha n}^2 - s_\alpha^2 n^2\right)\left(\alpha\, n - s_{\alpha n}c_{\alpha n} + n^2\left(\alpha - s_\alpha c_\alpha\right)\right)\right. \\
& \left. m\left(s_\alpha^2 - \alpha^2\right)\left(\alpha\, n + s_{\alpha n}c_{\alpha n}\right) + \left(s_{\alpha n}^2 - \alpha^2 n^2\right)\left(\alpha + s_\alpha c_\alpha\right)\right] \\
& - \frac{s^2}{4}\left(s_{\alpha n}^2 - s_\alpha^2 n^2\right)\left[m^2\left(s_\alpha^2 - \alpha^2\right)\left(\alpha^2 n^2 + c_{\alpha n}^2\right)\right. \\
& \left. -2m(n\alpha^2 - n^2\alpha^4 - s_\alpha c_\alpha s_{\alpha n}c_{\alpha n}) - \left(\alpha^2 + c_\alpha^2\right)\left(s_{\alpha n}^2 - \alpha^2 n^2\right)\right]
\end{aligned}
\tag{A5}
$$

$$
\begin{aligned}
k_{11} = & -\frac{s^2}{4\alpha^5}(m-1)\left(s_{\alpha n}^2 - s_\alpha^2 n^2\right)\left(\alpha\, n - s_{\alpha n}c_{\alpha n} + n^2\left(\alpha - s_\alpha c_\alpha\right)\right) \\
& \times\left[m(s_{\alpha n}c_{\alpha n} - \alpha\, n)\left(s_\alpha^2 - \alpha^2\right) + \left(s_\alpha c_\alpha - \alpha\right)\left(s_{\alpha n}^2 - \alpha^2 n^2\right)\right]
\end{aligned}
\tag{A6}
$$

$$
\begin{aligned}
k_{31} = & \frac{1}{16\alpha^3}\left(s_\alpha^2 - \alpha^2\right)\left(s_{\alpha n}^2 - \alpha^2 n^2\right)\left[\left(\alpha + s_\alpha c_\alpha\right)\left(s_{\alpha n}^2 - \alpha^2 n^2\right)\right. \\
& \left. +m(\alpha\, n + s_{\alpha n}c_{\alpha n})(s_\alpha^2 - \alpha^2)\right]^2
\end{aligned}
\tag{A7}
$$

$$
\begin{aligned}
k_{22} = & \frac{1}{8\alpha^9}\left(s_\alpha^2 - \alpha^2\right)\left(s_{\alpha n}^2 - \alpha^2 n^2\right)\left[m(s_{\alpha n}c_{\alpha n} - \alpha\, n)(s_\alpha^2 - \alpha^2)\right. \\
& \left. +(s_\alpha c_\alpha - \alpha)\left(s_{\alpha n}^2 - \alpha^2 n^2\right)\right]\left[m(s_{\alpha n}c_{\alpha n} + \alpha\, n)(s_\alpha^2 - \alpha^2)\right. \\
& \left. +(s_\alpha c_\alpha + \alpha)\left(s_{\alpha n}^2 - \alpha^2 n^2\right)\right]
\end{aligned}
\tag{A8}
$$

$$
\begin{aligned}
k_{13} = & \frac{1}{16\alpha^{11}}\left(s_\alpha^2 - \alpha^2\right)\left(s_{\alpha n}^2 - \alpha^2 n^2\right)\left[\left(\alpha - s_\alpha c_\alpha\right)\left(s_{\alpha n}^2 - \alpha^2 n^2\right)\right. \\
& \left. +m(\alpha\, n - s_{\alpha n}c_{\alpha n})(s_\alpha^2 - \alpha^2)\right]^2
\end{aligned}
\tag{A9}
$$

and the longwave approximations are

$$k_{20} \approx \frac{n^4 s^2}{108} \varphi (n-1)(n+1)^2 (m-n^2) \alpha^9 \tag{A10}$$

$$k_{11} \approx \frac{n^7 s^2}{81} (n-1)(m-1)(n+m)(n+1)^2 \alpha^9 \tag{A11}$$

$$k_{31} \approx \frac{n^6}{324} (n^3+m)^2 \alpha^{11} \tag{A12}$$

$$k_{22} \approx \frac{n^8}{486} (n+m)(n^3+m) \alpha^{11} \tag{A13}$$

$$k_{13} \approx \frac{n^{10}}{2916} (n+m)^2 \alpha^{11} \tag{A14}$$

2. Unequal viscosity ratio

Here the small wavenumber (α) approximations for the case of finite thickness, n, and small Marangoni number, Ma are given. The longwave approximation to expressions (50)-(55) are first written as a polynomial in Ma and Bo, then the coefficients are expanded (via Taylor series about $\alpha = 0$), so that keeping only the leading term in α, equations (50)-(55) are approximately

$$F_2 = \mathrm{Re}(F_2) \approx \frac{1}{3}\,\psi, \tag{A15}$$

$$\mathrm{Re}(F_1) \approx \frac{1}{9} n^3 (m+n) \alpha^4 + \frac{1}{3} n (m+n^3) \alpha^2 \mathrm{Ma} + \frac{1}{9}\ n^3 (m+n) \alpha^2 \mathrm{Bo}, \tag{A16}$$

$$\mathrm{Im}(F_1) \approx \frac{2}{3} n^2 s (n+1)(1-m) \alpha, \tag{A17}$$

$$\mathrm{Re}(F_0) \approx \frac{1}{36}\, n^4 \alpha^6 \mathrm{Ma} + \frac{1}{36} n^4 \alpha^4 \mathrm{MaBo}\,, \tag{A18}$$

$$\mathrm{Im}(F_0) \approx \frac{1}{6} n^2 s(1-n^2)\alpha^3 \mathrm{Ma}, \tag{A19}$$

where ψ is given by equation (68). In terms of the discriminant parts:

$$\begin{aligned}
\mathrm{Re}(F_1^2) \approx & -\frac{4}{9} n^4 s^2 (n+1)^2 (m-1)^2 \alpha^2 \\
& + \frac{2}{27} n^4 \left(n^3+m\right)(n+m)\,\alpha^6 \mathrm{Ma} \\
& + \frac{2}{81} n^6 (n+m)^2\,\alpha^6 \mathrm{Bo} \\
& + \frac{2}{27} n^4 (n^3+m)(n+m)\alpha^4 \mathrm{MaBo} \\
& + \frac{1}{9} n^2 (m+n^3)^2 \mathrm{Ma}^2 + \frac{1}{81} n^6 (n+m)^2 \alpha^4 \mathrm{Bo}^2
\end{aligned} \tag{A20}$$

$$\begin{aligned}
\mathrm{Im}(F_1^2) \approx & \frac{4}{27} s n^5 (n+m)(1-m)(n+1)\,\alpha^5 \\
& + \frac{4}{9} s n^3 (n^3+m)(1-m)(n+1)\alpha^3 \mathrm{Ma} \\
& + \frac{4}{27} s n^5 (n+m)(1-m)(n+1)\alpha^3 \mathrm{Bo}
\end{aligned} \tag{A21}$$

$$\mathrm{Re}(4F_2F_0) \approx \frac{1}{27} n^4 \psi \alpha^6 \mathrm{Ma} + \frac{1}{27} n^4 \psi \alpha^4 \mathrm{MaBo} \tag{A22}$$

$$\mathrm{Im}(4F_2F_0) \approx \frac{2}{9} s n^2 \left(1-n^2\right) \psi \alpha^3 \mathrm{Ma} \tag{A23}$$

The full discriminant split in the real and imaginary parts are:

$$\begin{aligned}\mathrm{Re}(F_1^2 - 4F_2F_0) \approx & -\frac{4}{9}n^4 s^2 (n+1)^2 (m-1)^2 \alpha^2 \\ & + \frac{1}{27}n^4(m^2 - 6mn^2 - 2nm - 2mn^3 + n^4)\alpha^6 \mathrm{Ma} \\ & + \frac{2}{81}n^6 \left(n+m\right)^2 \alpha^6 \mathrm{Bo} \\ & + \frac{1}{27}n^4(m^2 - 6mn^2 - 2nm - 2mn^3 + n^4)\alpha^4 \mathrm{MaBo} \\ & + \frac{1}{9}n^2(n^3+m)^2\alpha^4\mathrm{Ma}^2 + \frac{1}{81}n^6(n+m)^2\alpha^4\mathrm{Bo}^2\end{aligned}$$

$$\begin{aligned}\mathrm{Im}(F_1^2 - 4F_2F_0) \approx & \frac{4}{27}sn^5 \left(n+m\right)\left(1-m\right)\left(n+1\right)\alpha^5 \\ & + \frac{2}{9}n^2 s(n^4 + 2mn^3 - 2mn - m^2)(n+1)^2\alpha^3\mathrm{Ma} \\ & + \frac{4}{27}(n+m)(1-m)(n+1)n^5 s\alpha^3\mathrm{Bo}\end{aligned} \tag{A24}$$

3. Equal viscosity ratio

The longwave approximations for $m = 1$ are given here:

$$F_2 = \mathrm{Re}(F_2) \approx \frac{1}{3}\left(n+1\right)^4 \tag{A25}$$

$$\mathrm{Re}(F_1) \approx \frac{1}{9}n^3(n+1)\alpha^4 + \frac{1}{3}n(n^3+1)\alpha^2\mathrm{Ma} + \frac{1}{9}\ n^3(n+1)\alpha^2\mathrm{Bo} \tag{A26}$$

$$\mathrm{Im}(F_1) = 0, \tag{A27}$$

$$\mathrm{Re}(F_0) \approx \frac{1}{36}\,n^4\alpha^6\mathrm{Ma} + \frac{1}{36}n^4\alpha^4\mathrm{MaBo}\,, \tag{A28}$$

$$\mathrm{Im}(F_0) \approx \frac{1}{6} n^2 s(1-n^2)\alpha^3 \mathrm{Ma}. \tag{A29}$$

One should note that each of the above approximations has been divided by α. The discriminant parts are:

$$\begin{aligned}\mathrm{Re}(F_1^2) \approx & \frac{1}{81}(n+1)^2 n^6 \alpha^8 + \frac{2}{27}(n^2-n+1)(n+1)^2 n^4 \alpha^6 \mathrm{Ma} \\ & + \frac{2}{81}(n+1)^2 n^6 \alpha^6 \mathrm{Bo} \\ & + \frac{2}{27} n^4 (n^3+1)(n+1)\alpha^4 \mathrm{MaBo} + \\ & + \frac{1}{9} n^2 (n^3+1)^2 \alpha^4 \mathrm{Ma}^2 + \frac{1}{81} n^6 (n+1)^2 \alpha^4 \mathrm{Bo}^2\end{aligned} \tag{A30}$$

$$\mathrm{Im}(F_1^2) = 0 \tag{A31}$$

$$\mathrm{Re}(4F_2F_0) \approx \frac{1}{27} n^4 (n+1)^4 \alpha^6 \mathrm{Ma} + \frac{1}{27} n^4 (n+1)^4 \alpha^4 \mathrm{MaBo} \tag{A32}$$

$$\mathrm{Im}(4F_2F_0) \approx \frac{2}{9}(n+1)^5 (1-n) s n^2 \alpha^3 \mathrm{Ma} \tag{A33}$$

The full discriminant split in to the real and imaginary parts are:

$$\begin{aligned}\mathrm{Re}(F_1^2 - 4F_2F_0) \approx & \frac{1}{81} n^6 (n+1)^2 \alpha^8 + \frac{2}{81} n^6 (n+1)^2 \alpha^6 \mathrm{Bo} \\ & + \frac{1}{81} n^4 \alpha^4 \Big\{ \big(n^2(n+1)\mathrm{Bo} \ - 3n(n^3+1)\mathrm{Ma}\big)^2 \\ & + 9n^2 (n+1)^2 (n-1)^2 \mathrm{MaBo} \Big\}\end{aligned} \tag{A34}$$

$$\mathrm{Re}(F_1^2 - 4F_2F_0) \approx \frac{1}{81}n^6(n+1)^2\alpha^8 + \frac{2}{81}n^6(n+1)^2\alpha^6\mathrm{Bo}$$
$$+ \frac{1}{27}n^4(n^2-4n+1)(n+1)^2\alpha^4\mathrm{MaBo} \tag{A35}$$
$$+ \frac{1}{9}n^2(n^3+1)^2\alpha^4\mathrm{Ma}^2 + \frac{1}{81}n^6(n+1)^2\alpha^4\mathrm{Bo}^2 \tag{A36}$$

$$\mathrm{Im}(F_1^2 - 4F_2F_0) \approx \frac{2}{9}(n+1)^5(n-1)sn^2\alpha^3\mathrm{Ma} \tag{A37}$$

APPENDIX B: INFINITE ASPECT RATIO DETAILS

1. Expressions for coefficients A_{ij}

The coefficients A_{11}, A_{12}, A_{21} and A_{22} from (114) in section III A are:

$$B_{11} = \frac{1}{\alpha} \tag{B1}$$

$$B_{12} = -\frac{i\,(2\,\alpha\,m\gamma + \mathrm{Bo} + \alpha^2)\,(s_\alpha^2 - \alpha^2)\,m}{2\alpha^2}$$
$$- \frac{i\,(s_\alpha c_\alpha + \alpha^2 + \alpha)\,m\gamma}{\alpha} - s\,(m-1)\,\alpha \tag{B2}$$

$$B_{21} = \frac{2i\gamma}{\alpha^2} \tag{B3}$$

$$B_{22} = \frac{(2\,m\alpha\,\gamma + \mathrm{Bo} + \alpha^2)\,((s_\alpha^2 - \alpha^2)\,\alpha\mathrm{Ma} + 2\,\gamma(s_\alpha c_\alpha - \alpha\,))}{2\alpha^3}$$
$$+ \frac{(\,\gamma(\alpha + s_\alpha c_\alpha) - i\alpha^2 s)\,\mathrm{Ma}}{\alpha} + \frac{2\gamma^2\,(\alpha^2(1-m) + c_\alpha^2)}{\alpha^2} \tag{B4}$$

2. Unequal viscosity ratio

The longwave approximations to equations (115)-(119) are:

$$\mathrm{Re}(F_2) \approx 1, \tag{B5}$$

$$\mathrm{Re}(F_1) \approx \frac{1}{3}\alpha^4 + \alpha^2\mathrm{Ma} + \frac{1}{3}\alpha^2\mathrm{Bo}, \tag{B6}$$

$$\mathrm{Im}(F_1) = (1-m)s\alpha^2, \tag{B7}$$

$$\mathrm{Re}(F_0) \approx \frac{1}{12}\alpha^6\mathrm{Ma} + \frac{1}{12}\alpha^4\mathrm{MaBo}, \tag{B8}$$

$$\mathrm{Im}(F_0) = -\frac{1}{2}s\mathrm{Ma}\alpha^3, \tag{B9}$$

The discriminant parts are:

$$\begin{aligned}\mathrm{Re}(F_1^2) \approx \frac{1}{9}\alpha^8 - s^2(m-1)^2\alpha^4 + \frac{2}{3}\alpha^6\mathrm{Ma} + \frac{2}{9}\alpha^6\mathrm{Bo} \\ + \frac{2}{3}\alpha^4\mathrm{MaBo} + \alpha^4\mathrm{Ma}^2 + \frac{1}{9}\alpha^4\mathrm{Bo}^2\end{aligned} \tag{B10}$$

$$\begin{aligned}\mathrm{Im}(F_1^2) \approx \frac{2}{3}s(1-m)\alpha^6 + 2(1-m)s\alpha^4\mathrm{Ma} \\ + \frac{2}{3}s(1-m)\alpha^4\mathrm{Bo}\end{aligned} \tag{B11}$$

$$\mathrm{Re}(4F_2F_0) \approx \frac{1}{3}\alpha^6\mathrm{Ma} + \frac{1}{3}\alpha^4\mathrm{MaBo} \tag{B12}$$

$$\mathrm{Im}(4F_2F_0) \approx -2s\alpha^3\mathrm{Ma} \tag{B13}$$

And the full discriminant split in the real and imaginary parts are:

$$\begin{aligned}\mathrm{Re}(F_1^2 - 4F_2F_0) \approx \frac{1}{9}\alpha^8 - s^2(m-1)^2\alpha^4 + \frac{1}{3}\alpha^6\mathrm{Ma} + \frac{2}{9}\alpha^6\mathrm{Bo} \\ + \frac{1}{3}\alpha^4\mathrm{MaBo} + \alpha^4\mathrm{Ma}^2 + \frac{1}{9}\alpha^4\mathrm{Bo}^2\end{aligned} \tag{B14}$$

$$\begin{aligned}\mathrm{Im}(F_1^2 - 4F_2F_0) \approx \frac{2}{3}s(1-m)\alpha^6 + 2s\alpha^3\mathrm{Ma} + 2s(1-m)\alpha^4\mathrm{Ma} \\ + \frac{2}{3}s(1-m)\alpha^4\mathrm{Bo}\end{aligned} \tag{B15}$$

The discriminant given in equation (189) from section III B is

$$-\frac{C}{A} = \frac{\left(\left(s_\alpha^2 - \alpha^2\right)m^2 + \left(3\,s_\alpha c_\alpha - \alpha + s_\alpha^2 - \alpha^2\right)m + \alpha + s_\alpha c_\alpha + 2\,\alpha^2 + 2\,c_\alpha^2\right)^2 s^2(m-1)^2\alpha^6}{\left(q_1 m + q_0\right)\left(\left(s_\alpha^2 - \alpha^2\right)m + s_\alpha c_\alpha - \alpha\right)\left(\left(s_\alpha^2 - \alpha^2\right)m^2 + 2\,m s_\alpha c_\alpha + \alpha^2 + c_\alpha^2\right)} \tag{B16}$$

where

$$q_1 = s_\alpha^4 + 2\,s_\alpha^3 c_\alpha - 3\,s_\alpha^2\alpha^2 + s_\alpha^2 c_\alpha^2 - 2\,s_\alpha^2\alpha - 2\,c_\alpha s_\alpha\alpha - 2\,\alpha^2 s_\alpha c_\alpha + 2\,\alpha^4 + \alpha^2 c_\alpha^2 + 2\,\alpha^3,$$

$$q_0 = s_\alpha^3 c_\alpha + s_\alpha^2\alpha + 2\,s_\alpha^2 c_\alpha^2 + 2\,s_\alpha^2\alpha^2 + c_\alpha^3 s_\alpha - 2\,\alpha^4 - 2\,\alpha^2 c_\alpha^2 - 2\,\alpha^3 - \alpha\,c_\alpha^2.$$

Or separately,

$$A = \frac{\left(q_1 m + q_0\right)\left(\left(s_\alpha^2 - \alpha^2\right)m + s_\alpha c_\alpha - \alpha\right)\left(\left(s_\alpha^2 - \alpha^2\right)m^2 + 2\,m s_\alpha c_\alpha + \alpha^2 + c_\alpha^2\right)}{\alpha^2\left(\left(s_\alpha^2 - \alpha^2\right)m^2 + \left(3\,s_\alpha c_\alpha - \alpha + s_\alpha^2 - \alpha^2\right)m + \alpha + s_\alpha c_\alpha + 2\,\alpha^2 + 2\,c_\alpha^2\right)^2}, \tag{B17}$$

and

$$C = -s^2(m-1)^2\alpha^4. \tag{B18}$$

In the longwave limit $\alpha \downarrow 0$, to leading order (B16) is approximately

$$-\frac{C}{A} \approx 9s^2(m-1)^2 - 9s^2(2m-1)(m-1)^2\alpha$$